CHARACTERIZATION AND CELL-SEEDING OF DECELLULARIZED ADIPOSE TISSUE FOAMS FOR WOUND HEALING

by

Bryen Turco

A thesis submitted to the Department of Chemical Engineering

In conformity with the requirements for

the degree of Master of Applied Science

Queen's University

Kingston, Ontario, Canada

(September, 2014)

Abstract

Chronic wounds are common among diabetic patients and they are a leading cause of foot amputations. The standard of care has not been successful in healing these wounds so alternative cell-based approaches are being investigated. Each cell-based approach necessitates a delivery strategy that minimizes cell death and maximizes cell retention. To this end, an adipose-derived stem cell (ASC) delivery system was developed, using an extracellular matrix (ECM)-derived bioscaffold as the platform. Porous decellularized adipose tissue (DAT) foams were fabricated over a range of concentrations, and with different tissue processing methods (mincing vs. milling). These foams were characterized by quantitative assessment of equilibrium water content, porosity, protein loss, and swelling ratio (n = 3), with the aim of elucidating how protein concentration and tissue processing affect foam properties. DAT foams were hydrophilic, porous, and maintained their form in culture despite the gradual loss of protein. Also, increasing DAT foam concentrations resulted in reduced porosity and equilibrium water content. Immunofluorescence was then used to detect extracellular matrix (ECM) constituents including collagen IV, laminin and fibronectin in DAT foam cross-sections. DAT foams were positive for all three ECM proteins, suggesting that they could allow cell attachment, migration, and proliferation. In a previous study, it was identified that ASC do not infiltrate DAT foams using traditional static cell-seeding techniques. Therefore, cell-seeding studies were performed in an attempt to enhance cell infiltration into the central regions of the foams. dsDNA content and cell density were quantified in response to various seeding methods, scaffold concentrations, and orbital shaker speeds until an improved set of seeding conditions was identified. Proliferation of ASCs in foams was then determined by semi-quantitatively evaluating Ki67 expression and dsDNA content over 14 days. Finally, to determine the effects of cell-scaffold interactions on

ASC gene expression, cells were seeded onto various substrates and cultured in normoxic (21%) or hypoxic (1%) conditions. mRNA levels of VEGF-A and FGF-2 were quantified using qRT-PCR, and it was found that there were no noticeable trends in terms of the effects of oxygen tension or cell-scaffold interactions. However, protein analysis should be performed to confirm these trends.

Acknowledgements

First and foremost, I would like to thank my supervisor Dr. Lauren Flynn for her support, patience and mentorship throughout my Master's.

I'm grateful for the opportunity to have gotten to know the present and past members of the Flynn lab including Cody Brown, Andrew Carroll, Lydia Fuetterer, Ming Gong, Tim Han, Valerio Russo, Stuart Young and Claire Yu. Their friendship and inspiration has enriched my life over the last 2 years.

I would like to thank Sandra Lourenssen, Kurtis Miller and Dr. Michael Blennerhassett for assisting me with qRT-PCR. I would also like to thank Dr. Brian Amsden and Dale Marecak for allowing me to use lab equipment. Moreover, I would like to extend my thanks to Drs J. F. Watkins, K. Meathrel, J. Davidson, and D. McKay for their clinical collaborations.

Finally I would like to thank my family for their love and support.

Table of Contents

List of Figures

List of Tables

List of Abbreviations

ASC	Adipose-derived stem cell	HOX	Hypoxic
BSC	Biological safety cabinet	NOX	Normoxic
C_T	Cycle threshold number	PBS	Phosphate buffered saline
DAPI	4', 6-diamidino-2-phenylindole	PBST	Phosphate buffered saline with 0.2% TWEEN 20
DAT	Decellularized adipose tissue	qRT-PCR	Quantitative real-time polymerase chain reaction
DATsol	Homogenized decellularized adipose tissue	RNA	Ribonucleic acid
DDT	Decellularized dermal tissue	SEM	Scanning electron microscopy
DDTsol	Homogenized decellularized dermal tissue	SPB	Sorenson's phosphate buffer
DMEM	Dulbecco's modified eagle's medium	TCPS	Tissue culture poly(styrene)
DNA	Deoxyribonucleic acid	VEGF	Vascular endothelial growth factor
EDTA	Ethylenediaminetetraacetic acid	A	Area
EWC	Equilibrium water content	ρ	Density
FGF	Fibroblast growth factor	m	Mass
GAPDH	Glyceraldehyde-3-phosphate dehydrogenase	V	Volume

Chapter 1

Introduction

1.1 Project Motivation: Chronic Wound Treatment

Chronic wounds including diabetic foot ulcers are relatively common among the diabetic population, and can be caused by a combination of neuropathy, vasculopathy, and trauma [1]. Once developed, diabetic foot ulcers do not heal well, with complete healing occurring in only approximately 31% of patients after 20 weeks of care [2]. Additionally, up to 70% of healed ulcers will redevelop within 5 years [3]. Recurrent ulcers are prone to infection and are a leading cause of lower limb amputation [4]. The standard of care evidently can be improved, and cell-based treatment strategies that focus on delivering adipose-derived stem cells (ASCs) to the wound site are being explored.

1.2 Thesis Overview

Adipose tissue represents an easily acquired and expendable source of both ASCs [5] and extracellular matrix (ECM) for fabricating tissue-derived bioscaffolds [6] that holds promise for applications in soft tissue regeneration including chronic wound therapies. The efficacy of ASCs in the treatment of wounds has been primarily attributed to their ability to secrete beneficial paracrine growth factors [7] and chemokines [8] , which influence the function of nearby parenchymal cells, and recruit regenerative cells to the site of injury, respectively. However, in the development of any cell-based

therapeutic approach, it is important to consider the method of cell delivery. Based on clinical studies to date, injecting cell suspensions into ischemic tissue sites results in poor retention, low viability, and extremely limited engraftment [9]. A promising alternative in the context of wound healing would be to use a naturally-derived bioscaffold as an ASC-delivery platform. For example, the use of collagenous sponges in wound treatment has been shown to facilitate host cell infiltration, angiogenesis, and gradual remodeling of the wound environment [10].

Fabrication methods for decellularized adipose tissue (DAT)-derived foams have been described [11], and they have the potential to be used as chronic wound dressings since they support host cell infiltration, are gradually remodeled *in vivo,* and elicit a host angiogenic response [11]. Furthermore, due to preservation of the native adipose tissue ECM, DAT foams may retain bioactive ECM proteins, including laminin, collagen IV, and fibronectin, which could potentially enhance the wound healing response relative to bioscaffolds derived from purified collagens. In previous work, basement membrane proteins were histologically detected in DAT [6] prior to foam fabrication protocols. Further, DAT-based biomaterials have also been shown to be highly supportive of ASC attachment and proliferation [12], suggesting that the tissue-specific ECM may have advantages in designing ASC-delivery vehicles.

However, a limitation noted in the previous study with the DAT foams was the poor infiltration of seeded ASCs into the porous foams *in vitro*, with the static culture conditions employed resulting in monolayer growth on the scaffold surface. In

developing strategies with DAT-based foams as biological dressings for chronic wound healing, it would be advantageous to refine the scaffold properties and cell-seeding method to obtain a more homogeneous cellular distribution throughout the foams. Achieving a higher density of ASCs within the carrier would increase the "therapeutic dose" of cells that could be delivered in a single dressing. Moreover, the presence of ASCs within the central regions of the foam may help to further enhance the infiltration of endogenous progenitor cells through the secretion of chemotactic paracrine factors, thereby improving scaffold integration, tissue regeneration, and wound closure.

To address the previous limitations, this project focused on characterizing DAT foam scaffolds, optimizing cell-seeding strategies to enhance cellular distribution, and conducting a pilot study to explore the *in vitro* effects of cell-scaffold interactions on angiogenic factor gene expression, with a view towards potential applications in wound healing.

1.3 Research Objectives

The specific research objectives of this Master's thesis project were:

i. To characterize the structure and composition of the DAT foam scaffolds and to assess how DAT processing conditions and DAT concentration influenced the scaffold properties.

ii. To develop a reproducible seeding protocol, which resulted in a more uniform distribution of ASCs in the DAT foams by manipulating the seeding method, DAT foam concentration, and DAT processing steps.

iii. To investigate ASC interactions with the DAT foams *in vitro* by quantifying foam contraction and assessing ASC proliferation in culture.

iv. To conduct a pilot *in vitro* study to probe the effects of ECM interactions and oxygen tension on ASC angiogenic factor gene expression.

Chapter 2

Literature Review

2.1 Adipose Tissue

Adipose tissue is a depot for triacylglycerol storage, functioning to supply the body with a substrate from which energy may be produced [13]. Furthermore, subcutaneous and visceral adipose tissues are recognized as a source of both thermal insulation and cushioning. Although these roles have long been realized, research has revealed that adipose tissue also participates in regulating a broad range of bodily functions through the secretion of cell signaling proteins termed “adipokines” [13]. Moreover, there are two distinct types of adipose tissue found in the human body that have very different roles.

2.1.1 Brown Adipose Tissue

Brown adipose tissue is visually distinct from white adipose tissue. As the name implies, this tissue has a brown colour which is attributable to the numerous, large mitochondria present in the brown adipocytes and the tissue’s dense vascular supply [14]. It can therefore be deduced that brown adipocytes are highly metabolically active in nature and the tissue's primary function is to generate heat to maintain internal body temperatures. Brown adipocytes are able to generate large quantities of thermal energy since their mitochondria express high levels of uncoupling proteins (UCP1) in the inner mitochondrial membrane [15]. UCP1 allow protons in the mitochondrial intermembrane

space to travel down their electrochemical gradient, bypassing ATP synthase and generating heat [15].

Brown fat is localized in adults to cervical, supraclavicular, axillary, paravertebral, mediastinal, and upper abdominal regions [16]. The amount of brown fat decreases with increased age, however brown adipose tissue continues to be metabolically active during adulthood. For instance, van Marten Lichtenbelt *et al.* detected metabolic activity in brown adipose tissue after exposure to cold temperatures in 96% of healthy adult males subjects [17]. Interestingly, brown fat metabolic activity seems to be greater among lean individuals, however it is unknown if the higher metabolic activity of brown fat in lean individuals is a cause or effect of body composition [17].

2.1.2 White Adipose Tissue

In contrast to brown adipocytes that are derived from the same precursor cells as myocytes, white adipocytes are derived from a separate precursor [18]. White adipocytes are the major component of white adipose tissue, which includes visceral and subcutaneous fat. Adipocytes in white adipose tissue possess a distinctly large lipid droplet containing triacylglycerol for energy storage; additionally, white adipose tissue serves to thermally insulate and cushion the body. On top of these roles, white adipose tissue has now been recognized as an endocrine organ that produces numerous adipokines - most of which have functions that are largely unknown [19].

For example, leptin signaling is known to both suppress appetite and increase energy expenditure [20]; in fact, leptin deficiency causes severe early onset obesity [21]. Furthermore, decreased leptin signaling is reported in obese individuals despite higher circulating levels of leptin [20]. However, leptin affects more than simply appetite and energy expenditure. Similar to other adipokines, such as resisitin, adiponectin, and apelin, leptin can modulate a variety of bodily processes including inflammation, immunity, cardiovascular functions and eliminating free radicals. Wozniak *et al.* reviews many of these adipokines and their functions in detail. [19].

2.1.3 Extracellular Matrix Components of White Adipose Tissue

Histological examination of adipose tissue reveals that individual adipocytes and groups of adipocytes are enveloped in a fibrous network of collagen type I [22]. Collagen I is the primary structural heterotrimeric protein of the ECM that takes on a triple helical form, and it can be cross-linked to a host of other ECM proteins to form a complex network. Cells can bind to collagen I via integrin receptors (mainly the β_1 subgroup), or non-integrin receptors, and therefore influence cellular signaling [23].

Immediately surrounding the adipocyte is a thin layer of basement membrane comprised of intertwined networks of laminin and collagen type IV [22], [24], [25]. Moreover, a layer of basement membrane underlies the endothelial cells of blood vessels [22] and nerves dispersed throughout adipose tissue. Laminin is a four-armed heterotrimeric polymerizable glycoprotein which binds to the cellular transmembrane laminin receptor-1 (LAMR1) [26]. It was originally thought that the function of LAMR1

was to anchor cells to the basal lamina, but it is now understood - albeit poorly - that LAMR1 is capable of transducing signals that influence adhesion, differentiation, proliferation, and migration [26]. The network of collagen type IV in adipose tissue is not dependent on binding to cellular receptors [27]. However, cells can bind heterotrimeric collagen IV via integrin receptors (mainly the β_1 subgroup) and non-integrin receptors such as those belonging to the mannose receptor family and glycoprotein VI [23]. Like laminin, binding to collagen type IV influences proliferation, differentiation, migration, survival and adhesion.

Cellular fibronectin is a glycoprotein that is also found surrounding adipocytes and in the interstitium [24], as it is a significant component of the ECM. Upon binding to preadipocytes mainly via β_1 integrin receptors, fibronectin is known to affect cytoskeletal organization and gene expression [28]. In addition to affecting cellular activity, cellular fibronectin also influences ECM properties since it can be cross-linked to collagen I [29] and influence fibrillar organization. Adipose tissue is comprised of many more ECM proteins that further influence ECM organization and cellular responses by directly stimulating cells through receptor proteins and by sequestering growth factors or matrix metalloproteinases [30]. Some ECM proteins become biologically active only after proteolytic cleavage; for example irisin is a cleavage fragment of fibronectin that enhances cell adhesion via integrin interaction [31]. Since adipose tissue contains an abundance of ECM and ECM-associated proteins, it is an attractive potential biomaterial for soft tissue engineering applications.

2.2 Biomaterials in Tissue Engineering

Tissue engineering often involves the use of biomaterials that act as carriers for therapeutic cells, growth factors, or a combination of both. Additionally, biomaterials may be used on their own to enhance the body's innate capacity to regenerate - one example is the use of collagen foams in wound healing [32]. There are two classes of biomaterials - namely synthetic biomaterials and naturally derived biomaterials. Synthetic biomaterials are often designed to recapitulate the structure of natural ECM by using polymer processing techniques such as electrospinning that yield nano-fibers [33]; moreover, well-defined ligand-functionalized groups can be grafted onto polymer backbones to elicit cellular responses that mimic the bioactivity of natural ECM [34]. Since synthetic biomaterials may be fabricated with a relatively high degree of control over polymer composition, grafting, cross-link density, and polymer processing methods (among others), they have been invaluable in the elucidation of how cells respond to isolated elements of their microenvironment [35]. However, since the natural ECM is comprised of complex interwoven networks of proteins, proteoglycans, glycosaminoglycans, soluble and sequestered growth factors, synthetic materials often fail to accurately mimic the native ECM milieu [35]. On the other hand, naturally derived biomaterials may encompass a milieu more representative of native ECM, however these materials are usually not well-defined relative to synthetic materials, and control over parameters such as scaffold composition is limited [35]. Of particular interest in the context of the current project are naturally derived ECM biomaterials. Generally,

biomaterials of this nature involve the collection, decellularization and potential processing of excised tissues [36]. Finally, a hybrid approach to biomaterial fabrication exists, incorporating both synthetic and natural elements in the final product.

2.2.1 Extracellular Matrix-Derived Biomaterials

ECM-derived biomaterials are typically produced via decellularization protocols of excised tissues. They represent an attractive class of natural biomaterials because of their cell adhesion properties, biocompatibility, and ability to degrade over time. The processing strategies are designed to extract cells and cellular components that would initiate an immune response, allowing these materials to be applied allogenically with low risk for rejection [37]. However, for some types of tissue, this class of biomaterial may even have the potential to act as an autologous scaffold, further minimizing the risk of an adverse immune response. To date, commercially available allogenic and xenogeneic tissues such as dermis, small intestinal submucosa, urinary bladder and pericardium are available and have been used effectively in the clinic for a range of applications in soft tissue regeneration [36].

2.2.2 Host Response to Biomaterials

The success of a biomaterial is largely attributed to the elicitation of a favorable healing response in the host. It is understandable to presume that the ideal host response to an implanted tissue would be non-existent. However, a host immune response - in particular the activation of macrophages in remodeling the ECM - is necessary [38]. In

fact, the actions of macrophages can dictate the success or failure of an implanted biomaterial. For example, macrophages can take on a destructive, pro-inflammatory (M1) phenotype or a more constructive regenerative (M2) phenotype depending on interactions with the implanted biomaterial [39]. The mechanism by which ECM biomaterials mediate the macrophage phenotypic transition is not well understood, but a few factors are known to impair constructive M2 macrophage transitions [36].

First, chemical cross-linking appears to prevent the constructive macrophage phenotype, and instead results in a foreign body response, involving encapsulation and multinucleate giant cell formation [40]. This was demonstrated in a study where both chemically cross-linked and non-cross-linked porcine small intestine submucosa (SIS) were used for skeletal muscle formation in a rodent [41]. More specifically, non-cross-linked SIS resulted in the production of organized, contractile, and vascularized skeletal muscle, while chemically cross-linked SIS yielded little to no new muscle that was generally non-contractile.

Degradation of ECM-derived biomaterials generate bioactive fragments [42] that can affect cellular differentiation, migration, and proliferation. These degradation products are also likely to influence macrophage activity. Since cross-linking slows the rate of degradation, bioactive fragments may not be released as quickly and this might also explain why cross-linked biomaterials result in macrophage M1 phenotypes [36]. However, cross-linking can be used to enhances structural rigidity and slow degradation,

thereby preventing structural breakdown as the biomaterial is gradually replaced with new tissue [36].

The amount of residual cellular debris following a decellularization protocol can also impair constructive macrophage (M2) transition. For instance, a study evaluated the M1/M2 phenotypic polarization profile of SIS decellularized to different extents (defined by the abundance of residual DNA) and concluded that more cellular debris present in the decellularized tissue elicited an macrophage M1 phenotype [43]. In addition to the factors mentioned the decellularization, sterilization protocol and each processing step afterwards may influence macrophage activity.

2.2.3 Decellularized Adipose Tissue Foams

Adipose tissue is abundant and it can be collected with minimally invasive liposuction procedures, making it an attractive source of ECM for tissue engineering applications. Decellularized adipose tissue (DAT) can be processed further to yield porous DAT foam scaffolds [11], and parameters such as pore size of the foams can be controlled by manipulating the rate of freezing or the concentration of ECM suspension used to generate the foams. Moreover, these DAT foams were implanted in an immunocompetent rat and were gradually resorbed, remodeled, and integrated with surrounding tissue over a period of 12 weeks [11]. Furthermore, DAT foams facilitated the invasion of host immune cells and functional blood vessels were visualized at the center of the foam suggesting a potent angiogenic effect [11].

2.2.4 Cell-Seeding

Porous scaffolds have the capacity to support cell populations and act as both a delivery vehicle and structural network that can regenerate tissue. However, development of strategies to optimize cell infiltration into scaffolds prior to implantation is necessary to increase the cell density and promote homogenous distribution. Traditional static seeding methods are the most commonly used to date because of their simplicity [44]. Static seeding involves dripping a concentrated cell suspension over scaffolds and then allowing time for cells to adhere and equilibrate. Generally, static seeding results in very little cell infiltration when compared to other seeding methods [44]. However, cell infiltration can also be affected by other factors such as cell size and scaffold properties including pore size and void fraction [45]. As such, many seeding strategies exist with the aim of seeding scaffolds uniformly, reproducibly, and with minimal cost.

Dynamic seeding protocols involve the movement of cell suspension around a scaffold to facilitate seeding. For instance, spinner flask seeding involves stirring a cell suspension in a flask containing scaffolds [46]. Agitation seeding involves placing a vessel containing scaffolds and cell suspension on an orbital shaker [44]. More intricate dynamic seeding methods use oscillatory flow perfusion techniques to force cell suspension through stationary scaffolds [47]. Each seeding technique has advantages and limitations, and the application of one technique over another might be determined by the mechanical properties of the scaffold, cell-seeding objectives, and costs.

2.3 Adipose-derived Stem Cells

In addition to containing an ECM rich in bioactive proteins, white adipose tissue houses a population of multipotent stromal cells capable of *in vitro* expansion called adipose-derived stem cells (ASCs). An ideal stem cell source for regenerative medicine applications is one that can be: found in abundant quantities, harvested by a minimally invasive procedure, reproducibly differentiated into different cell lineages, safely transplanted into an autologous or allogenic host, and produced according to Good Manufacturing Practice Guidelines [48]. The stem cell yield of ASC from 1 g of adipose tissue has been reported to be at least 500-fold greater than the stem cell yield from 1 g of bone marrow stem cells (BMSC) [49]. Moreover, adipose tissue can easily be collected from routine liposuction procedures that often yield 100 mL - 3 L of lipoaspirates [48]. Once isolated, ASCs can be expanded in culture, with a doubling time of 2-4 days [50].

In culture, ASCs can be differentiated into adipogenic, chondrogenic, osteogenic, and myogenic lineages, and can be induced to display markers of other mature cell types, with lineage-specific differentiation media. Moreover, it was shown that over half of clonal ASC populations could differentiate into 2 or more lineages, supporting the notion that ASCs represent a multipotent stromal cell population rather than a mixed population of unipotent progenitors [51]. Interestingly, ASCs suppress the *in vitro* alloreactivity in lymphocyte cultures, with a more potent effect observed when there was direct cell-to-cell contact [52]. Furthermore it was shown that ASC passage number is inversely proportional to immunogenicity as determined by allogenic responder T-cell

proliferation; moreover, higher passage ASCs were shown to suppress allogenic responder T-cell proliferation [53], thereby providing supporting evidence for safety in allogenic transplantation. Clearly, ASCs meet the criteria of an ideal stem cell source as described above.

2.3.1 Isolation and Culture of ASCs

The isolation procedure for ASCs was originally described in 1964 [54] when Rodbell *et al.* were isolating mature adipocytes. Many advances have been made in the isolation process and ASCs can be now be isolated from either whole fat or lipoaspirates. Whole fat needs to be minced, while the liposuction procedure effectively minces adipose tissue to a size dependent on the diameter of the cannula [48]. Moreover, ASC viability is not significantly affected by the liposuction procedure [55]. Following tissue collection and potential mincing, adipose tissue is subject to collagenase digestion usually followed by centrifugation to separate the floating mature adipocytes from the stromal vascular fraction (SVF). Mature adipocytes are aspirated to collect the SVF, which contains a mixed population of cells including ASCs, fibroblasts, pre-adipocytes, blood cells, endothelial cells, and pericytes [54]. In order to further isolate ASCs from the SVF, the SVF cells are cultured on plastic to separate non-adherent populations. Automated ASC isolation prototypes now exist and are capable of isolating ASCs from up to 1 L of lipoaspirate [56]. Once isolated, ASCs can be cultured for extended periods of time, although there is evidence that the differentiation capacity towards soft tissue lineages decreases with repeated serial passaging [57].

2.3.2 Immunophenotype of ASCs

Although no universal definition with respect to immunophenotype exists for ASCs, they are known to express several surface antigens. Cells of the SVF are heterogeneous, but after culturing the cell population tends to become more homogeneous because of the selective effects of culturing (only 1 in 30 SVF cells is plastic-adherent [50]) and because existing adherent cells begin to change their phenotype (a maximum of 54% of SVF cells express stromal markers, while 98% of later passage ASCs express stromal markers [50]). Moreover, ASCs can be isolated from cryo-preserved lipoaspirates with a yield of 90% compared to cell isolation from fresh lipoaspirates, and maintain their ability to differentiate [58].

ASCs are often compared to bone marrow-derived mesenchymal stem cells (BMSCs) and these two populations are indistinguishable based on a panel of 22 surface antigens [59]. However, some basic distinguishing factors have been determined and the Tissue Stem Cell Committee of the International Society for Cellular Therapy identified some basic criteria for identification of ASCs [60]. ASCs must: (i) be plastic-adherent; (ii) express CD105, CD73 and CD90; (iii) lack expression of CD45, CD14 or CD11b, CD79a or CD19 and HLA-DR surface molecules; and (iv) be able to differentiate to cells of the osteogenic, chondrogenic and adipogenic lineages [60].

2.3.3 ASCs in Regenerative Medicine

ASCs have shown great promise in numerous regenerative applications in animal models however their exact mechanisms of action are yet well understood. There is a

general consensus that ASCs exert their effects primarily through paracrine factor secretions, which mediate endogenous cell recruitment and cell survival. For example, when ASCs were co-cultured with endothelial cells, endothelial cells displayed increased viability and migration; however, once neutralizing antibodies against vascular endothelial growth factor (VEGF) and hepatocyte growth factor (HGF) are added to ASC-conditioned medium, endothelial cell viability and migration returned to baseline levels [61]. Moreover, transduced ASCs that have 80% reduced expression of HGF *in vitro* have an impaired ability to enhance ischemic tissue reperfusion after implantation into a mouse model [62].

ASCs also secrete factors that recruit other cell types. For instance, SDF-1 is expressed by ASCs [63]. In a previous study, SDF-1 was shown to play a role in vasculogenesis through the recruitment of *ex vivo* expanded endothelial progenitor cells to sites of ischemia in a mouse model [64]. After implantation of ASCs in an ischemic mouse model and subsequent injection of a neutralizing antibody against SDF-1, the efficacy of ASCs in improving revascularization was reduced [63]. This evidence supports the notion that ASCs exert their therapeutic effects through secreted factors. In contrast with the paracrine mechanism of action, ASCs may also directly contribute to the parenchymal cell population via differentiation, although evidence for this hypothesis is lacking relative to the paracrine factor secretion hypothesis.

2.4 Wound Healing and Angiogenesis

Wound healing is a complex process that depends on cell-ECM interactions, cell-cell interactions, and the cellular response to various secreted signaling proteins [65]. All of these interactions are at play in the three overlapping phases of acute wound healing, namely the inflammatory phase, the proliferative phase, and the maturation phase.

By the end of the inflammatory phase, hemostasis is achieved, a provisional matrix susceptible to cell infiltration is established, and circulating leukocytes are recruited to the site of injury [65]. Immediately following injury, the endothelial lining of blood vessel walls is damaged and subendothelial cells, along with various ECM components become exposed in the lumenal space [66]. ECM components may directly or indirectly bind circulating platelets that aggregate and form a barrier that prevents hemorrhage. Simultaneously, exposed ECM and subendothelial cells initiate two converging coagulation cascades that yield a cross-linked fibrin network that acts to reinforce the platelet plug [66]. As the fibrin network expands, it becomes interspersed with adherent platelets and collectively; the fibrin and platelet components constitute the hemostatic plug. In addition to preventing hemorrhage, the hemostatic plug acts as a provisional matrix to support cell infiltration. Furthermore, embedded platelets secrete protein factors that facilitate the extravasation of leukocytes into the wound space [67].

Towards the end of the inflammatory phase, leukocytes (macrophages and neutrophils) enter the hemostatic plug and phagocytose cellular debris and pathogens [65]. Simultaneously, macrophages secrete factors from within the hemostatic plug that

signal regenerative cells surrounding the provisional matrix (i.e.: fibroblasts, endothelial cells, and more leukocytes) to proliferate and migrate into the wound. This event marks the transition from the inflammatory phase to the proliferative phase in wound healing.

One of the most prominent features during the proliferative phase is the appearance of granulation tissue. Granulation tissue consists mainly of ECM, fibroblasts and newly formed vasculature [65]. As activated fibroblasts migrate into the wound bed, they remodel the provisional matrix mainly by increasing the proportion of collagen in the ECM [68]. During tissue formation, a new epidermal layer is created. Epidermal cells located near the edge of the wound mobilize and migrate along the granulation tissue-hemostatic clot border [69]. Once a monolayer of epidermal cells separates the overlying clot from the underlying granulation tissue, epidermal cells begin to re-establish connections with newly synthesized underlying basement membrane and neighboring cells [65].

In the final remodeling phase, a subset of fibroblasts differentiate into myofibroblasts [68] and compact the ECM using contractile force [65]. Undifferentiated fibroblasts continue to secrete collagen and remodel the ECM, eventually forming scar tissue. Once the dermal layer is regenerated, many of the resident cells begin to apoptose [70] and wound healing is complete.

2.4.1 Diabetic Foot Ulcers

Diabetic foot ulcers are examples of chronic wounds where healing is impaired. It is estimated that between 15-25% of diabetic patients will develop foot ulcers in their

lifetime [71]. Diabetic foot ulcers are difficult to heal because of a unique combination of neuropathy, vasculopathy, infection, and cellular abnormalities. One study demonstrated neuropathy was present in 78% of diabetic patients with foot ulcers [72]. Neuropathy includes the physiological changes of motor, sensory and autonomic neurons in response to a prolonged diabetic state [1]. Damaged motor neurons alter intrinsic foot muscle activation patterns and result in unevenly distributed loads during walking. Consequently, areas of high pressure develop and they contribute to trauma that may initiate or maintain foot ulceration [73]. Autonomic neuronal damage increases ateriovenous shunting, effectively leading to edema and a dry, warm environment permissive to bacterial infection [74]-[76].

In addition to neuropathy, peripheral vascular disease (PVD) was present in 30% of patients with foot ulcers [77]. Both macro and microvascular dysfunction may contribute to impaired tissue perfusion, nutrient exchange and cellular migration during wound repair [78]. Furthermore, cellular abnormalities like unresponsive fibroblasts may contribute to impaired healing [79].

2.4.2 Treatment of Chronic Wounds with ASCs

Standard care for non-healing wounds such as diabetic foot ulcers focuses on offloading the wounded area, controlling bacterial infections [80], and surgical debridement to remove necrotic or infected tissue and callouses. Following surgical debridement, a standard saline-soaked gauze dressing is usually applied over an extended period of time and changed frequently with the aim of accelerating wound regeneration.

The standard of care for treating non-healing wounds of the diabetic foot usually results in ~ 30% healing rate after 20 weeks [2]. Further, recurrence rates are high and often necessitate lower limb amputation, which has devastating psycho-social consequences and high associated rates of mortality. The annual cost of treating chronic wounds in North America is approaching $25 billion [81]. Not surprisingly, many groups have worked to develop alternative wound dressings that are available on the market (Table 2.1). Since the pathophysiology of wounds is heterogeneous, a large variance between wounds is often observed with respect to: presence/absence of infection, exudation, wound size, wound location, the presence of necrotic tissue, and the presence of foot deformities [82]. Many wound dressings are useful in certain classes of wounds, but none of these products are without their disadvantages. For instance, alginate wound dressings are particularly useful in heavily exudating wounds because they are absorbent, hemostatic and bacteriostatic; however, residual alginate may serve as a source of infection, so care must be taken to ensure that all residual alginate is removed from the wound during dressing changes [83]. Unfortunately, there is a lack of research-based evidence that supports the use of one dressing type over another [83].

In addition to studying alternative wound dressing materials, the use of cell-based therapies is being explored for applications in chronic wounds. In particular, ASCs have been investigated in treating non-healing wounds since they secrete a wide array of angiogenic growth factors including VEGF and FGF-2, and chemotactic factors including SDF-1 [84]. Moreover, secretion of these factors can be upregulated through *in vitro*

hypoxic preconditioning [85]. To date, no clinical trials using ASCs for wound healing have been reported, however a phase II clinical trial is ongoing. In contrast, animal models have been used to demonstrate that delivery of ASC to the wound site can improve healing. However, there is a lack of research comparing the effectiveness of different ASC delivery strategies [86].

Table 2.1: Wound dressing classifications taken from Hilton *et al.* [83]

Dressing	Advantages	Disadvantages
Low-adherence	Simple	Minimal absorbency
	Hypoallergenic	
	Inexpensive	
Hydrocolloids	Absorbent	Concerns about use for infected wounds
	Can be left for several days	May cause maceration
	Aid autolysis	Unpleasant odor
Hydrogels	Absorbent	Concerns about use for infected wounds
	Aid autolysis	May cause maceration
	Donate liquid	
Foams	Thermal insulation	Can adhere to wound
	Good absorbency	Occasional dermatitis with adhesive
	Confirm to contours	
Alginates	Highly absorbent	May need wetting before removal
	Bacteriostatic	
	Hemostatic	
	Useful in cavities	
Iodine preparations	Antiseptic	Iodine allergy
	Moderately absorbent	Discolors wounds
		Avoid in case of thyroid disease or pregnancy
Silver-impregnated	Antiseptic	Cost
	Absorbent	No proven advantage

Chapter 3

Materials and Methods

Unless otherwise stated, all reagent used were purchased from Sigma-Aldrich (Oakville, Canada).

3.1 Obtaining Human Adipose Tissue

Subcutaneous or breast adipose tissue samples were obtained from female patients undergoing abdominoplasty or breast reduction procedures at Hotel Dieu Hospital or Kingston General Hospital in Kingston, Canada. Upon excision, adipose samples were placed in sterile tubs containing 100 mL of sterile, cation-free phosphate buffered saline (PBS) and transported back to the lab within two hours of harvesting. PBS was supplemented with 2% (w/v) bovine serum albumin (BSA) if samples were used for ASC isolation. Research ethics board approval from Queen's University was obtained for this research (REB No. CHEM-002-07).

3.2 Decellularization of Human Adipose Tissue

Subcutaneous and breast adipose tissue samples from multiple patients were decellularized over 5 days using an established detergent-free protocol consisting of freeze-thaw cycles, mechanical agitation, polar solvent extractions, and enzymatic treatments [6]. Prior to decellularization, cauterized tissue and large blood vessels were removed and discarded. The remaining adipose tissue was then divided into 20-25 g

portions and transferred to 250 mL plastic containers. Tissue samples were submerged in series of decellularization solutions (100 mL working volume) supplemented with 1% (v/v) antibiotic/antimycotic solution (Invitrogen, Burlington, ON, Canada) and 0.27 mM phenylmethylsulfonylfluoride solution (protease inhibitor) according to table *3.1*. Unless stated otherwise, adipose tissue was decellularized under constant agitation (100 RPM) at 37°C using an Excella^{TM} 24 Benchtop Incubator (New Brunswick Scientific, Edison, NJ, USA).

First, Solution A (hypotonic tris-ethylenediaminetetraacetic acid (Tris-EDTA) solution at pH 8) was added to the plastic tubs containing adipose tissue. Samples were then frozen at -80°C and thawed under agitation at 37°C. Following the first freeze-thaw cycle, Solution A was replaced with fresh Solution A. Samples underwent an additional 2 freeze-thaw cycles and following the final freeze-thaw cycle, Solution A was replaced with 50 mL of Enzymatic Digestion Solution 1 (0.25% (m/v) Trypsin-EDTA (Life Technologies Inc., Burlington, ON, Canada) and incubated under agitation overnight.

The next day, Enzymatic Digestion Solution 1 was removed and lipids were extracted from adipose tissue over the next 48 hours using 99% isopropanol that was replaced every eight hours. Tissue was gently massaged during isopropanol replacement to enhance lipid extraction. On the fourth day, the tissue was rinsed 3 times (30 minutes each) in Sorenson's Phosphate Buffer (SPB) Rinsing Solution (8 g/L NaCl, 200 mg/L KCl, 1 g/L Na_2HPO_4, and 200 mg/L KH_2PO_4, at pH 8.0) before digesting samples with Enzymatic Digestion Solution 1 (0.25% Trypsin-EDTA, Gibco, Life Technologies) for 6

hours. Next, samples were rinsed 3 times (30 minutes each) using SPB Rinsing Solution before Enzymatic Digestion Solution 2 (55 mM Na_2HPO_4, 17 mM KH_2PO_4, 4.9 mM $MgSO_4 \cdot 7H_2O$, 15,000 U DNase Type II (from bovine pancreas), 12.5 mg RNase Type III A (from bovine pancreas), and 2000 Units Lipase Type VI-S (from porcine pancreas)) was added. Samples were incubated overnight and Enzymatic Digest Solution 2 was replaced with 99% isopropanol the following morning for the final 8-hour polar solvent extraction. After 8 hours, samples were rinsed three times (30 minutes each) with SPB Rinsing Solution and then stored in 70% ethanol at 4°C for future use.

Table 3.1: Adipose tissue decellularization protocol.

Day	Steps
1	• 3 freeze-thaw cycles in Solution A (Freezing Buffer Solution) • Enzymatic Digestion Solution 1
2	• Polar solvent extraction in 99% Isopropanol
3	• Polar solvent extraction in 99% Isopropanol
4	• Rinse 3 x 30 min in SPB Rinse (Rinsing Buffer Solution) • Enzymatic Digestion Solution 1 for 6 h • Rinse 3 x 30 min in SPB Rinse (Rinsing Buffer Solution) • Enzymatic Digestion Solution 2
5	• Polar solvent extraction using 99% Isopropanol • Rinse 3 x 30 min in SPB Rinse (Rinsing Buffer Solution)

3.3 Obtaining Porcine Skin

Porcine skin was collected from Quinn's Meats located in Yarker, Canada. Upon arrival at the lab, porcine skin samples were wrapped in tin foil and stored frozen at -80°C for future use.

3.4 Porcine Dermis Isolation

Frozen porcine skin samples were thawed at 4°C for 24 hours prior to dermis isolation. Once the skin was thawed, subcutaneous adipose tissue was carefully removed using a razor blade and discarded. Samples were then subjected to a modified heat-shock protocol [87] to loosen bonds between the basement membrane and overlying epidermis. Briefly, porcine skin samples were cut to ~10 cm x 10 cm portions before being immersed in a 55°C water bath for 2 minutes. Porcine skin samples were then quickly transferred into a bath of ice-cold PBS for 3 minutes. In order to remove the epidermis from the dermis, a razor blade was used to carefully scrape away the epidermal layer and the isolated dermal tissue was placed in 70% ethanol and stored at 4°C prior to decellularization the following day.

3.5 Porcine Dermis Decellularization adopted from Reing *et al.* [88]

Previously isolated porcine dermal tissue was immersed in a series of decellularization solutions and agitated at room temperature using an Excella™ 24 Benchtop Incubator set to 300 RPM unless otherwise stated. Initially, dermal tissue was washed 3 times (30 minutes each) with deionized water prior to the addition of 0.25% (m/v) trypsin-EDTA solution (Life Technologies Inc., Burlington, ON, Canada). Samples were then agitated in trypsin-EDTA solution for 6 hours and then rinsed with deionized water 3 times (15 minutes each) before agitating dermal tissue in 70% ethanol for 10-12 hours. 70% ethanol was then replaced with 3% $H_2O_{2(aq)}$ for 15 minutes and washed twice (15 minutes each) with deionized water. Samples were then placed in Triton X-100

solution (1% Triton X-100 in 0.26% EDTA/0.69% Tris) for 6 hours, and then again overnight.

The following day, dermal tissue was washed 3 times in deionized water (15 minutes each) before being placed into 0.1% (v/v) peracetic acid/4% (v/v) ethanol solution for 2 hours. Samples were then rinsed twice in PBS (15 minutes each) and then twice in deionized water (15 minutes each) before being stored in 70% ethanol at 4°C until future use.

3.6 Homogenization and Sterilization of Decellularized Human Adipose Tissue and Decellularized Porcine Dermal Tissue

DAT and decellularized dermal tissue (DDT) were rinsed in PBS 3 times (10 minutes each) under agitation at room temperature. After the final rinse, DAT and DDT were frozen at -20°C overnight in a 50 mL centrifuge tube and then lyophilized for at least 48 hours.

Samples were retrieved from the lyophilizer and then minced into small fragments (~0.2 cm^3). Minced DAT and DDT were collected in a glass vial and stored in a desiccator for future use. A fraction of minced DAT was further processed into a fine powder using a ball mill homogenizer (Mikro-Dismembrator Homogenizer by Sartorius Canada Inc., Mississauga, Canada). Briefly, 75-100 mg minced DAT was loaded into a stainless steel milling chamber with 4 small (1 mm) and 1 large (4 mm) stainless steel milling balls. The milling chamber was immersed in liquid nitrogen for 3 minutes before

being loaded into the ball mill homogenizer. DAT was milled at 2550 RPM for 3 minutes, collected in a glass vial, and stored in a desiccator for future use.

Minced or milled tissue was processed to form a homogenous suspension using established methods in the Flynn lab [11], adapted from the previous approach described by Steven F.S. (1964). Briefly, 350-1040 mg of minced/milled tissue was loaded into a 50 mL centrifuge tube and rinsed with 0.22M $NaH_2PO_{4(aq)}$ under agitation at room temperature for 10 minutes. Minced/milled tissue was then centrifuged at 1500 xg for 10 minutes. The supernatant was discarded and the pellet was resuspended in fresh 0.22M $NaH_2PO_{4(aq)}$ to achieve a concentration of 35 mg/mL based on the original dry mass of the minced or milled tissue. 1% (m/m) α-amylase was added. Tissue was allowed to digest under agitation at room temperature for 72 hours.

Following digestion, minced/milled tissue was centrifuged at 1500 xg for 10 minutes and the supernatant was discarded. The pellet was resuspended in 5% (m/v) $NaCl_{(aq)}$ and agitated for 10 minutes at room temperature before being centrifuged again. Pellets were resuspended in distilled water, agitated at room temperature for 10 minutes and centrifuged at 1500 xg for 10 minutes. Pellets were rinsed in distilled water once more before adding an appropriate volume of 0.2 M acetic acid. Minced DAT and DDT were resuspended in a volume of acetic acid sufficient to yield a concentration of 50 mg/mL based on the starting dry mass; and milled DAT was resuspended in a volume of acetic acid sufficient to yield a concentration of 75 mg/mL. Centrifuge tubes were then agitated at 100 RPM in 37°C for 24 hours before being homogenized using a

PowerGen™ Model 125 Homogenizer (Fisher Scientific, Ottawa, Canada). Centrifuge tubes were intermittently cooled in an ice water bath during homogenization to avoid protein denaturation. After homogenization, centrifuge tubes were again agitated at 100 RPM for another 24 hours at 37°C. Minced and milled DAT suspensions (DATsol), and minced DDT suspensions (DDTsol) were collected and stored at 4°C.

DATsol and DDTsol were chloroform-sterilized according to methods outlined in an established protocol [89]. DATsol or DDTsol was placed into Spectra/Por® Membrane Dialysis tubing (132628, SpectrumLabs, Rancho Dominguez, CA, USA) and then immersed in a 1% (v/v) chloroform solution in a chemical fume hood. Dialysis bags were stirred in chloroform solution overnight and the next morning, sterilized DATsol and DDTsol was aseptically transferred into a beaker containing 0.2 M acetic acid in a biological safety cabinet (BSC). DATsol and DDTsol were equilibrated over the next 6 days in acetic acid solution, which was replaced every 48 hours. Finally, sterilized DATsol and DDTsol were placed into sterile 50 mL centrifuge tubes and stored at 4°C for future use.

3.7 Fabrication of DAT Foams and DDT Foams

DATsol and DDTsol were diluted to desired concentrations using sterile distilled water before loading 500 μL of diluted DATsol/DDTsol into 1cm x 1 cm x 0.5 cm cryomolds (Sakura Finetek, Torrance, CA, USA). Each cryomold was suspended in a well of a 24-well plate and the lid was closed before freezing samples at -20°C overnight.

The next day, samples were lyophilized for at least 24 hours and foams were aseptically removed for future use.

3.8 ASC Isolation and Culture

Adipose tissue was transported to the lab within 2 hours of harvesting and all work was carried out within a BSC unless otherwise stated. Cell isolation was performed according to a published protocol [90]. Upon arrival, adipose tissue was inspected and large blood vessels and cauterized tissue were excised and discarded. The adipose tissue was then minced to increase surface area before being transferred into a 50 mL centrifuge tube containing 25 mL of sterile-filtered digest solution (3 mM glucose, 2 mg/mL collagenase type I (Worthington Biochemical Corporation, Lakewood, NJ, USA), and 5 mM HEPES in Kreb's Ringer Bicarbonate Buffer (KRB) solution) supplemented with 1.4 mL of 35% BSA. Tissue was placed in an Excella^{TM} 24 Benchtop Incubator (New Brunswick Scientific, Edison, NJ, USA) set to 100 RPM and 37°C for 45 minutes.

Digested tissue was passed through a 250 μm pore size stainless steel filter to remove undigested fragments and then allowed to stand for 5 minutes as mature adipocytes rose to the top. The adipocyte layer was aspirated and an equal volume of complete culture medium (Dulbecco's Modified Eagle's Medium (DMEM): Ham's F-12, 10% (v/v) fetal bovine serum (FBS) and 1% (m/v) pen-strep (100 U/mL penicillin and 0.1 mg/mL streptomycin)) was added to deactivate the collagenase. Cells were centrifuged at 1200 xg for 5 minutes, supernatant was aspirated, and the pellet was resuspended in 20 mL of erythrocyte lysing buffer (0.154 M ammonium chloride, 10 mM

potassium bicarbonate, and 0.1 mM EDTA in sterile deionized water). The cell suspension was then gently agitated at room temperature for 10 minutes before again centrifuging at 1200 xg for 5 minutes. Supernatant was aspirated and the pellet was resuspended in 20 mL complete culture medium and passed through a 100 μm pore size nylon mesh filter (Corning Life Sciences Plastic, Tewksbury, MA, USA) to remove any remaining debris. Filtrate was again pelleted, supernatant was aspirated, and the cell pellet containing ASCs was resuspended in an appropriate volume of complete culture medium. Cell suspension was divided into 1-3 T-175 culture flasks (Corning Life Sciences Plastic, Tewksbury, MA, USA) and flasks were topped up to 50 mL using complete culture medium before being transferred into incubators set to 37°C with 5% CO_2. Cells were allowed to adhere to the bottom of flasks for 24 hours and then non-adherent cells/debris were removed by rinsing with PBS. Flasks were labeled "P0", 50 mL of fresh complete culture medium was added to each flask, and then flasks were placed back into incubators. Complete culture medium was replaced every 2-3 days until cells became ~80% confluent.

Once cells reached ~80% confluence, they were detached using 0.25% trypsin/0.1% EDTA (Gibco®, Invitrogen, Burlington, ON, Canada) and divided into 2-4 new T-175 flasks. Cells were expanded to passage 2-3 for all experiments unless otherwise stated.

3.9 DAT Foam Characterization Studies

3.9.1 Stereomicroscope Images of and Scanning Electron Micrographs

Minced and milled DAT foams were fabricated over a range of concentrations: milled foams were fabricated using 10, 15, 25, 50, and 75 mg/mL DATsol; while minced foams were fabricated using 10, 25 and 50 mg/mL DATsol. After foams were produced, the outer surfaces were imaged using a stereomicroscope.

In addition, cross-sections of DAT foams were visualized using a scanning electron microscope (SEM). To prepare for SEM, freeze-dried DAT foams were immersed in liquid nitrogen for approximately 1 minute to make them brittle before a razor was carefully used to fracture the foams to reveal cross-sections. To remove residual condensation, DAT foams were frozen overnight at -20°C and then lyophilized for 24 hours. DAT foams were then mounted, pulse coated with gold, and visualized with a JOEL JSM-840 microscope using an accelerating voltage of 10 kV and a working distance of 15 mm.

3.9.2 Immunofluorescence Microscopy

Minced and milled DAT foams were fabricated and cut using a razor blade to reveal cross-sections. DAT foams were then submersed in 100% ethanol and agitated at room temperature for 10 minutes. Samples were then rinsed with PBS 3 times (30 minutes each) under agitation at room temperature. After the final rinse, DAT foams were fixed overnight at 4°C using 4% paraformaldehyde solution (PFA). The next morning, PFA was replaced with 70% ethanol and then embedded in paraffin. Paraffin-embedded samples were cut into 6 μm sections using a Shandon™ Finesse™ ME+

microtome (Thermo Scientific) and then de-waxed using xylene and rehydrated through a series of ethanol solutions.

De-waxed and rehydrated sections were subjected to various antigen retrieval protocols according to Table 3.2. Sections subjected to enzymatic antigen retrieval using trypsin (10 mL of 0.25% Trypsin-EDTA, 35 mL deionized water, and 5 mL 1% $CaCl_{2\,(aq)}$) were incubated at 37°C for 20 minutes. Sections subjected to enzymatic antigen retrieval using proteinase K (20 µg/mL proteinase K (iNtRON Biotechnology, Korea) in Tris-EDTA buffer) were incubated at 37°C for 20 minutes. Finally, all sections subjected to heat-mediated antigen retrieval were immersed in Dako Target Retrieval solution (DAKO Canada Inc. Burlington, Canada) and incubated just below 100°C for 30 minutes.

Following antigen retrieval, sections were rinsed 3 times with PBS (5 minutes each) before primary antibody solution (diluted in 0.2% (v/v) TWEEN 20 in PBS (PBST)) was added according to Table 3.2. Sections were incubated in primary antibody solution overnight in a humidity chamber at room temperature. The next morning, primary antibody was aspirated and sections were rinsed again in PBS (3 x 5 minutes) before diluted secondary antibody solution was added according to Table 3.2. The samples were incubated in secondary antibody solutions for 1 hour in a humidity chamber protected from light. Sections were then rinsed in PBS (3 x 5 minutes) before fluoroshield mounting medium with DAPI (Abcam, Toronto, Canada) was used to bond

coverslips to the microscope slides. Slides were protected from light and air-dried prior to imaging using fluorescence microscopy.

Table 3.2: Immunostaining antigen retrieval protocols and antibodies used for several targets in unseeded DAT foams.

Target	Antigen Retrieval	Primary Antibody	Secondary Antibody
Collagen 1	Enzymatic (trypsin)	1:100 Monoclonal Mouse Anti-Collagen 1 (ab90935, Abcam Toronto, Canada)	1:200 Alexa Fluor® 555 Goat Anti-Mouse (A-21422, Life Technologies Burlington, Canada)
Collagen 4	Dako Target Retrieval	1:500 Polyclonal Rabbit Anti-Collagen 4 (ab6586, Abcam Toronto, Canada)	1:500 Alexa Fluor® 488 Goat Anti-Rabbit (A-11008, Life Technologies Burlington, Canada)
Fibronectin	Enzymatic (proteinase K)	1:100 Monoclonal Mouse Anti-Fibronectin (ab6328, Abcam Toronto, Canada)	1:200 Alexa Fluor® 555 Goat Anti-Mouse (A-21422, Life Technologies Burlington, Canada)
Laminin	Dako Target Retrieval	1:25 Polyclonal Rabbit Anti-Laminin (ab11575, Abcam Toronto, Canada)	1:50 Alexa Fluor® 488 Goat Anti-Rabbit (A-11008, Life Technologies Burlington, Canada)

3.9.3 Porosity and Equilibrium Water Content of DAT Foams

Minced and milled DAT foams were fabricated at range of concentrations and used to quantify porosity based on a technique similar to the liquid displacement method [91]. For each fabrication method (minced vs. milled), a total of 3 foams were measured

at a given concentration (n = 3). Immediately after lyophilization, foams were weighed ($m_{dry\ foam}$) and then immersed in 100% isopropanol. To remove air bubbles, foams were placed into an ultrasonic cleaner (Cole-Parmer, Montreal, Canada) and pulsed 4 times (15 seconds each) with intermittent breaks (15 seconds each). Foams were then placed under vacuum for 30 minutes before 2 more cycles of pulsing in the sonic bath. Foams were placed under vacuum for another 30 minutes before blotting away excess isopropanol around the foams. Isopropanol-saturated DAT foams were then weighed ($m_{saturated\ foam}$). The following equation was used to calculate porosity:

$$Porosity\ [\%] = \left(\frac{V_{isopropanol}}{V_{total}}\right)\ x\ 100\%$$

$$V_{total} = V_{foam} + V_{isopropanol}$$

$$V_{foam} = \frac{m_{saturated\ foam}}{\rho_{DAT}}$$

$$V_{isopropanol} = \frac{(m_{saturated\ foam} - m_{dry\ foam})}{\rho_{isopropanol}}$$

The density of DAT (ρ_{DAT}) was assumed to be equal to the density of collagen, which was reported in the literature to be 1.343 g/cm^3 [92].

After isopropanol-saturated foams were weighed, foams were then rinsed using distilled water under agitation at room temperature 3 times (30 minutes each). After the last rinse, fresh distilled water was added to the foams and they were allowed to

equilibrate over 72 hours at 37°C. Following equilibration, excess water was carefully blotted from hydrated DAT foams and they were weighed ($m_{hydrated\ foam}$). The following equation was used to calculate equilibrium water (EWC) content:

$$Equilibrium\ Water\ Content\ [\%] = (\frac{m_{hydrated\ foam} - m_{dry\ foam}}{m_{hydrated\ foam}})\ x\ 100\%$$

3.9.4 Swelling Ratio and Protein Release of DAT Foams

Minced and milled DAT foams were fabricated over a range of concentrations. Milled foams were made using 10-75 mg/mL DATsol, while minced foams were produced using 10-50 mg/mL DATsol, with 3 foams fabricated per group (n = 3). DAT foams were imaged immediately after being lyophilized using a stereomicroscope and then submersed in 100% ethanol under agitation at room temperature for 10 minutes. Foams were then rinsed with Ringer's buffer solution (8.6 mg/mL NaCl, 0.3 mg/mL KCl and 0.33mg/mL $CaCl_2$) 3 times for 30 minutes each under agitation at room temperature. After the final rinse, 3 mL of fresh Ringer's buffer solution was added and vacuum was applied to scaffolds for 30 minutes to remove air bubbles. Foams were then equilibrated for 72h in 37°C before images were taken of hydrated foams. Images were imported into ImageJ (National Institutes of Health, USA) and surface areas of dry foams ($A_{dry\ foam}$) and hydrated foams ($A_{hydrated\ foam}$) were measured. Swelling ratios were calculated using the equation below:

$$Swelling\ [\%] = \left(\frac{A_{dry\ foam}}{A_{hydrated\ foam}}\right)\ x\ 100\%$$

After images were taken, the buffer solution was collected and frozen at -20°C. Each foam was submerged in 3 mL of fresh Ringer's buffer solution and then incubated at 37°C for another 4 days. After 4 days, the buffer solution was collected and frozen (day 7), replaced with 3 mL of fresh Ringer's buffer solution, and incubated for another 7 days at 37°C. On day 14, Ringer's buffer solution was collected and frozen.

In order to measure the amount of protein (primarily comprised of structural collagens) released from the DAT foams, a modified Lowry assay was performed on the Ringer's buffer solutions collected after 72 hours, 7 days, and 14 days. The protocol is outlined in Komsa-Penkova *et al.* (1996). Briefly, standard solutions were produced using milled DATsol diluted in Ringer's buffer solution to a stock concentration of 2 mg/mL. A standard dilution series was made from this stock solution by further diluting with Ringer's buffer solution. 40 µL of each sample (either standards or Ringer's buffer solution collected from DAT foams) was then incubated at 50°C for 20 minutes with 36 µL of Reagent A (0.4% (m/v) potassium-sodium tartrate, 10% (m/v) Na_2CO_3 and 0.5 M NaOH (Fischer Scientific, Ottawa, Canada) in deionized water). Samples were cooled to room temperature before adding 4 µL of Reagent B (2% (m/v) potassium-sodium tartrate, 3% (m/v) $CuSO_4 \cdot 5\ H_2O$, and 0.1 M NaOH in deionized water) and incubating at room temperature for 10 minutes. 120 µL of 0.15 M Folin-Coicalteu reagent (Millipore, Etobicoke, Canada) was added to samples and incubated for 10 minutes at 50°C before

cooling to room temperature. The absorbance (650 nm) of each sample was measured and protein release concentrations were calculated.

3.10 DAT Foam Cell-Seeding Studies

In all seeding studies, the ViaCount assay (Millipore, Etobicoke, Canada) was employed to quantify cell number and cell viability according to the manufacturer's instructions using a Guava EasyCyte 8HT flow cytometer (Millipore, Etobicoke, Canada). Moreover, DATsol and DDTsol used in cell-seeding studies were chloroform sterilized using the methods outlined previously unless otherwise stated. All work involving ASCs was performed aseptically within a BSC.

3.10.1 Chloroform Sterilization Cytotoxicity Study

DATsol was sterilized using established chloroform sterilization procedures [93]. Briefly, DATsol was transferred into a glass container and 100% chloroform was carefully layered below the homogenized tissue before capping the container and storing it overnight at 4°C. The volume of chloroform added was ~ 10% of the total volume of DATsol loaded into the container. The next morning, DATsol was aseptically transferred into a centrifuge tube ensuring that the residual underlying chloroform layer was not disturbed.

Chloroform-sterilized DATsol was then used to make foams at a concentration of 50 mg/mL using methods previously described. Lyophilized foams were then immersed in 100% ethanol and agitated for 10 minutes at room temperature. Foams were then

agitated in PBS twice for 10 minutes before equilibrating foams at 37°C overnight in complete culture medium without antibiotic supplementation.

ASCs were seeded onto the bottom of 12-well cell culture plates and allowed to adhere and equilibrate in complete media without antibiotic supplementation for 24 hours before rinsing each well with PBS to remove non-adherent cells and debris. Wells were then topped up to 3 mL with complete culture medium (antibiotic-free).

Equilibrated foams were aseptically placed into 12-well inserts (Greiner Bio-One, North Carolina, USA). 1 mL of complete medium (antibiotic-free) was added to each insert before being suspended into wells of the 12-well plate containing the pre-plated ASCs. Overall, there were 4 conditions included in this experiment: ASCs were seeded at a density of either 10,000 cells/cm^2 or 30,000 cells/cm^2; and cultured either with or without chloroform-sterilized DAT foams. Chloroform-sterilized foams were cultured with ASCs for 72 hours before quantifying cell number and cell viability with the ViaCount assay.

3.10.2 Cell-Seeding Methods Pilot Study

In an effort to increase cell infiltration into the DAT foams, 3 cell-seeding protocols: i) static hydrated seeding, ii) static dry seeding, and iii) orbital shaker hydrated seeding were investigated using triplicate DAT foams (n = 3) at a concentration of 35 mg/mL. After the DAT foams were lyophilized, groups i) and iii) were immersed in 100% ethanol and agitated at room temperature for 10 minutes before being rinsed twice

in PBS for 10 minutes each. Rinsed scaffolds were then immersed in complete culture medium and allowed to equilibrate overnight at 37°C.

The next day, scaffolds were seeded with ASCs using the 3 protocols. Cell-seeding protocols i) and ii) involved statically drip seeding either dry or complete culture medium-equilibrated DAT foams using 350 µL of cell suspension containing a total of 1 x 10^6 ASCs. Briefly, DAT foams were placed into 12-well plate inserts (Greiner Bio-One, North Carolina, USA) and then inserts were suspended into wells of a 12-well plate. Cell suspension was then slowly dripped over the DAT foams and then inserts were topped up with 150 µL of complete culture medium, while underlying wells were topped up with 3 mL of complete culture medium. Cell suspensions were incubated with DAT foams for 24 hours before seeded DAT foams were removed from the inserts and placed into the underlying wells and incubated for 7 days at 37°C and 5% CO_2.

The final group of complete culture medium-equilibrated DAT foams was seeded using an orbital shaker. The orbital shaker was used to allow cell suspension to perfuse DAT foams and this method was selected based on the findings in two other studies ([44], [46]. Briefly, all 3 foams were placed in a 50 mL centrifuge tube containing a total of 3 x 10^6 ASCs and suspended in 21 mL of complete culture medium. The centrifuge tubes were placed in an Excella^{TM} 24 Benchtop Incubator (New Brunswick Scientific, Edison, NJ, USA) set to 60 RPM at 37°C for 20 hours. Seeded foams were then removed from the centrifuge tubes, placed in 12-well plates containing 3 mL of fresh complete culture medium, and incubated for 7 days at 37°C and 5% CO_2.

After 7 days of culture, all 3 groups of ASC-seeded foams were fixed using 4% PFA overnight at 4°C. Then foams were cut using a razor blade to expose cross-sections, paraffin embedded, and sectioned using a microtome to a thickness of 6 μm. Sections were de-waxed using xylene and then rehydrated through a series of ethanol solutions before performing a Masson's trichrome stain by following the manufacturer's instructions (HT15, Sigma-Aldrich, Oakville, Canada). Stained sections were visualized and imaged under a microscope to visualize cell infiltration resulting from the 3 cell-seeding protocols.

3.10.3 Orbital Shaker Cell-Seeding Pilot Study

In order to determine which DAT foam fabrication method (minced vs. milled) was the most permissive to cell infiltration using the orbital shaker cell-seeding protocol, minced and milled foams were fashioned at "low" (minced and milled = 20 mg/mL) and "high" (milled = 50 mg/mL; minced = 40 mg/mL) concentrations. Triplicate foams at each concentration and fabrication method were produced (n = 3). After being lyophilized, foams were immersed in 100% ethanol and agitated at room temperature for 10 minutes before rinsing twice with PBS under agitation at room temperature for 10 minutes. DAT foams were then equilibrated in complete culture medium overnight at 37°C.

The next day, each group of three DAT foams was placed into a 50 mL centrifuge tube containing 3×10^6 ASCs in 21 mL complete culture medium. Centrifuge tubes were loaded into an orbital shaker set to 60 RPM at 37°C for 20 hours. After seeding, foams

were placed into 12-well plates and wells were toped up with 3 mL of complete culture medium. Foams were incubated at 37°C and 5% CO_2 for 7 days before fixing samples with 4% PFA overnight at 4°C. Foams were then cut using a razor blade to expose cross-sections, paraffin embedded, and sectioned using a microtome to a thickness of 6 μm. To visualize ASCs in the foams, sections were stained using fluoroshield mounting medium with DAPI (Abcam, Toronto, Canada) and then imaged using fluorescence microscopy. Cell infiltration was assessed in each group.

3.10.4 DAT Foam Contraction Study

Minced and milled foams were fabricated over a range of concentrations. each group consisted of 3 foams (n = 3). DAT foams were immersed in 100% ethanol and agitated for 10 minutes before rinsing twice in PBS under agitation for 10 minutes each. Foams were then equilibrated in complete culture medium overnight at 37°C. Each group of 3 foams was placed in a 50 mL centrifuge tube containing 3 x 10^6 ASCs in 21 mL of complete culture medium. Centrifuge tubes were then loaded into an orbital shaker set to 60 RPM at 37°C for 20 hours. Seeded foams were placed into 12-well plates, 3 mL of complete culture medium was added to each well, and the foams were immediately imaged using a stereomicroscope. After imaging, foams were incubated at 37°C and 5% CO_2 over a period of 28 days with complete culture medium changes every 2-3 days. Foams were imaged at timepoints of 0 days, 4 days, 7 days, 14 days, and 28 days, and surface areas were measured using ImageJ.

3.10.5 Orbital Shaker Cell-Seeding Optimization

To further enhance ASC infiltration into milled DAT foams using the orbital shaker cell-seeding protocol, the effects of DAT foam concentration, orbital shaker RPM, and cell suspension concentration were investigated. Each group consisted of 3 foams (n = 3). Milled foams were fabricated at three concentrations (15 mg/mL, 25 mg/mL or 50 mg/mL), and immersed in 100% ethanol and agitated for 10 minutes before rinsing twice in PBS under agitation for 10 minutes. Foams were then equilibrated in complete culture medium overnight at 37°C. Each group of 3 foams was placed into a 50 mL centrifuge tube containing either 3×10^6 ASCs or 1.5×10^6 ASCs in 21 mL complete culture medium. Centrifuge tubes were then loaded into an orbital shaker set to either 60 or 120 RPM at 37°C for 20 hours. Seeded foams were placed into 12-well plates and 3 mL of complete culture medium was added to each well. Foams were incubated at 37°C and 5% CO_2 for 72 hours. One set of seeded foams was used to assess total double stranded deoxyribonucleic acid (dsDNA) content and another set of seeded foams was used for histological studies.

In order to quantify dsDNA, foams were rinsed 3 times in PBS (10 minutes each) under agitation at room temperature. Each foam was placed into a 15 mL centrifuge tube containing 5 mL of collagenase digest solution (same digest solution used for ASC isolation) and agitated at 37°C and 100 RPM for 30 minutes. Partially digested foams were carefully pipetted up and down to enhance digestion and then agitated for another 30 minutes at 100 RPM at 37°C. An equal volume of complete culture medium was

added to inactivate the collagenase and then cells/scaffold debris was centrifuged at 1200 xg for 5 minutes. Supernatant was then aspirated and pellets were resuspended in 2 mL of Tris-EDTA (TE) buffer (Fischer Scientific, Ottawa, Canada). Cells were lysed with a sonic dismembrator (Model-100, Fisher Scientific, Toronto, Canada) (3 pulses of 10 seconds with intermittent cooling on ice). To remove cellular debris, samples were centrifuged at 12,000 xg for 5 minutes and then supernatant containing dsDNA was collected and analyzed using a Quant-iT™ PicoGreen® dsDNA Assay (Life Technologies Inc., Burlington, ON, Canada) according to the manufacturer's instructions.

To process cells for histology, foams were fixed in 4% PFA overnight at 4°C. Next, foams were cut using a razor blade to expose the cross-section, paraffin embedded, and sectioned using a microtome to a thickness of 6 μm. Sections were then de-waxed using xylene and rehydrated through a series of ethanol solutions. Sections were incubated in Dako Target Retrieval solution for 30 minutes just below 100°C. Sections were then rinsed 3 times (5 minutes each) in PBS and primary antibody diluted with PBST was added according to Table 3.8. Primary antibody solution was incubated overnight at room temperature in a humidity chamber and then washed 3 times with PBS (5 minutes each) before diluted secondary antibody solution was added according to Table 3.8. Secondary antibody solution was incubated for 1 hour in a humidity chamber protected from light and then washed 3 times with PBS before mounting slides using fluoroshield mounting medium with DAPI (Abcam, Toronto, Canada).

Once dried, sections were imaged using using fluorescence microscopy (10 x magnification). Briefly, 2 cross-sections of each seeded foam were imaged and then digitally reassembled by manual stitching using Photoshop CS6 (Adobe, USA). Total cell density, "outer" cell density (defined as the cell density from the surface of the cross-section to a depth of 25% total cross-section length), and "inner" cell density (defined as the cell density excluding the "outer" areas of the cross-section) were calculated for each cross-section (Figure 3.2). Moreover, ASC proliferation was assessed in each seeded foam by quantifying cellular Ki67 expression. Briefly, 5 random, non-overlapping images (20 x magnification) of every foam were taken. In each of the 5 images, the number of cells expressing Ki67 was expressed relative to the total number of cells and then expressed as an average.

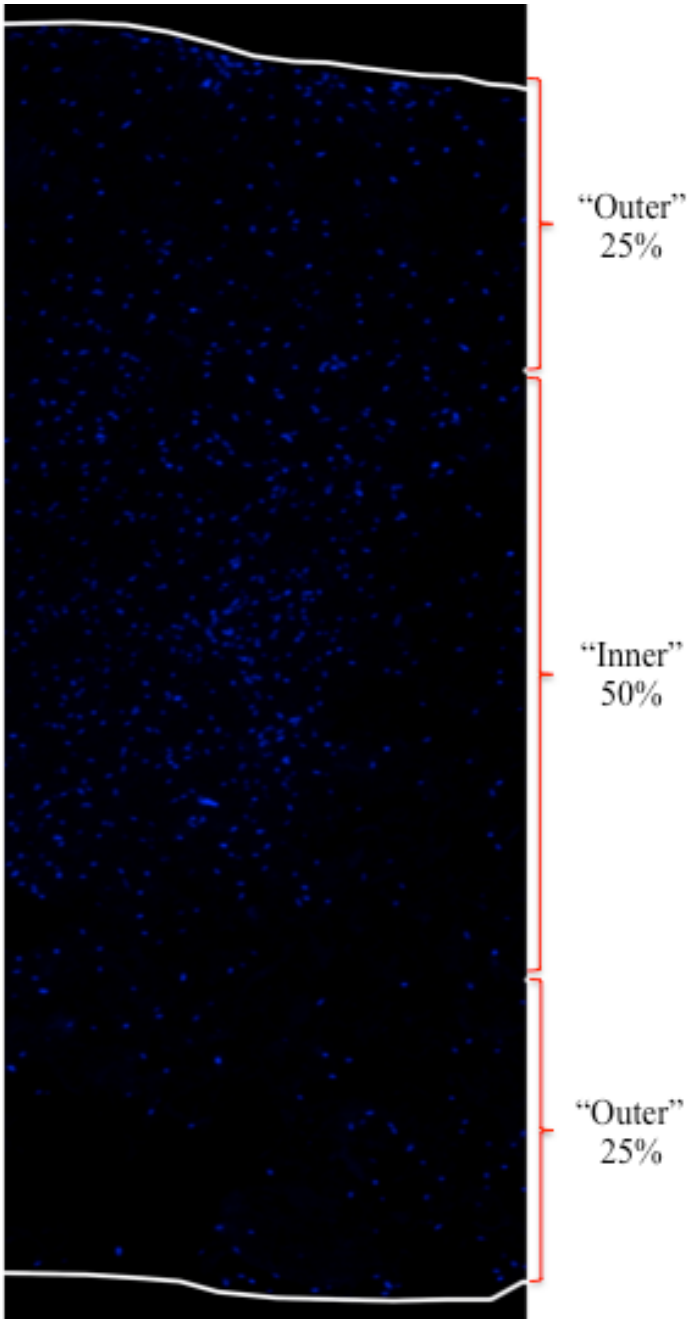

Figure 3.1: Representative cross-section of a seeded DAT foam highlighting the "inner" and "outer" regions in which cell densities were measured. White lines indicate the surfaces of the foam.

Table 3.3: Immunostaining antigen retrieval protocols and antibodies used for several targets in orbital shaker cell-seeded DAT foams.

Target	Antigen Retrieval	Primary Antibody	Secondary Antibody
Ki67	Dako Target Retrieval	1:100 Monoclonal Rabbit Anti-Ki67 (ab16667, Abcam Toronto, Canada)	1:250 Alexa Fluor® 488 Goat Anti-Rabbit (A-11008, Life Technologies Burlington, Canada)

3.11 ASC Gene Expression Study

Milled DAT foams (25 mg/mL) and DDT foams (25 mg/mL) were fabricated, immersed in 100% ethanol and agitated for 10 minutes before rinsing twice in PBS under agitation for 10 minutes. Foams were then equilibrated in complete culture medium overnight at 37°C. Each group of 3 foams was placed into a 50 mL centrifuge tube containing 1.5 x 10^6 ASCs in 21 mL complete culture medium. Centrifuge tubes were loaded into an orbital shaker set to 120 RPM at 37°C for 20h and then foams were moved into wells of a 12-well plate with 3 mL of complete culture media.

Collagen gels (PureCol®, Advanced BioMatrix, Poway, CA, USA) were also made in parallel according to the manufacturer's instructions. 5 x 10^5 ASCs were encapsulated within the gels before loading them into cryomolds (Sakura Finetek, Torrance, CA, USA). Gels were allowed to set for 2 hours at 37°C and then carefully transferred into a 12 well-plate containing 3 mL of complete culture media per well.

ASCs were also plated onto the bottom of 12-well plates at a density of 30,000 cells/cm^2 and served as controls.

Once cell-seeding was complete, all groups were allowed to equilibrate for 24 hours in complete culture media at 37°C. After 24 hours, complete culture media was replaced. An experimental subgroup was then transferred into a hypoxic subchamber system (Biospherix, Lacona, NY) with a ProOx 110 oxygen controller set to 1% O_2, while another subgroup was placed back into a normoxic incubator (21% O_2). Both groups were incubated for 48 hours at 37°C and 5% CO_2 before total ribonucleic acid (RNA) was extracted. Three samples were included for each experimental group in the study (n = 3).

TRIzol® Reagent (Life Technologies Inc., Burlington, ON, Canada) was used to extract RNA from the ASCs cultured on tissue culture poly(styrene) (TCPS), DAT foams, DDT foams, and collagen gels. After complete culture medium was aspirated, wells were rinsed with PBS under agitation at room temperature for 10 minutes. 1 mL of TRIzol® Reagent was added to each TCPS well, pipetted up and down, and then transferred into a 2 mL eppendorf tube. All foams and gels were transferred into a 2 mL eppendorf containing 1 mL TRIzol® Reagent and then homogenized by pulsing a sonic dismembrator (Model-100, Fisher Scientific, Toronto, Canada) (3 x 10 second pulses with intermittent cooling on ice). RNA was extracted using standard methods [6].

Before first strand cDNA synthesis, the concentration of RNA was determined using a Qubit® RNA Assay Kit in a Qubit® 2.0 Fluorometer (Life Technologies Inc.,

Burlington, ON, Canada) according to the manufacturer's instructions. RNA solutions were diluted appropriately using sterile DNAse-free water and up to 1 μg of RNA was loaded into each reaction. A reaction volume of 20 μL was used and included first-strand buffer (50 mM Tris-HCl, 75 mM KCl, 3 mM $MgCl_2$), 10 mM dithiothreitol (DTT), 0.09 OD_{260} units of random primers (Invitrogen, Burlington, ON, Canada), 0.5 mM of each dNTP (Invitrogen, Burlington, ON, Canada), and 200 units of SuperScript™ II RT (Invitrogen, Burlington, ON, Canada). Minus RT-controls were prepared for samples with over 1 μg yield of total RNA. cDNA was stored at -80°C until future use.

Quantitative real-time polymerase chain reaction (qRT-PCR) was used to assess ASC gene expression of VEGF-A and fibroblast growth factor-2 (FGF-2) transcripts using TaqMan® Gene Expression assays from Life Technologies (Burlington, ON, Canada). Briefly, using a 20 μL reaction volume and duplicate reactions per sample, 10 μL of TaqMan® Universal Master Mix II 2x (Life Technologies Inc., Burlington, ON, Canada), 9 μL cDNA solution, and 1 μL of TaqMan® Gene Expression Assay (Life Technologies Inc., Burlington, ON, Canada) was loaded into a 96-well plate and the reaction was carried out and monitored using a StepOnePlus™ Real-Time PCR System (Life Technologies Inc., Burlington, ON, Canada). Refer to Table 3.9 for assay information.

Once data was collected, the comparative C_T method was used to calculate relative gene expression of both FGF-2 and VEGF-A according to the manufacturer's instructions. Briefly, cycle threshold numbers (C_T) of targets (FGF-2 and VEGF-A) were

normalized to C_T values of the endogenous control (glyceraldehyde-3-phosphate dehydrogenase) (GAPDH). Then gene expression was calculated relative to a calibrator sample (TCPS cultured in normoxic conditions) and expressed as a fold change value.

Table 3.4: Assays used in qRT-PCR

Target	Accession #	TaqMan® Gene Expression Assay ID
FGF-2	NM_002006.4	Hs00266645_m1
GAPDH	NM_001256799, NM_002046	Hs03929097_g1
VEGF-A	NM_001025466-70, NM_001033756 NM_001171622-30 NM_001204384-5 NM_003376	Hs00900055_m1

3.12 Statistical Analysis

All data are expressed as means ± standard deviation of the mean. Statistical analyses were performed using the software program Prism 6 (GraphPad Software Inc., La Jolla, CA, USA). 2-way and 1-way ANOVAs with a Tukey's or Sidak's post-hoc test were used and all differences were considered statistically significant at $p < 0.05$.

Chapter 4

Results and Discussion

4.1 Characterization of DAT Foams

The DAT scaffold fabrication protocols yielded porous, tissue-derived foams suitable for investigation as a biomaterial for applications in wound healing and soft tissue regeneration (Figure 4.1). Comprised of a network of entangled collagen fibers and other ECM constituents, the DAT foams were soft, deformable, and stable following re-hydration without the need for chemical cross-linking. In fabricating these scaffolds, the effects of both DATsol concentration and tissue processing prior to homogenization (i.e.: mincing vs. milling) were assessed. The mass of decellularized tissue that could be homogenized to create a suspension depended upon whether DAT was minced or milled. More specifically, a larger mass of DAT could be homogenized using the milling protocol, likely associated with higher packing density of the more fragmented ECM fibers. Consequently, the stock concentration of the milled DATsol was higher than the stock concentration of the minced DATsol (75 mg/mL vs. 50 mg/mL, respectively). Since the described DAT processing methods (mincing vs. milling) may impact the bioactivity and architecture of DAT foams, scaffolds fabricated from these DATsol variants were characterized and compared.

To qualitatively assess the effects of DATsol concentration and DAT processing on the scaffold architecture, foams were fabricated over a range of concentrations using

both the mincing and milling processing protocols described in Chapter 3. After fabrication, foams were imaged using a stereomicroscope and a SEM (Figure 4.2). SEM micrographs revealed that both minced and milled DAT foams possessed a porous microarchitecture at all concentrations. Qualitatively, it appeared that increasing the DATsol concentration used to fabricate foams resulted in a denser network. This trend was also evident in images taken with the stereomicroscope. Moreover, a comparison of micrographs of minced vs. milled foams revealed differences in network structure - these differences were especially evident at low (10 mg/mL) and high (50 mg/mL) concentrations. For instance, 10 mg/mL milled DAT foams seemed to have discontinuous porous network (Figure 4.2), while 10 mg/mL minced foams had a well-defined, continuous porous network. Furthermore, 50 mg/mL minced foams possessed irregularities in the porous network that 50 mg/mL milled foams did not have (Figure 4.1). These differences may be attributed to the more inhomogeneous nature of the DAT suspension prepared using the mincing protocol, which would be expected to better preserve long ECM fibers and fiber bundles.

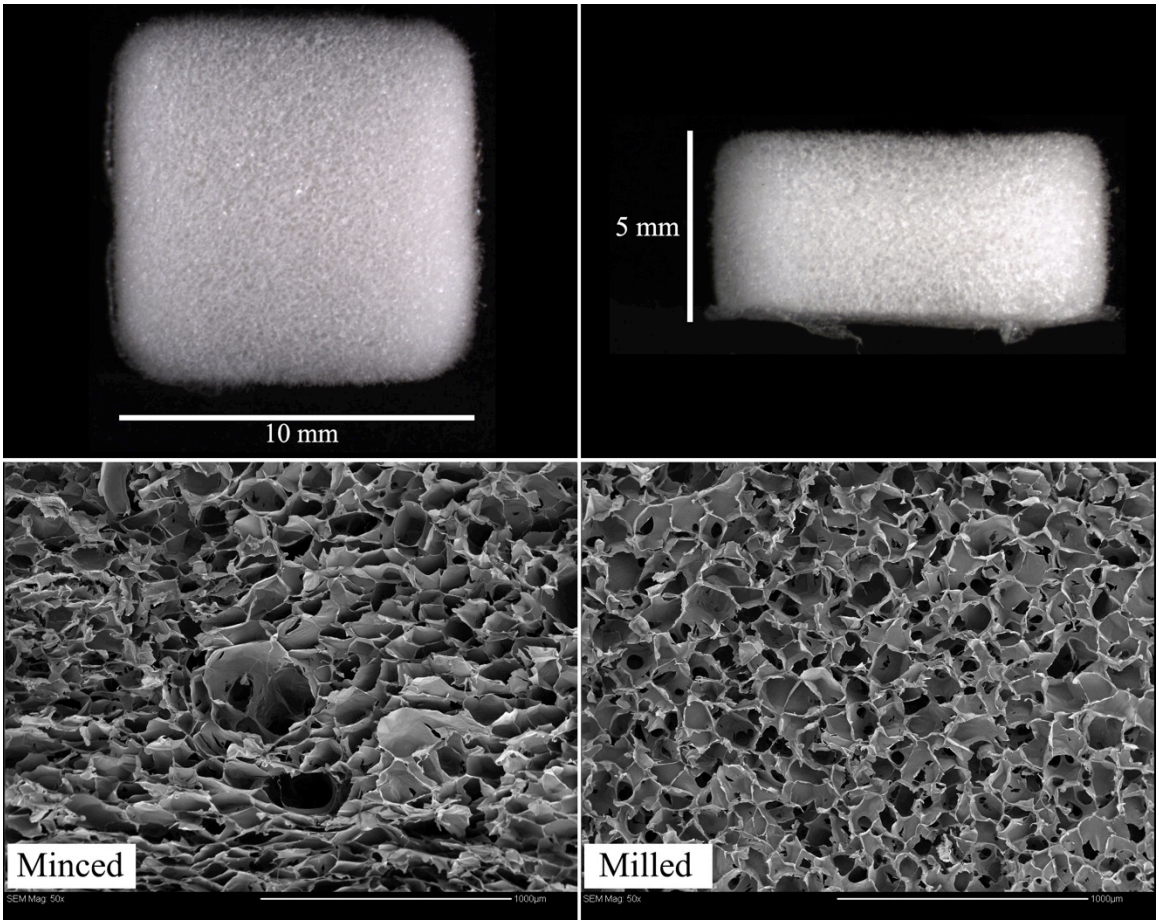

Figure 4.1: Representative images of a lyophilized DAT foam (top) and scanning electron micrographs of minced (50 mg/mL) and milled (50 mg/mL) DAT foam cross-sections (bottom, Scale bars represent 1 mm).

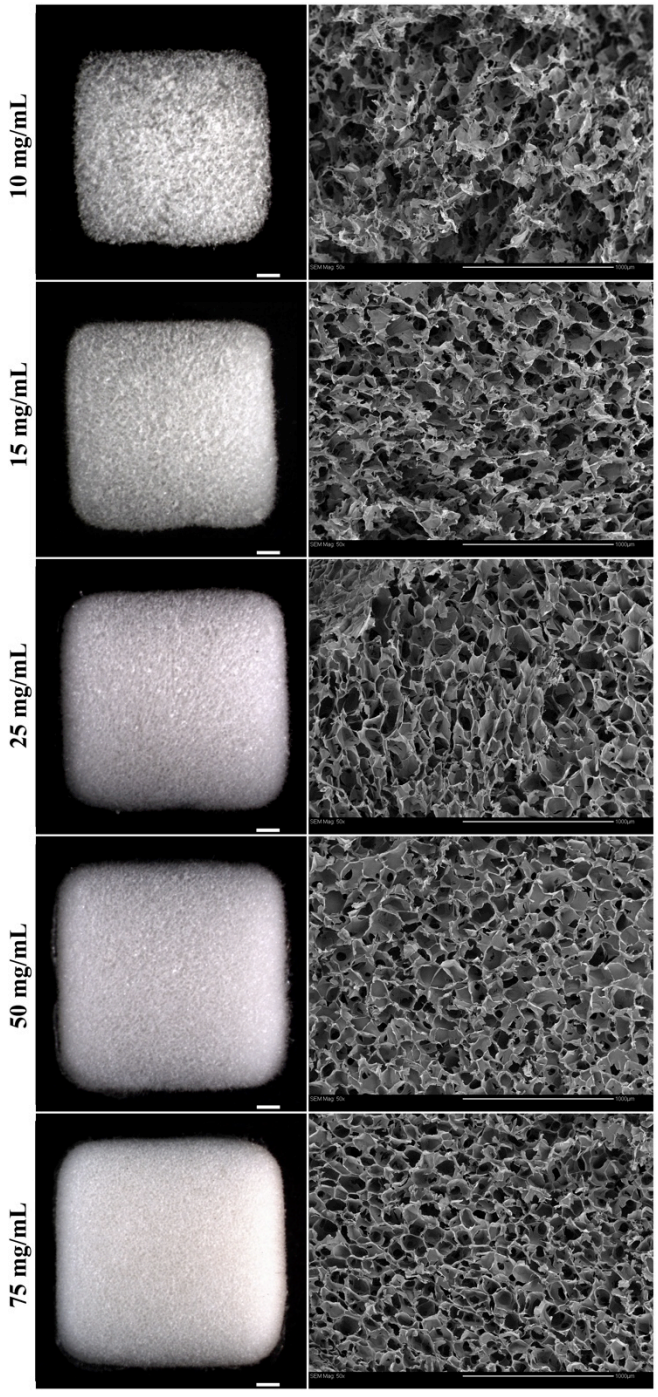

Figure 4.2: Stereomicroscope images of representative milled DAT foams (left, Scale bars represent 1 mm) and respective scanning electron micrographs of the associated foam cross-sections, showing internal structure (right, Scale bars represent 1 mm).

4.1.1 Porosity

To validate the observations made using SEM and stereomicroscope images, the porosity of the DAT foams was quantified (Figure 4.3). A variation of the liquid displacement method [91] was used to quantify porosity (see Chapter 3). In general, DAT foams were porous at all concentrations, with the least porous group possessing 96.4 ± 0.1% porosity and the most porous group possessing 99.3 ± 0.1% porosity. In agreement with the previous observations made, increasing DAT foam concentration generally resulted in a reduction in porosity (Figure 4.3).

Moreover, the data suggests that the DAT processing protocols (mincing vs. milling) did not statistically impact overall porosity with the exception of foams fabricated at lower concentrations (i.e.: 10 and 15 mg/mL). It is important to note that one reason for the statistical differences in porosity observed at these low concentrations may have resulted from the methodology used. For instance, prior to weighing isopropanol-saturated foams, "excess" isopropanol was gently blotted away. At low concentrations, the DAT foams are less rigid, as evidenced by an decreased Young's modulus in previous work [11], and it is possible that the scaffolds partially collapsed prior to blotting. This compressive force may have resulted in porosity values that were artificially low. Based on observation, minced DAT foams qualitatively appeared to be more rigid than milled DAT foams for a given concentration; the differences between the groups were more noticeable at low concentrations. As such, the milled foams may have been more prone to collapse than the minced DAT foams at the same concentration, and this could have

resulted in lower porosity measurements among milled foams, which was observed in the data at 10 mg/mL and 15 mg/mL concentrations.

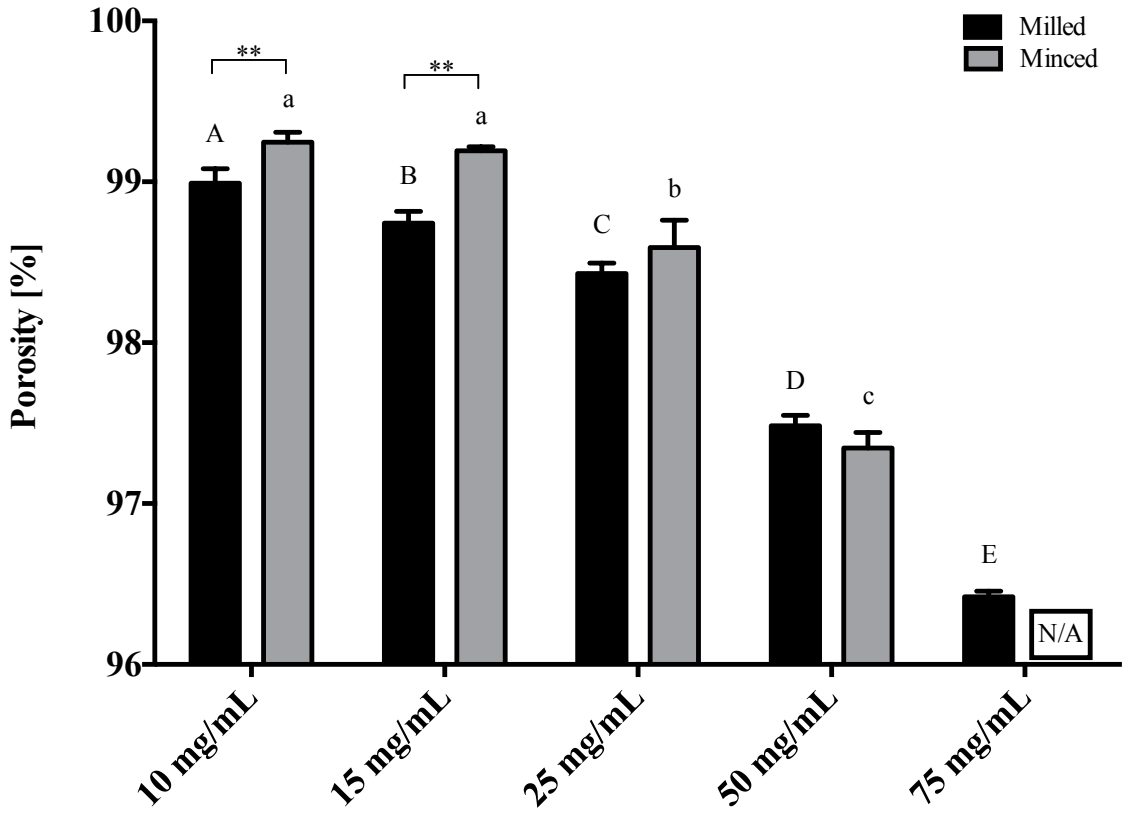

Figure 4.3: **Porosity of minced and milled DAT foams (n = 3).** A 2-way ANOVA with a Sidak's multiple comparisons post-hoc test was performed to compare means of identical foam concentrations, while a Tukey's multiple comparisons post-hoc test was performed to compare means of identical DAT foam fabrication method (i.e.: minced or milled). Means were considered to be statistically different if $p < 0.05$. At a given concentration, "**" was used to indicate a statistical difference between means. For a given DAT foam fabrication method, means were statistically different if they were assigned a unique letter (i.e.: means that are assigned "a" are statistically different from means that are assigned "b"). N/A = not applicable, Minced DAT foams were not fabricated at this concentration.

4.1.2 Equilibrium Water Content

As a potential biomaterial, it was important to characterize DAT foams in an aqueous environment. Therefore the EWC of minced and milled DAT foams was measured (Figure 4.4). In general, the scaffolds were hydrophilic as evidenced by their high EWC, with water content ranging from 96.3 ± 0.1% to 98.9 ± 0.1%. For minced foams, an increased foam concentration generally decreased the EWC. Although not statistically significant, the same general trend was found in the milled foams (with the exception of 15 mg/mL). This can be explained using the data obtained from the porosity measurements. Increasing the foam concentration reduced porosity, and therefore reduced potential space for water.

At each concentration, the minced DAT foams had a statistically greater EWC compared to the milled DAT foams. Similar to the methodology used to measure porosity, EWC was quantified by weighing liquid-saturated foams that had been blotted. If the milled foams were structurally weaker than the minced foams, the milled foams may have collapsed to a greater extent during rehydration and/or blotting, resulting in a reduction in the measured EWC.

Another contributing factor to the lower EWC measurements in the milled group may have arisen due to protein loss during the 3-day incubation period in water. As discussed previously, the network structure of the DAT foams was generated through physical cross-links formed during lyophilization. During scaffold formation, it is likely that there were protein fragments that were only loosely incorporated into the foam

network. Since the foams were incubated in water for 3 days, small protein fragments likely diffused out of the foams and into the surrounding water. If protein is lost during the incubation period, this might have also affected the EWC measurements. Due to the more disruptive nature of the processing conditions for preparing the milled foams, it is possible that there may have been more protein loss in that group.

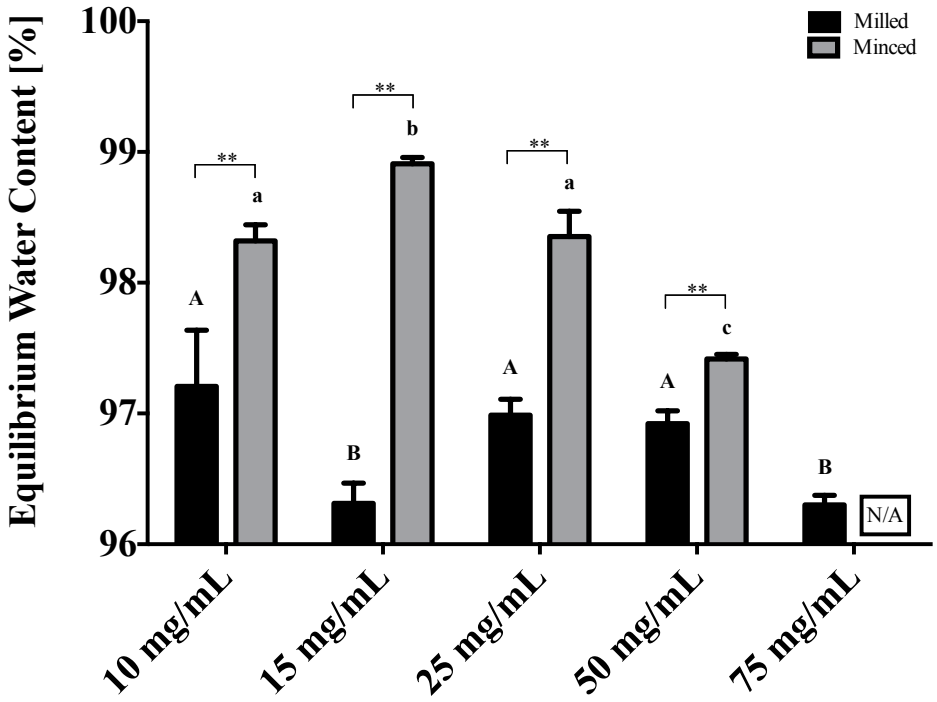

Figure 4.4: Equilibrium water content of minced and milled DAT foams after 72 hours of equilibration at 37°C (n = 3). A 2-way ANOVA with a Sidak's multiple comparisons post-hoc test was performed to compare means of identical foam concentration, while a Tukey's multiple comparisons post-hoc test was performed to compare means of identical DAT foam fabrication method (i.e.: minced or milled). Means were considered to be statistically different if $p < 0.05$. At a given concentration, "**" was used to indicate a statistical difference between means. For a given DAT foam fabrication method (i.e.: milled or minced) means were statistically different if they were assigned a unique letter (i.e.: means that are assigned "a" are statistically different from means that are assigned "b"). N/A = not applicable, Minced DAT foams were not fabricated at this concentration.

4.1.3 Protein Release

To further investigate the possibility of small protein fragments diffusing from the DAT foams into surrounding aqueous medium, a protein release study was conducted (Figure 4.5). DAT foams were immersed in Ringer's solution and incubated over a period of 14 days. Ringer's solution was collected and replaced after 3, 7 and 14 days. The concentration of protein was determined in each of the collected Ringer's solutions using a modified Lowry assay [94]. Since the modified Lowry assay detects the concentration of proteins including collagen, the loss of other components (i.e.: proteoglycans or other structural components) was not determined. In all groups, the amount of protein loss from the DAT foams was highest after the initial 3 days of incubation. This finding could be attributed to the rapid initial loss of the smaller and more loosely incorporated ECM fragments present in DAT foams, which gradually decreased over time. Presumably, the fragments closest to the surface of the foam would be lost more quickly relative to fragments located towards the interior of the foam. This would explain the initial protein "burst" at day 3. After day 3, less protein was released and this could be due to the fact that small ECM fragments in the interior of the foam were more entrapped in the scaffold network and released more gradually.

Moreover, minced DAT foams appeared to lose more protein than milled DAT foams at the same concentration. This is especially evident for foams fabricated using 50 mg/mL DATsol. Although not statistically significant, minced foams at concentrations below 50 mg/mL showed more protein loss than their milled counterparts.

A possible explanation for this observation is that the ECM fibers in the minced samples would be predicted to be larger in the minced samples than in the milled samples, so even if fewer ECM fibers were lost during the course of the study from the minced sample group, the total mass of protein released may have been greater.

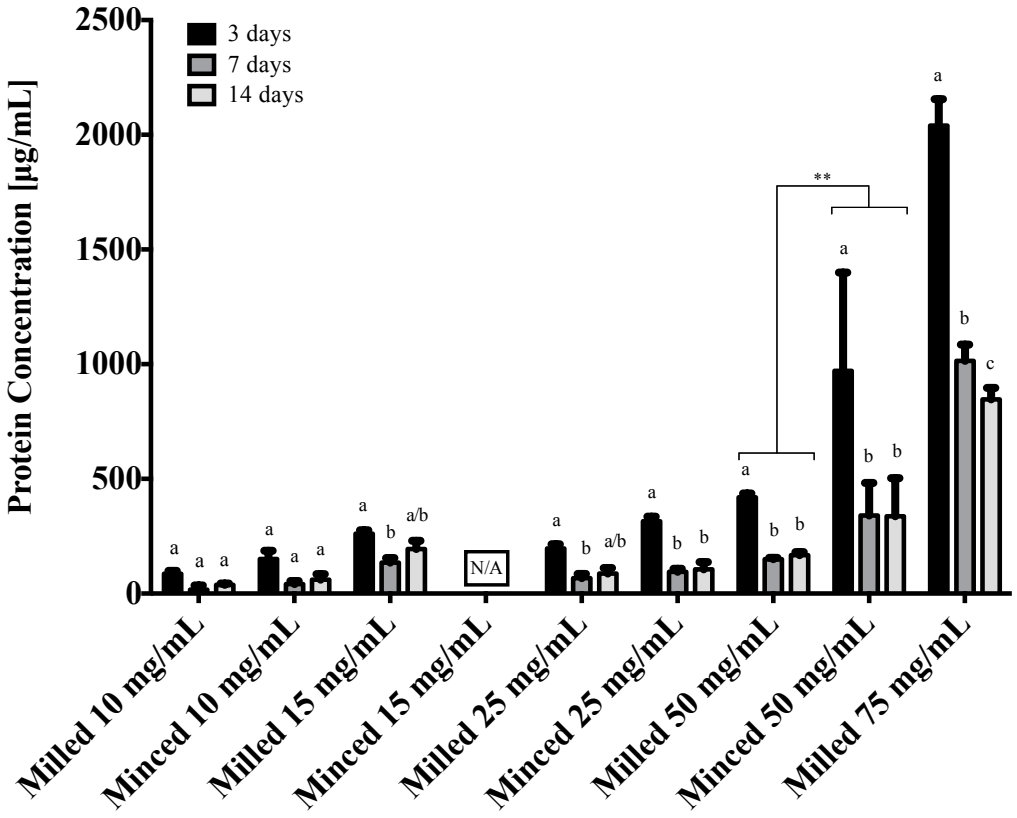

Figure 4.5: Protein release study of minced and milled DAT foams after 72 hours, 7 days and 14 days of incubation in ringer buffer solution (n = 3) at 37°C. A 2-way ANOVA with Tukey's multiple comparisons post-hoc test was performed to compare means. Means were considered to be statistically different if $p < 0.05$. Within each group, means are statistically different if they are assigned a unique letter (i.e.: means that are assigned "a" are statistically different from means that are assigned "b"; however, means that are assigned "a/b" are not statistically different than means that are assigned "b" or "a"). For a given concentration, statistical differences between means of milled and minced foams at the same timepoint were denoted by "**". N/A = not applicable, Minced DAT foams were not fabricated at this concentration.

4.1.4 Swelling Ratio

The swelling ratio of DAT foams was also determined by comparing the surface area of the foams equilibrated in Ringer's solution for 3 days to the surface area of the dry foams (Figure 4.6). In all groups, there were no significant changes in the size of the foams following rehydration. Likewise, there were no significant differences in swelling between the minced and milled foams fabricated for each given concentration. This is consistent with previous findings from our group [11].

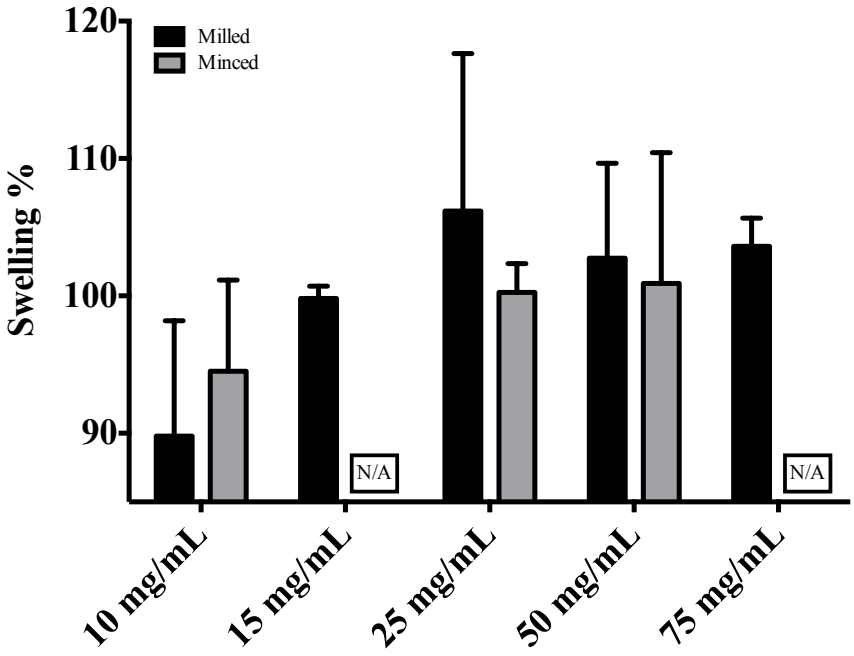

Figure 4.6: Swelling ratio of minced and milled DAT foams equilibrated in ringer buffer solution for 72 hours at 37°C (n = 3), based on surface area calculations. A 1-way ANOVA with a Tukey's multiple comparisons post-hoc test was performed to compare means. Means were considered to be statistically different if $p < 0.05$. N/A = not applicable, Minced DAT foams were not fabricated at this concentration.

4.1.5 Immunostaining of Extracellular Matrix Proteins

ECM components including structural proteins, proteoglycans, and bioactive growth factors can be affected by decellularization, homogenization and sterilization protocols. To determine if the DAT foams retained the epitopes of structural proteins found in native adipose tissue, immunostaining for major ECM constituents (collagen 1, collagen 4, fibronectin and laminin) was performed. Native adipose tissue was positive for collagen 1, collagen 4, fibronectin and laminin (Figures 4.7-4.10). Similarly, intact DAT, minced DAT foams, and milled DAT foams also retained a positive signal for all four proteins (Figures 4.7-4.10). Qualitatively, the intensity of the staining was higher in the minced DAT foam groups as compared to the milled DAT foam groups, which suggests that there may be better preservation of the ECM in this group. The presence of these ECM epitopes is a positive indicator that the foams may support cell adhesion, survival, migration, and function.

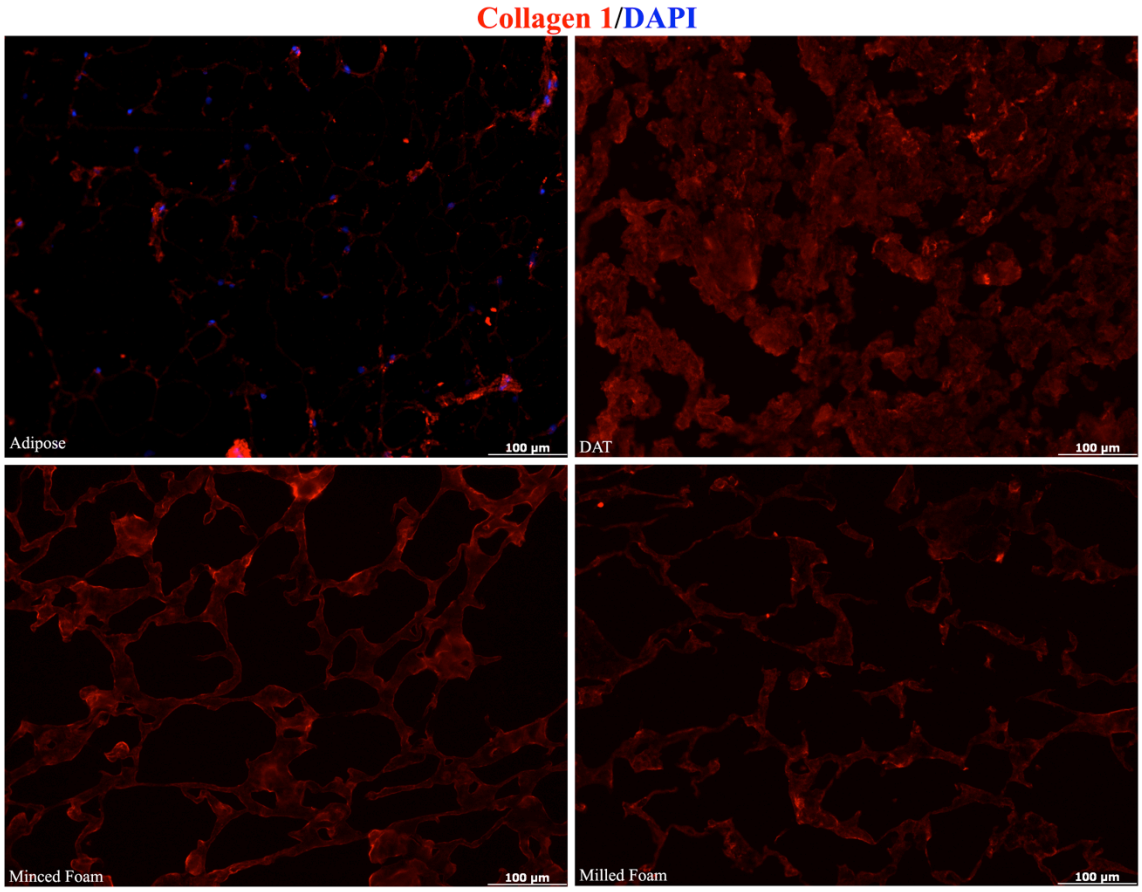

Figure 4.7: Immunostaining for collagen type I (red) (upper left = human fat; upper right = human DAT; bottom left = minced DAT foam 50 mg/mL; bottom right = milled DAT foam 50 mg/mL). All slides were counterstained with DAPI to visualize nuclei (blue). Images were taken at a magnification of 20x.

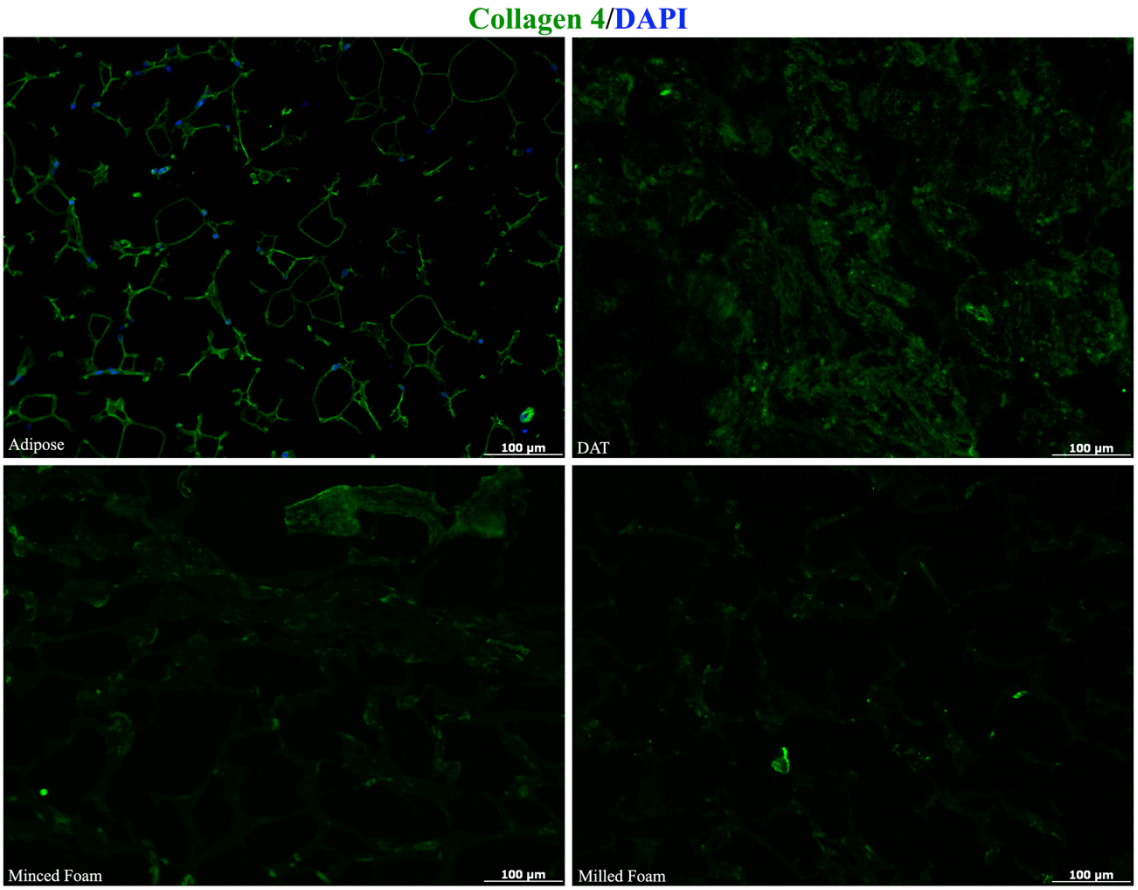

Figure 4.8: Immunostaining for collagen type IV (green) (upper left = human fat; upper right = human DAT; bottom left = minced DAT foam 50 mg/mL; bottom right = milled DAT foam 50 mg/mL). All slides were counterstained with DAPI to visualize nuclei (blue). Images were taken at a magnification of 20x.

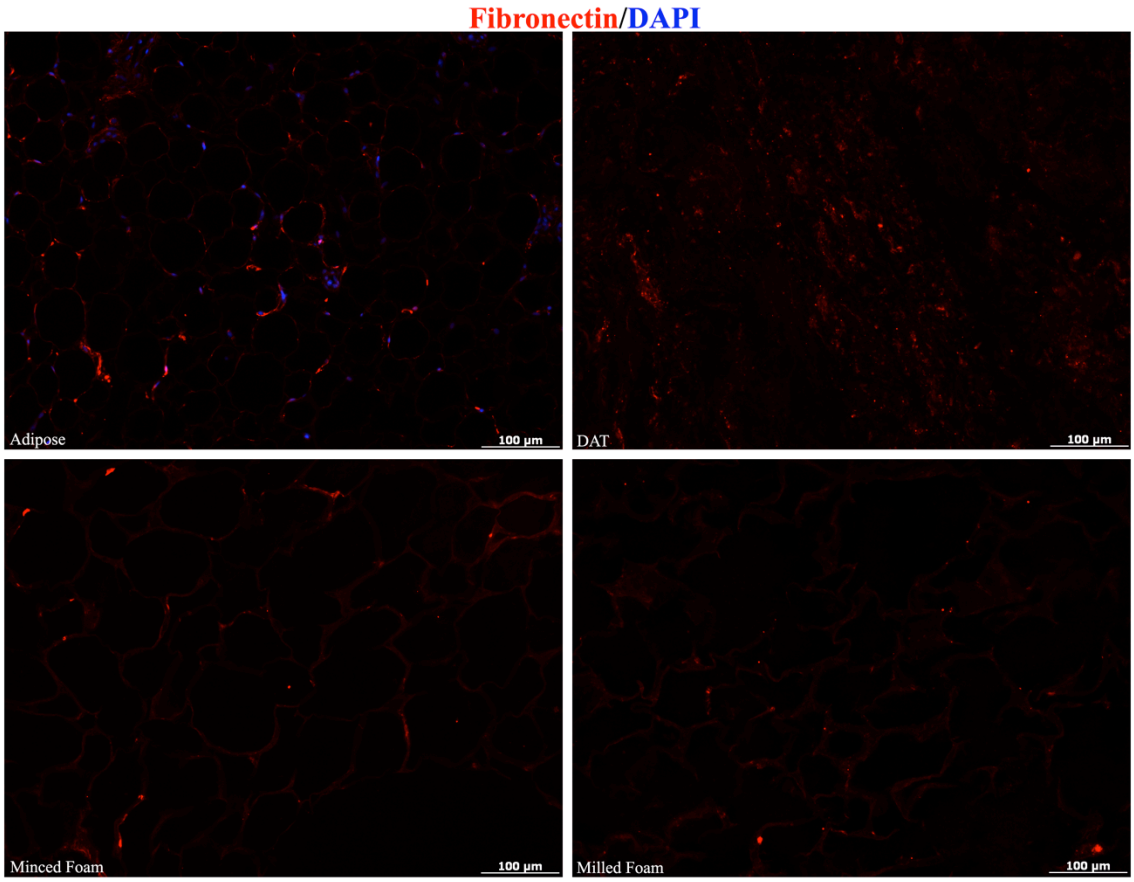

Figure 4.9: Immunostaining for fibronectin (red) (upper left = human fat; upper right = human DAT; bottom left = minced DAT foam 50 mg/mL; bottom right = milled DAT foam 50 mg/mL). All slides were counterstained with DAPI to visualize nuclei (blue). Images were taken at a magnification of 20x.

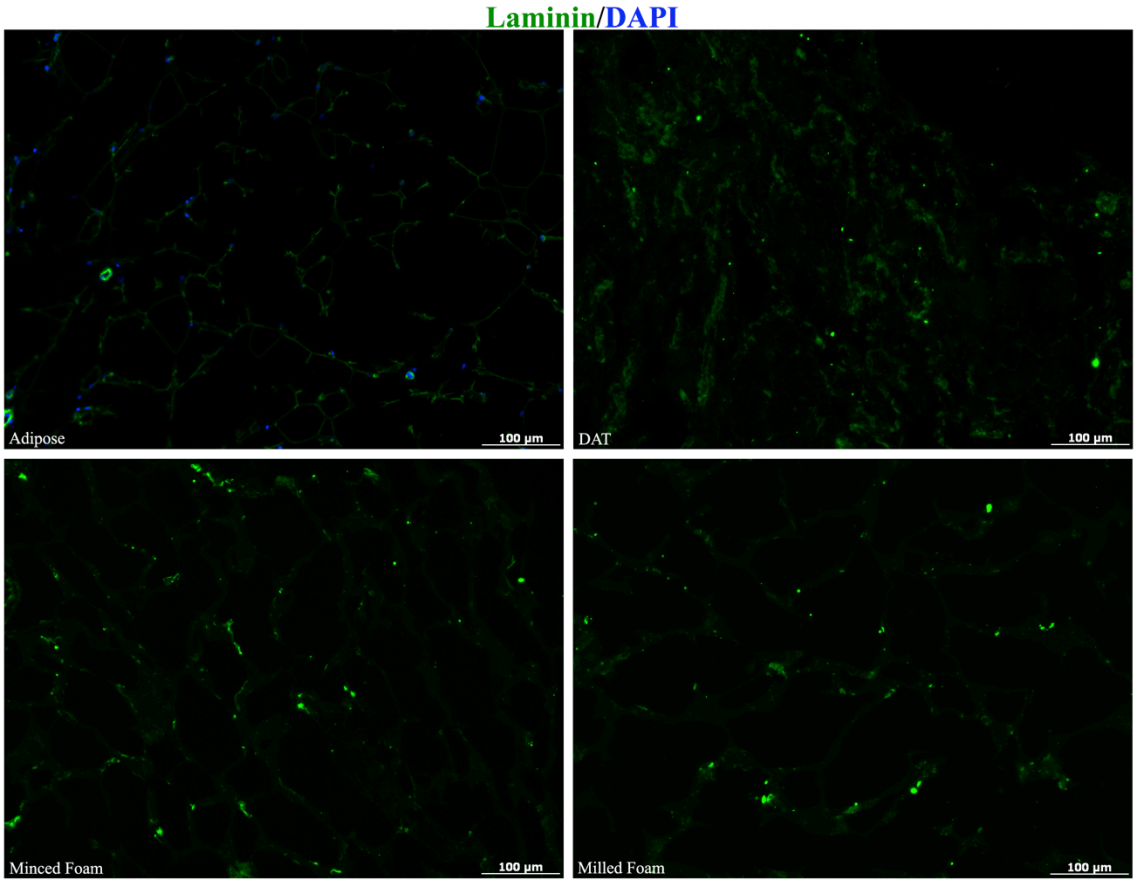

Figure 4.10: Immunostaining for laminin (green) (upper left = human fat; upper right = human DAT; bottom left = minced DAT foam 50 mg/mL; bottom right = milled DAT foam 50 mg/mL). All slides were counterstained with DAPI to visualize nuclei (blue). Images were taken at a magnification of 20x.

4.2 Cell-Seeding Studies

4.2.1 Chloroform Sterilization Cytotoxicity Pilot Study

DATsol was sterilized using chloroform (see Chapter 3) and the potential cytotoxic effects on human ASCs were investigated to determine if the sterilization protocol was suitable prior to cell-seeding. After sterilizing DATsol with chloroform, the DAT foams were fabricated and then suspended in inserts, to create an indirect culture system where the human ASCs were plated on the tissue culture well-plates. ASCs were seeded at a density of 10,000 and 30,000 cells/cm^2 and after 3 days of culture, ASC cell number and viability were determined following trypsinization using a viability staining assay analyzed by flow cytometry (Figure 4.11). At both cell-seeding densities, ASCs cultured in the presence of chloroform-sterilized DAT foams did not have a statistically different viability or cell count as compared with ASC controls cultured without the DAT foams. This confirmed that chloroform sterilization of the foams would not impact the ASCs.

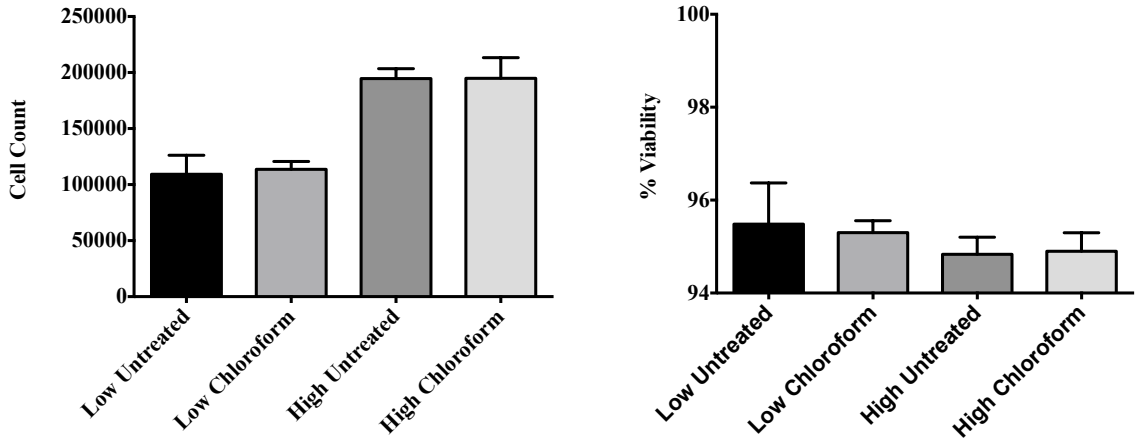

Figure 4.11: Chloroform sterilization cytotoxicity study results for viable ASC counts (left) and ASC percent viabilities (right). ASCs were seeded at "low" (10,000 cells/cm^2) and "high" (30,000 cells/cm^2) cell densities on tissue culture well plates and cultured in the presence of DAT foams, either pre-treated with chloroform or without chloroform (untreated controls) sterilization, for 72 hours (n = 3). A 1-way ANOVA with a Tukey's multiple comparisons post-hoc test was performed to compare means. Means were considered to be statistically different if $p < 0.05$.

4.2.2 Cell-Seeding Methods Pilot Study

In previous work, DAT foams were seeded using a static droplet seeding method, which involved dripping a highly concentrated cell suspension over the surface of the scaffolds. However, Masson's trichrome staining revealed that the ASCs seeded in this fashion were localized to the surface of foams, with little to no penetration after 14 days of culture *in vitro* [11]. Since ASCs secrete factors that augment wound healing and angiogenic responses [7], [84]**,** it was of great interest to investigate a cell-seeding strategy that could increase the cellular dose within a given scaffold. In addition to increasing cellular dose, increasing ASC infiltration in the DAT foams may be beneficial, as ASCs present within the interior of the foam may help to promote scaffold integration

and tissue regeneration through the recruitment of endogenous host progenitor cells into the central scaffold regions through paracrine factor secretion.

The aim of the first pilot study was to compare cell infiltration with 3 different seeding protocols – (i) traditional static droplet seeding of a hydrated scaffold, (ii) static droplet seeding of a dry scaffold, and (iii) dynamic seeding using an orbital shaker. The rationale for using a dry scaffold in place of a hydrated one was that cells might be naturally drawn towards the scaffold center during the rehydration process. Alternatively, reports in the literature demonstrate that dynamic seeding strategies, such as using an orbital shaker, allow for a greater degree of cell infiltration compared to traditional static seeding strategies [44], [46]. Therefore, DAT foams of the same concentration were fabricated, seeded with the same number of viable ASCs and then cultured for 7 days to allow cells to proliferate. After 7 days, the foams were paraffin-embedded, sectioned and stained with Masson's trichrome that coloured collagen fibers blue and cell nuclei dark purple (Figure 4.12).

During static droplet cell-seeding, dry foams were observed to rapidly shrink and collapse upon contact with the cell suspension. This loss of structure is evident when viewing the histological image of the foam in Figure 4.12 and comparing it to the overall foam structure in the other two groups. Moreover, dry foams were not equilibrated in complete culture medium and this may have impaired cell adhesion, survival, and function since bioactive proteins present in the FBS included in the complete culture medium would not have had the opportunity to pre- adsorb to the scaffold during the

equilibration period. Regardless, ASCs were detected - albeit very few - at the center of the scaffold. On the other hand, traditional static droplet seeded hydrated foams had no detectable ASCs in the central regions. Most cells were located at the surface of the foam, consistent with previous findings [11]. Dynamic seeding using an orbital shaker resulted in the highest cell density at the center of scaffolds; moreover there seemed to be a relatively uniform cellular distribution. Moving forward, dynamic cell-seeding using an orbital shaker was selected as the seeding method of choice to maximize cell infiltration within the DAT foams.

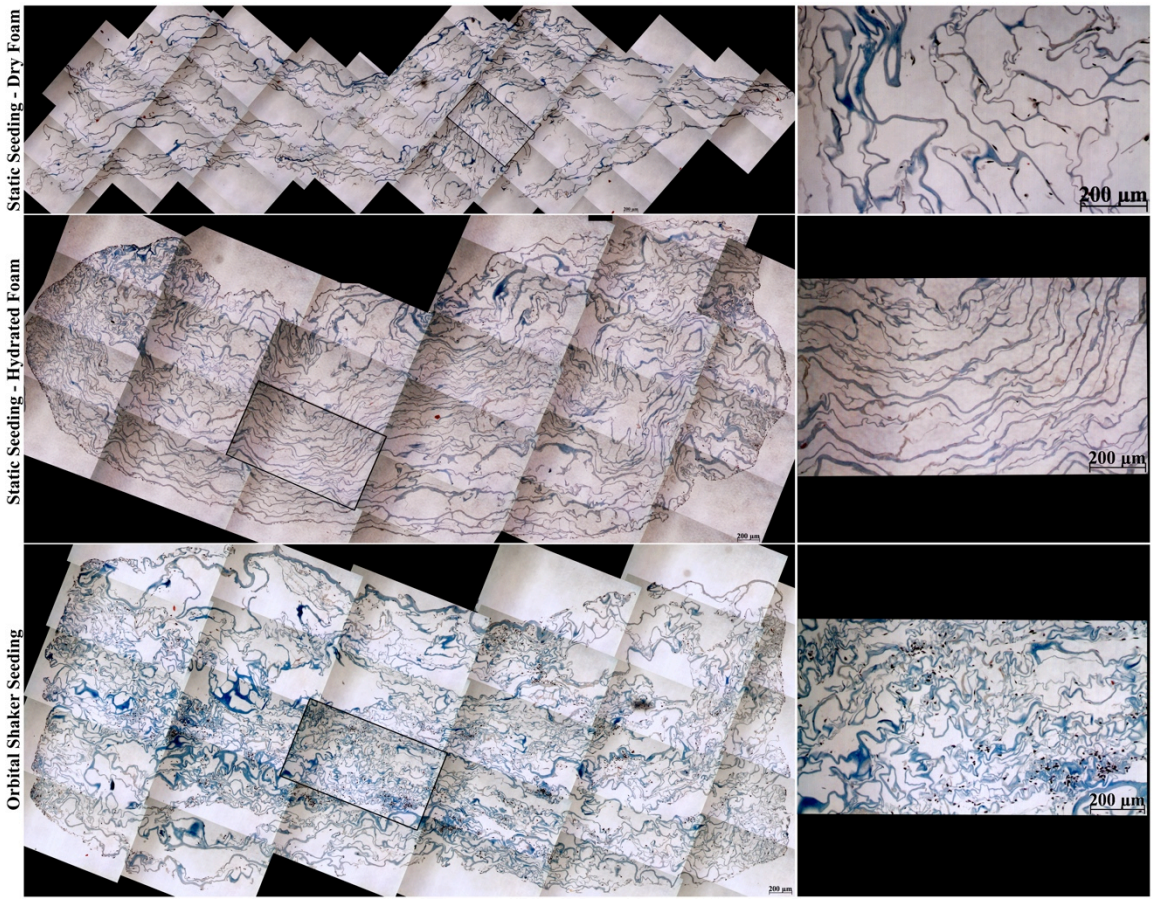

Figure 4.12: Representative images from the seeding methods pilot study showing reconstructed cross-sections of DAT foams seeded with ASCs using three different protocols (left). Seeded DAT foams were cultured for 7 days before fixing for histological analysis by Masson's trichrome staining (n = 3). An enlarged image taken at the center of each cross-section is shown to reveal ASC nuclei (right).

4.2.3 DAT Foam Contraction

After observing that seeded DAT foams contracted in culture over time, a contraction study was performed to quantify the change in scaffold size after the foams were seeded with ASCs using the dynamic orbital shaker method described in 4.2.2. Minced and milled DAT foams were fabricated at 10, 25, and 50 mg/mL concentrations.

One group of 75 mg/mL milled foams was also included in the study. Seeded scaffolds were imaged immediately following the cell-seeding protocol (day 0), and again after 4, 7, 14, and 28 days in culture (Figure 4.13). Surface areas were calculated and then plotted at the end of the study (Figure 4.14).

Generally, foams of lower concentration had a significantly smaller surface area than foams of higher concentration by day 28. Moreover, minced and milled foams of the same concentration contracted to statistically similar sizes by day 28, with the exception of a few timepoints in which the minced foams had a significantly higher surface area than the milled foams for a given concentration, suggesting that the minced foams were more resistant to contraction. These findings are consistent with better preservation of the ECM fiber structure in the minced foam groups.

Contraction of scaffolds seeded with cells is a common phenomenon and it is a result of the contractile forces generated by cells on the scaffold. The amount of contraction has been shown to increase with increased cell-seeding density [95], [96], and it is largely dependent on the mechanical properties of the foam. To that end, it has been reported that collagen scaffolds fabricated with a higher concentration of protein tend to be more resistant to contraction [95] presumably because of augmented mechanical properties. This finding is consistent with the results in this study since foams of higher concentration tended to be more resistant to contraction than foams of lower concentration. However, it is difficult to say that scaffold concentration alone influenced contraction unless it is assumed that the cell-seeding densities are identical at all

concentrations. It is likely that scaffold concentration may have influenced cell-seeding efficiency via porosity changes, as evidenced by the findings in the previous porosity study. Moreover, DAT processing methods (mincing vs. milling) may also influence cell-seeding efficiency due to differences in the foam architecture.

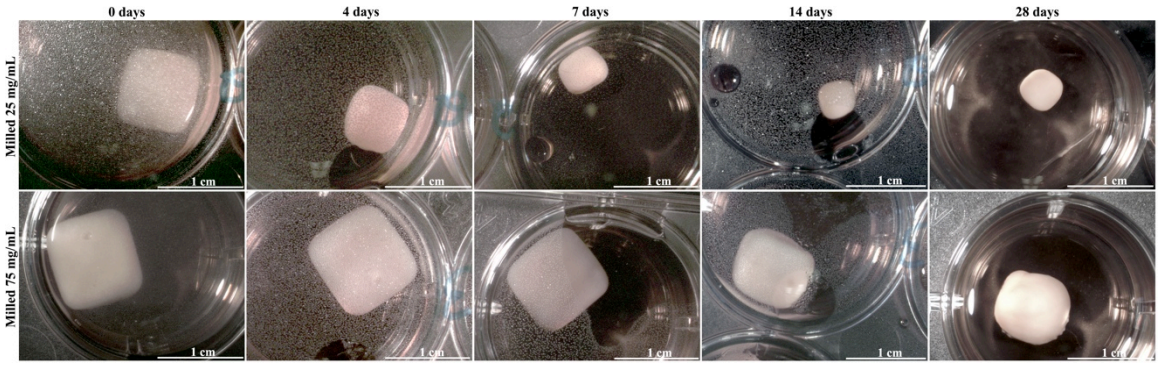

Figure 4.13: Representative images of a low concentration milled DAT foam (top row) and a high concentration milled DAT foam (bottom row) taken during the contraction study. Foams were imaged and surface areas were measured immediately after orbital shaker cell-seeding and then periodically until day 28.

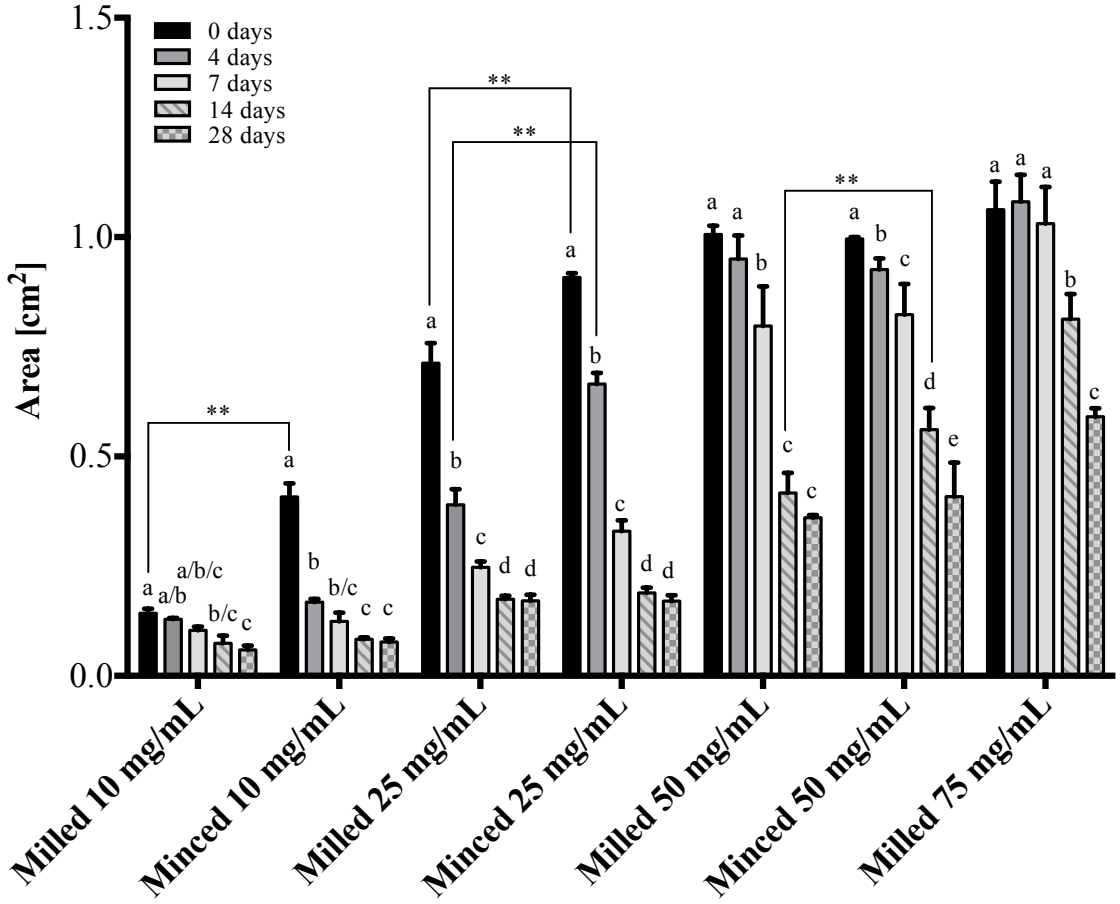

Figure 4.14: Contraction study of minced and milled DAT foams seeded with ASCs using the orbital shaker cell-seeding method. Surface areas were measured immediately after seeding (0 days) and 4 days, 7 days, 14 days, and 28 days thereafter. A 2-way ANOVA with a Tukey's multiple comparisons post-hoc test was performed to compare means. Means were considered to be statistically different if $p < 0.05$. Within each group, means are statistically different if they are assigned a unique letter (i.e.: means that are assigned "a" are statistically different from means that are assigned "b"; however, means that are assigned "a/b" are not statistically different than means that are assigned "b" or "a"). For a given concentration, statistical differences between means of milled and minced foams at the same timepoint were denoted by "**".

4.2.4 Orbital Shaker Cell-Seeding Pilot Study

In order to test if DAT processing and foam concentration influenced cell-seeding efficiency using the orbital shaker cell-seeding protocol, a pilot study was carried out in which 2 different concentrations of minced (20 and 40 mg/mL) and milled (20 and 50 mg/mL) DAT foams were seeded. Seeded foams were cultured for 7 days before being paraffin-embedded, sectioned, and stained. Cell infiltration was assessed for each group, and representative images are shown in Figure 4.15**.**

In general, ASCs infiltrated further into scaffolds fabricated at a lower concentration. Furthermore, at the same concentration (20 mg/mL), ASCs infiltrated further into the milled foams as compared to the minced foams. In fact, milled foams fabricated at 20 mg/mL contained high numbers of ASCs homogeneously distributed throughout the cross-sections of the scaffolds. To demonstrate this, images of 20 mg/mL milled foams were taken at the center of the foam rather than at the surface of the foam.

This pilot study demonstrated that both foam concentration and DAT processing impacted cell-seeding efficiency. More specifically, lower concentration DAT foams had greater cell infiltration presumably because of an increase in porosity. This assumption is in agreement with the findings of Zeltinger *et al.* who found that cell infiltration of scaffolds seeded using agitation was a function of porosity in three different cell types [45]. Additionally, milled DAT foams had greater cell infiltration than minced foams. SEM micrographs of foam cross-sections (Figure 4.1) revealed a greater degree of heterogeneity in minced foams compared to milled foams. Therefore, it is possible that

the interconnectivity of the pores within the minced foams is more interrupted. This could explain why cell infiltration was lower in the minced foams seeded with an orbital shaker.

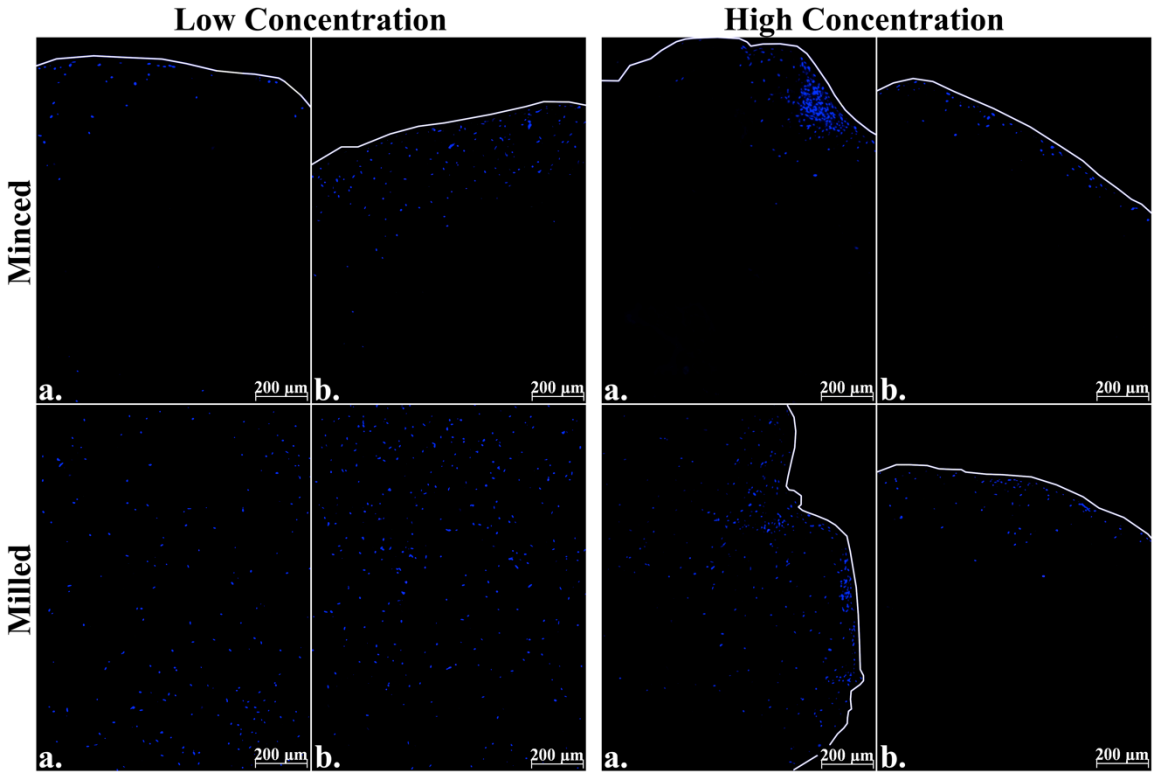

Figure 4.15: Representative cross-sections from the orbital shaker cell-seeding pilot study using "low" concentration (minced & milled = 20 mg/mL) and "high" concentration (minced = 40 mg/mL; milled = 50 mg/mL) DAT foams (n = 2). Cross-sections of 2 foams per group are shown ("a" and "b"), and the edge of the DAT foams is outlined in white where appropriate.

4.2.5 Orbital Shaker Cell-Seeding Optimization (Short-Term Culture)

In order to further enhance the orbital shaker cell-seeding protocol, the effects of orbital shaker RPM and cell suspension concentration on the total DNA content in the DAT foams were investigated. milled DAT foams at 15, 25, and 50 mg/mL were seeded using an orbital shaker set to 60 or 120 RPM; additionally, each group of 3 foams was seeded using 21 mL of complete medium containing either 3×10^6 or 1.5×10^6 ASCs. After 72 hours in culture, the foams were digested using collagenase and dsDNA was quantified using methods described in Chapter 3. Moreover, a subset of the scaffolds was paraffin-embedded, sectioned, and immunostained for Ki67 in order to quantify ASC proliferation, cell density, and cellular distribution (see 4.2.6).

When data was arranged to show the effect of cell suspension concentration on dsDNA content (Figure 4.16), only 2/6 groups had significantly increased DNA content at the higher cell-seeding density. However, most groups were observed to have an increased DNA content at the higher cell suspension concentration, albeit not statistically significant. Since doubling the concentration of the seeding suspension did not yield statistically significant increases in DNA content, it was decided that the lower concentration would be used in future experiments to minimize time and resources required for ASC expansion.

When the data was arranged to show the effect of orbital shaker RPM (Figure 4.17), 3/6 groups showed a statistically increased DNA content as the RPM increased from 60 to 120. Since the lower cell-seeding density was selected, groups seeded using

this cell suspension concentration (any group with "0.5M") were analyzed as the primary focus. Among them, 2/3 groups had an increased DNA content as RPM increased from 60 to 120. Therefore, it was decided that an orbital shaker speed of 120 RPM was preferable for future experiments.

Finally, when data was arranged to show the effect of DAT foam concentration on DNA content (Figure 4.18), 25 mg/mL foams were observed to have the statistically highest DNA content. This is clearly demonstrated for foams seeded at 120 RPM with 0.5 x 10^6 cells/foam. Therefore, in future experiments it was decided to seed milled 25 mg/mL foams using a seeding density of 0.5 x 10^6 cells/foam and an orbital shaker speed of 120 RPM.

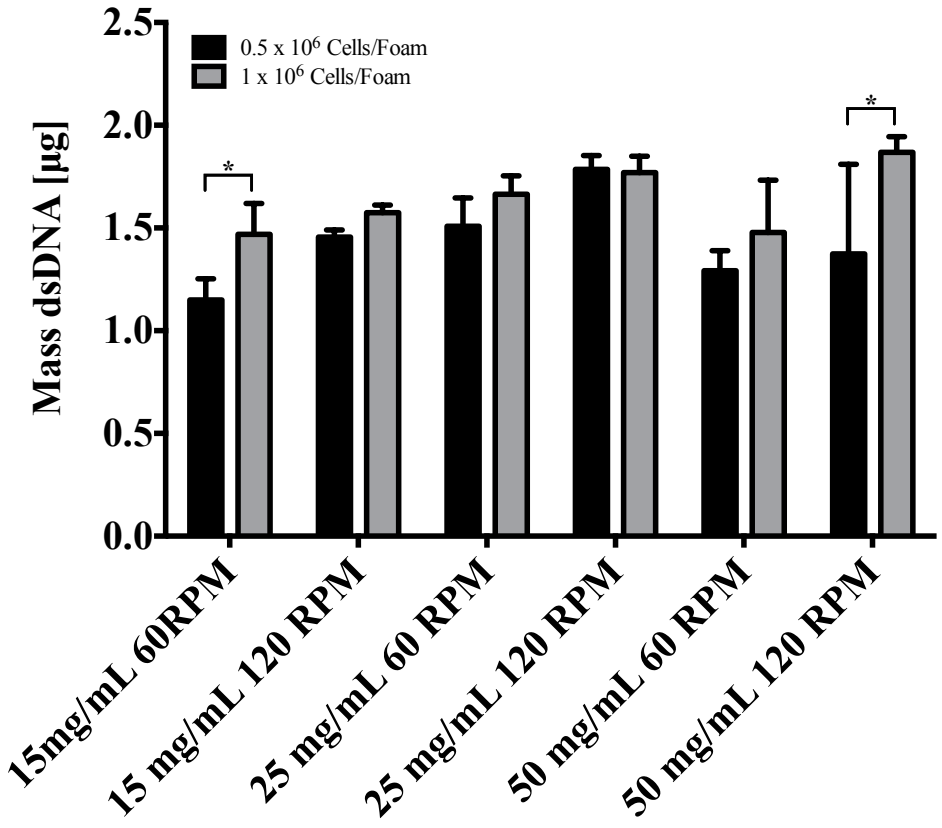

Figure 4.16: dsDNA content of milled DAT foams seeded using an orbital shaker, and cultured for 72 hours (n = 3). Experimental variables under investigation included DAT foam concentration, orbital shaker RPM, and cell-seeding density. The data in this figure is organized to show the effect of seeding density on dsDNA content. A 2-way ANOVA with a Sidak's multiple comparisons post-hoc test was performed to compare means of identical foam concentration and orbital shaker RPM. Means were considered to be statistically different if $p < 0.05$. Statistical differences between means are indicated by "*".

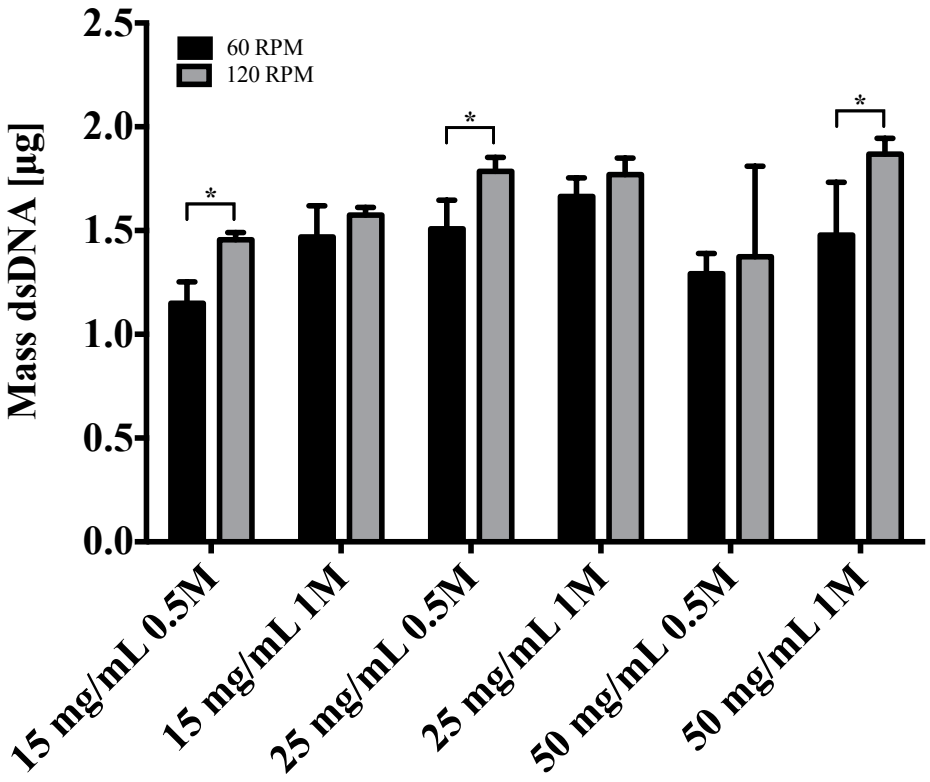

Figure 4.17: dsDNA content of milled DAT foams seeded using an orbital shaker, and cultured for 72 hours (n = 3). Experimental variables under investigation included DAT foam concentration, orbital shaker RPM, and cell-seeding density. The data in this figure is organized to show the effect of orbital shaker RPM on dsDNA content concentration. A 2-way ANOVA with a Sidak's multiple comparisons post-hoc test was performed to compare means of identical foam concentration and cell-seeding density. Means were considered to be statistically different if $p < 0.05$. Statistical differences between means are indicated by "*".

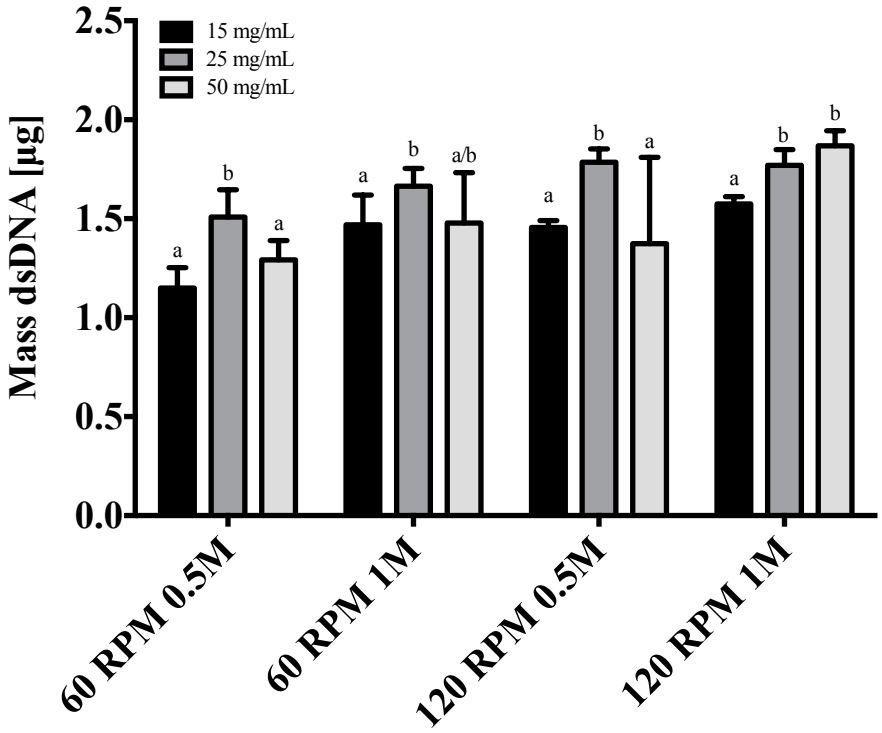

Figure 4.18: dsDNA content of milled DAT foams seeded using an orbital shaker, and cultured for 72 hours (n = 3). Experimental variables under investigation included DAT foam concentration, orbital shaker RPM, and cell-seeding density. The data in this figure is organized to show the effect of DAT foam concentration on dsDNA content. A 2-way ANOVA with a Tukey's multiple comparisons post-hoc test was performed to compare means of identical orbital shaker RPM and cell-seeding density. Means were considered to be statistically different if $p < 0.05$. Within each group, means are statistically different if they are assigned a unique letter (i.e.: means that are assigned "a" are statistically different from means that are assigned "b"; however, means that are assigned "a/b" are not statistically different than means that are assigned "b" or "a").

4.2.6 Orbital Shaker Optimization (Long-Term Culture)

To gain a better understanding of DNA content, cell distribution, cell density, and proliferative activity within orbital shaker seeded milled DAT foams, the previous experiment (4.2.5) was repeated using a smaller subset of seeding conditions and culturing the foams for 7 and 14 days. All foams were seeded at 120 RPM with 0.5 x 10^6 cells/foam, and the DAT foam concentrations included were 25 mg/mL and 50 mg/mL. 50 mg/mL foams were selected to validate a previous finding: ASC infiltration is reduced in higher concentration foams compared to lower concentration foams. Moreover, a group of 25 mg/mL minced DAT foams that were cultured in serum-free culture medium was included in order to observe how culture medium might impact DNA content, cell distribution, cell density and proliferative activity.

DNA content in both groups of milled foams was consistent from day 3 to day 7, but then significantly decreased in both groups by day 14 (Figure 4.19). One explanation for this concerns nutrient/waste diffusion. It is possible that the ASCs residing in the center of the foams were gradually cut off from nutrient/waste exchange during static culture as the foams contracted. Since milled 50 mg/mL foams contracted significantly less than 25 mg/mL foams by day 14 (Figure 4.14), the interconnectivity between pores may have been better preserved in the 50 mg/mL foams. This could explain the finding that the 50 mg/mL foams had a statistically higher DNA content than the 25 mg/mL foams at 14 days.

On the other hand, minced foams cultured in serum-free culture medium had a statistically similar DNA content at all 3 timepoints. Minced foams have been shown to have lower cell infiltration compared to their milled counterparts; therefore it was postulated that there would be fewer cells within the interior of the foams in this group. This would be consistent with the findings that the 25 mg/mL milled foams, which were observed to be highly supportive of cell infiltration in the previous study, had a significantly higher DNA content as compared to the minced foam group at day 3. In this case, the impairments with nutrient/waste diffusion mediated by scaffold contraction may not have influenced the cells as significantly in the minced foam group. Alternatively, it is possible that the serum-free culture medium enhanced cell proliferation. By day 7, cell sheets were observed surrounding the minced foams cultured in serum-free culture medium, while cell sheets were not observed in either of the groups cultured in standard culture medium containing FBS. Therefore, if cells at the center of the minced foams were affected by reduced nutrient/waste diffusion, it is possible that the enhanced ASC proliferation at the surface of the foam (induced by serum-free medium) compensated for this loss. This would explain why the DNA content seemed to be stable in the minced foam group.

To validate the findings of DNA content, the cell density in the foam cross-sections was semi-quantitatively analyzed through nuclei counting (Figure 4.20). Similar to the trend observed with DNA content, both groups of milled foams had a reduced cell density by day 14, although this difference was not statistically significant in the 50

mg/mL foam group. However, a discrepancy between cell density and DNA content data exists at day 7. By day 7, cell density in the milled DAT foams was significantly reduced while DNA content in both groups was statistically greater (50 mg/mL) or the same (25 mg/mL). It may have been possible that by day 7, cells at the center of the scaffold underwent apoptosis in response to nutrient deprivation. This would explain why cell density (as measured through histology) decreased. However, it might have also been possible that DNA from the apoptotic cells remained inside the scaffold; therefore the Quant-iT™ PicoGreen® dsDNA Assay may have detected this DNA. Another possibility is that the methodology used to quantify cell density has limitations. To calculate cell density, two cross-sections of each foam were imaged and counted - however, it is quite possible that the cross-sections selected were not truly representative of the entire foam.

To better understand cell distribution within the foam cross-sections, regional cell densities were measured (Figure 4.21). Briefly, cell densities towards the surface of the foam (outer) were compared with cell densities at the center of the foam (inner). In both milled foam groups, there was a statistical difference between inner and outer cell densities by day 3, although this difference was less pronounced in the 25 mg/mL foams. This may be explained by the increased cell infiltration demonstrated in the 25 mg/mL foams as compared to 50 mg/mL foams. By days 7 and 14, there was no difference in cell density between the outer and inner regions of the foam, likely due to contraction. In the minced foam group cultured in serum-free medium, there was no statistically significant difference between the outer and inner cell densities at 72 h, although there was a trend

for higher density in the outer regions with large variations observed. However, by day 7 and 14, there was a statistical difference between the outer and inner cell densities. These trends are consistent with the observation that cell sheets were formed on the surface of the foams by day 7 and 14.

Finally, proliferation of ASCs within the foams was assessed by immunostaining cross-sections for Ki67. 5 non-overlapping fields of view per cross section were imaged and the number of Ki67-positive cells was averaged (Figures 4.22-4.23). It is worth noting that most images of the minced 25 mg/mL foams were taken at the surface, while most images of the milled groups were taken at random locations throughout the cross-section of the foams. Ideally random areas of the minced foam cross-sections would also have been imaged, but there were very few nuclei detected beneath the surface of the foam in this group. Consequently, images of minced foam cross-sections were usually taken at the surface. Therefore, regional bias may have skewed results making it difficult to compare the milled and minced groups.

Interestingly, there was an absence of Ki67-positive nuclei at day 3 in both the 25 and 50 mg/mL milled groups. By day 7 and 14, both milled groups had a detectable number of Ki67-positive nuclei but there was no significant difference between the groups. On the other hand, a large proportion of ASCs seeded at the surface of minced foams and cultured in serum-free medium conditions were Ki67-positive. It is postulated that the higher number of Ki67-positive cells in the minced group was likely related to enhanced ASC expansion in the serum-free culture medium, rather than the effects of the

foam structure. In previous studies in our group, it was found that the proliferation of ASCs in the MesenGro medium is significantly enhanced as compared to expansion in conventional culture medium. The number of proliferative cells decreased after day 7 and there was no significant difference between day 7 and day 14. The number of proliferating cells may have been reduced at the later timepoints due to the high cell density as the surface of these foams.

Overall, ASCs were able to proliferate in the DAT foams and survive (as determined by detectable proliferative activity) for 14 days in culture. The absence of Ki67-positive cells in the milled foams at 3 days may suggest that the ASCs were still equilibrating with the environment. In minced foams, the significant reduction in Ki67-positive cells by day 7 might be attributed to contact-inhibition of proliferation. Histological analysis of minced foam cross-sections revealed a confluent layer of ASCs growing at the foam surface by day 7 (Figure 4.22). It is possible that the foam surfaces were not completely populated by ASCs by day 3. Therefore the ASCs could proliferate without being impeded by contact-mediated growth inhibition.

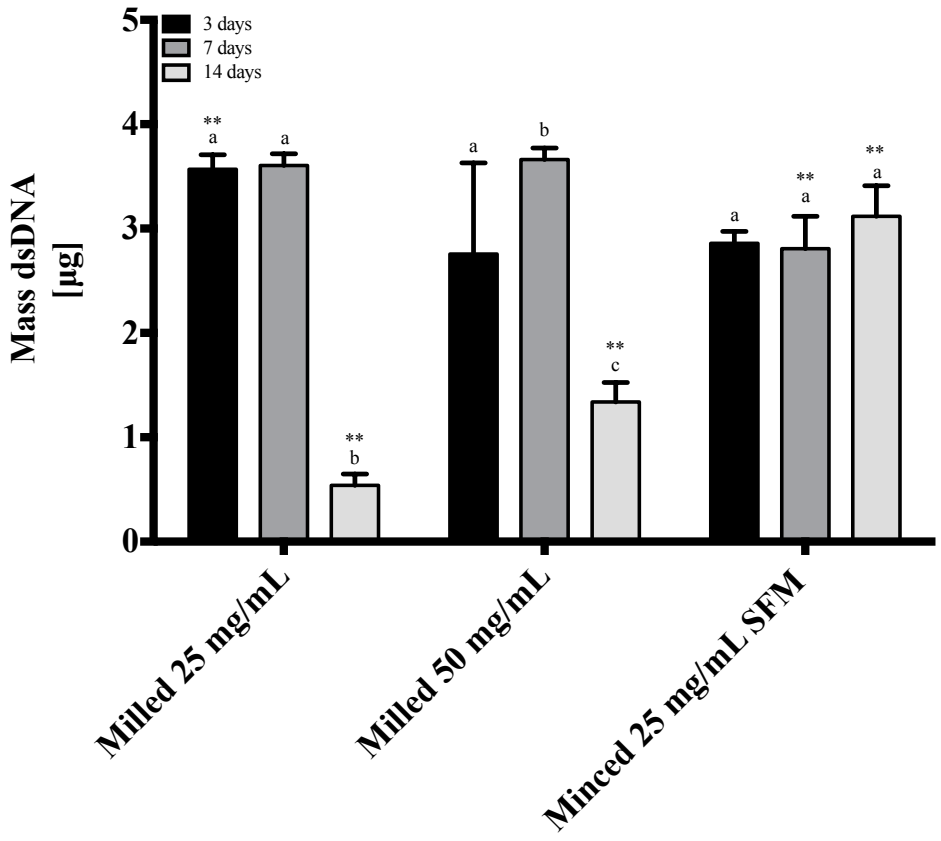

Figure 4.19: Orbital shaker cell-seeding optimization study results showing dsDNA content of DAT foams seeded using an orbital shaker after 3 days, 7 days, and 14 days in culture (n = 3). Both groups of milled DAT foams were cultured in complete culture medium, while the minced DAT foam group was cultured using MesenGro® Human MSC Medium. A 2-way ANOVA with a Tukey's multiple comparisons post-hoc test was performed to compare means. Means were considered to be statistically different if $p < 0.05$. Within a group, means were statistically different if they were assigned a unique letter (i.e.: means that are assigned "a" are statistically different from means that are assigned "b"). In comparing the different types of foams, means marked with "**" indicate statistical difference from all other means within the same timepoint.

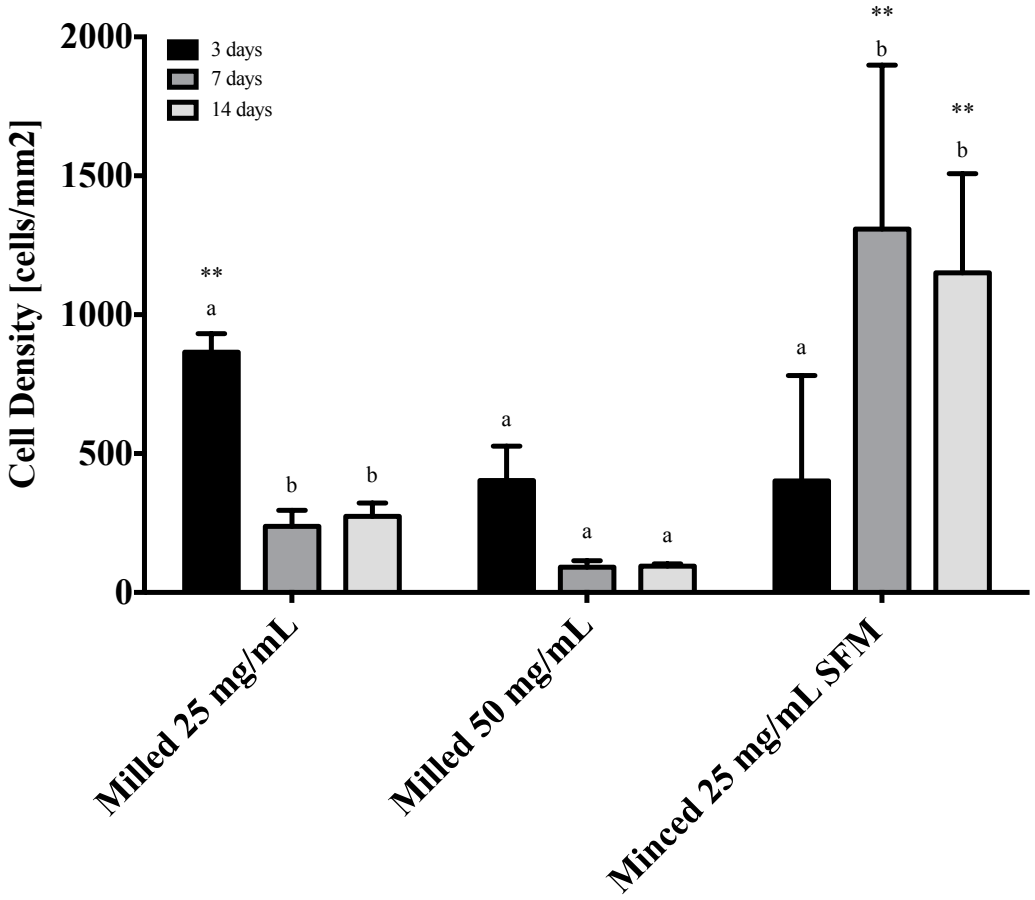

Figure 4.20: **Orbital shaker cell-seeding optimization study results showing total cross-sectional cell density of DAT foams seeded using an orbital shaker after 3 days, 7 days, and 14 days in culture (n = 3).** A 2-way ANOVA with a Sidak's multiple comparisons post-hoc test was performed to compare means for the different foam groups within a given timepoint, while a Tukey's multiple comparisons post-hoc test was performed to compare means over time for a given foam group. Means were considered to be statistically different if $p < 0.05$. Within a group, means were statistically different if they were assigned a unique letter (i.e.: means that are assigned "a" are statistically different from means that are assigned "b"). In comparing the different types of foams, means marked with "**" indicate statistical difference from all other means within the same timepoint.

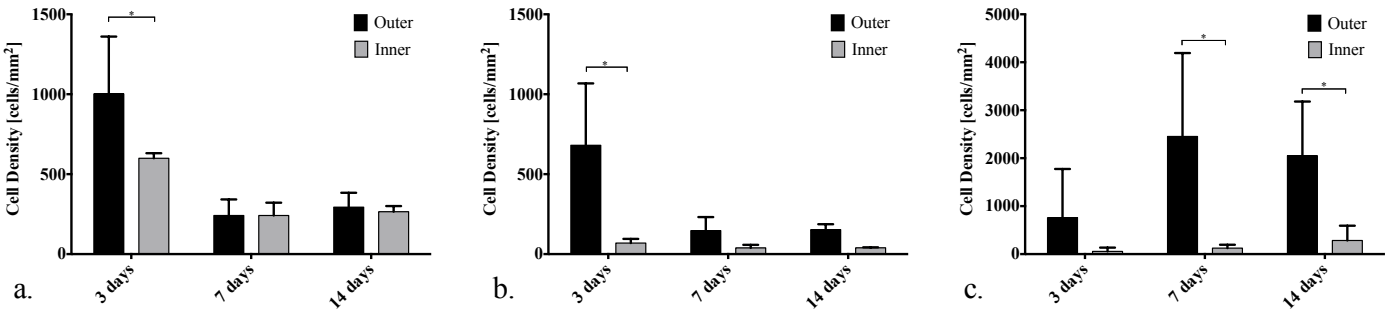

Figure 4.21: Orbital shaker cell-seeding optimization study results showing regional cross-section cell density of DAT foams seeded using an orbital shaker after 3 days, 7 days, and 14 days in culture (n = 3). Cell densities near the surface of the foam (outer) are compared to cell densities at the center of the foam (inner). The outer region was defined by the area from the surface of the foam to a distance of 25% total cross-sectional length; whereas the inner region was defined by the remaining cross-sectional area at the center of the foam Figure a. shows data for 25 mg/mL milled foams; figure b. shows data for 50 mg/mL milled foams; and figure c. shows data for 25 mg/mL minced foams cultures using MesenGro® Human MSC Medium. A 2-way ANOVA with a Sidak's multiple comparisons post-hoc test was performed to compare means within a given timepoint. Means were considered to be statistically different if $p < 0.05$. Statistical differences between means were denoted by "*".

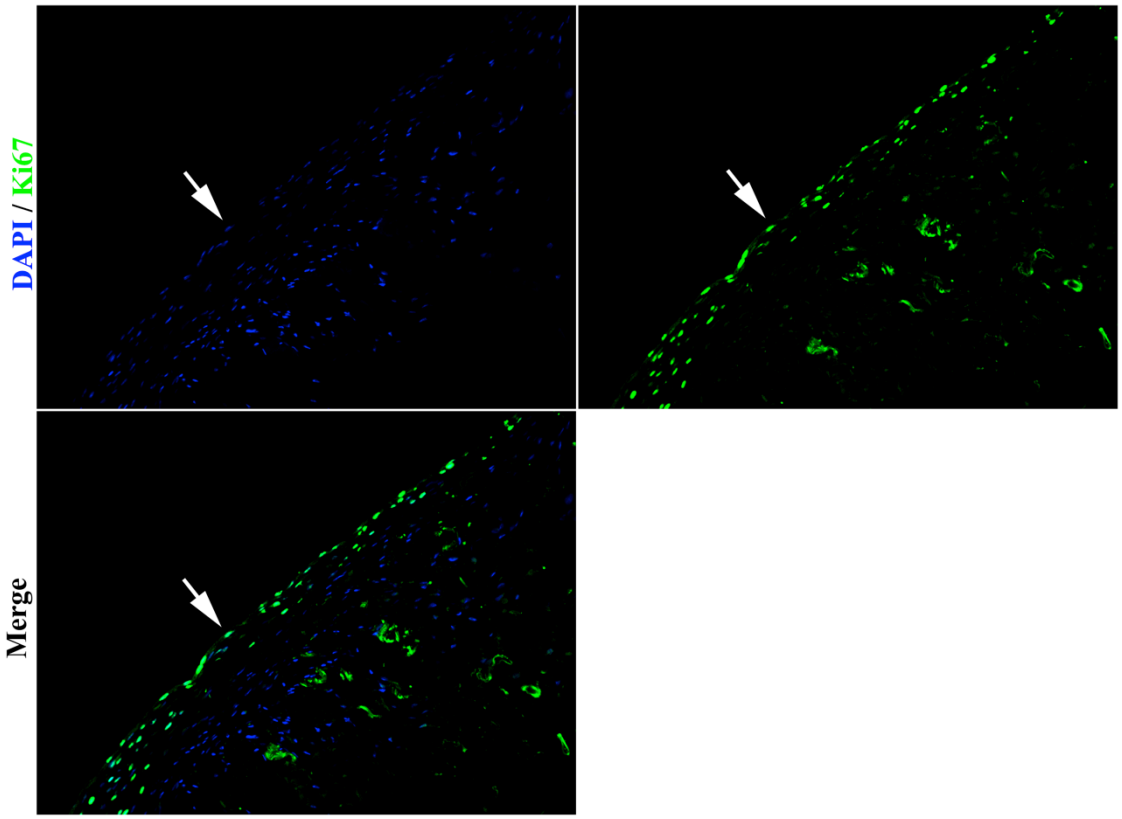

Figure 4.22: Orbital shaker cell-seeding optimization study showing ASC proliferation within DAT foams. DAT foams were seeded using an orbital shaker and cultured for 3 days, 7 days and 14 days before being processed for immunohistochemistry. Cross-sections of seeded foams were stained for Ki67 (green) with DAPI counterstaining (blue) and the percentage of $Ki67^{+}$ cells was determined.

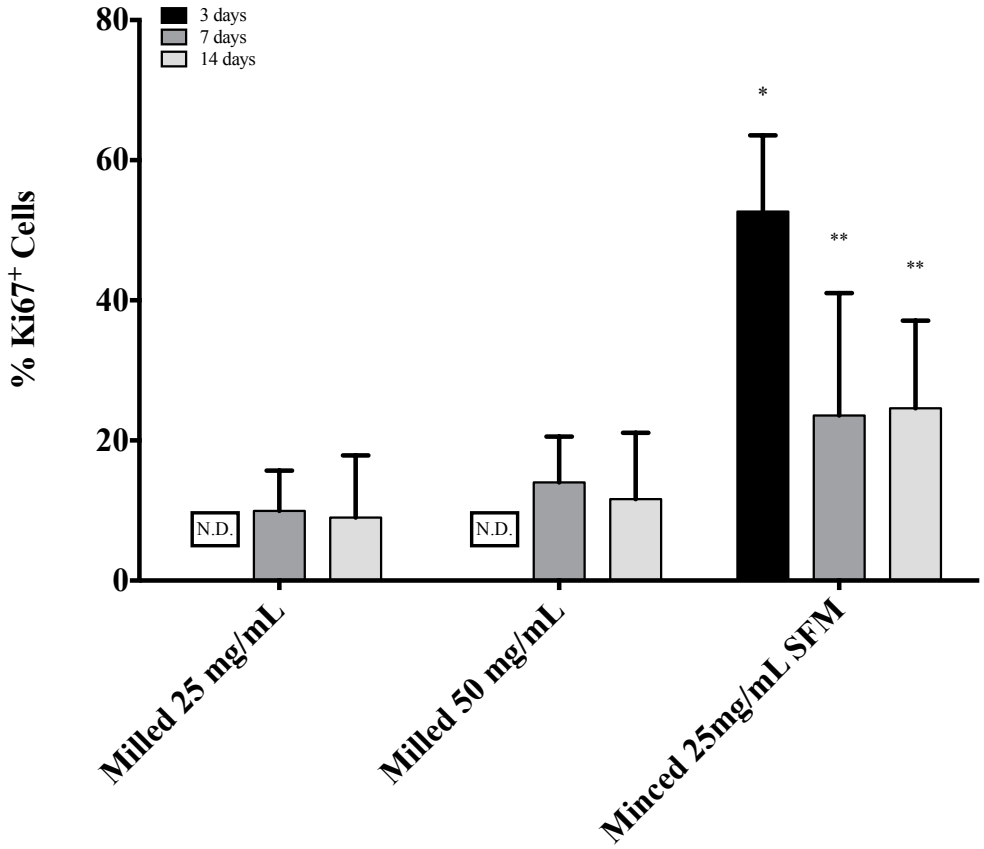

Figure 4.23: Orbital shaker cell-seeding optimization study showing ASC proliferation within DAT foams. DAT foams were seeded using an orbital shaker and cultured for 3 days, 7 days and 14 days before being processed for immunohistochemistry. Cross-sections of seeded foams were stained for Ki67 and the percentage of $Ki67^+$ cells was determined. A 2-way ANOVA with a Tukey's multiple comparisons post-hoc test was performed to compare means. Means were considered to be statistically different if $p < 0.05$. Within a group, means marked with "*" are statistically different from all other means. For means at a given timepoint, "**" denotes statistical difference from all other means. N.D. = not detected, no positive cells visualized at this timepoint.

4.3 Gene Expression of ASC Seeded on Various Substrates

The use of ASCs for therapeutic angiogenesis is well documented in animal studies models [8], [97]**.** In particular, it is thought that ASCs exert their effects mainly through soluble factor secretion [84], [98]. However, soluble factor secretion is modulated by many factors including oxygen tension [85], interactions with the ECM [99], and interactions with paracrine factors [98]**.** To that end, gene expression of ASCs seeded onto the ECM-derived scaffolds was compared in a pilot study quantitatively assessing VEGF-A and fibroblast growth factor-2 FGF-2 gene expression of ASCs grown in 2-D on various substrates to test if the cell culture substrate mediated ASC expression of these two angiogenic factors.

To investigate relative gene expression of ASCs seeded on DAT foams, DDT foams, collagen gels or tissue culture plates, qRT-PCR was used to quantify FGF-2 and VEGF-A mRNA levels. ASCs were seeded in milled DAT foam scaffolds using the orbital shaker protocol described in 4.2.6. Additionally, porcine dermal foams fabricated from decellularized dermal tissue (Figure 4.24), bovine collagen gels, and well plates were seeded using protocols described in Chapter 3. After a brief equilibration period immediately following cell-seeding, groups were cultured under normoxic (21% O_2) or hypoxic (1% O_2) conditions for 48 hours before collecting RNA. Gene expression was normalized to GAPDH expression, and then expressed as a fold change value relative to ASCs seeded in 2-D on TCPS under normoxic conditions (NOX TCPS).

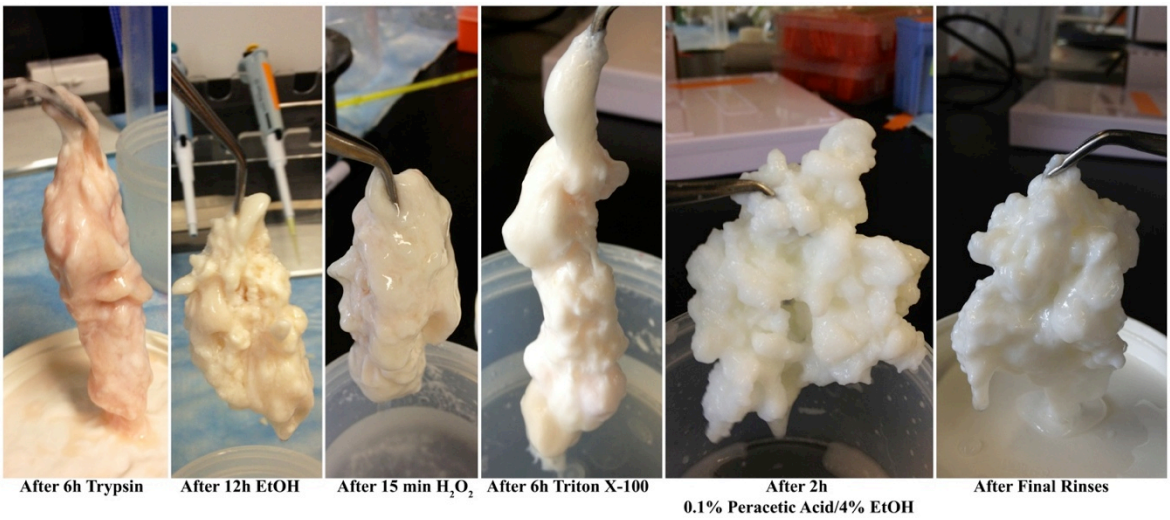

Figure 4.24: Porcine dermal decellularization process.

FGF-2 expression was significantly higher than all other groups for ASCs seeded in the dermal foams (Figure 4.25a); however ASCs seeded in DAT foams had elevated gene expression, albeit not statistically significant. Moreover, FGF-2 expression was observed to decrease under hypoxic conditions for most groups, although this decrease was not statistically significant. There was one exception to this trend, as FGF-2 gene expression was not detected in the collagen gel group cultured under normoxic conditions.

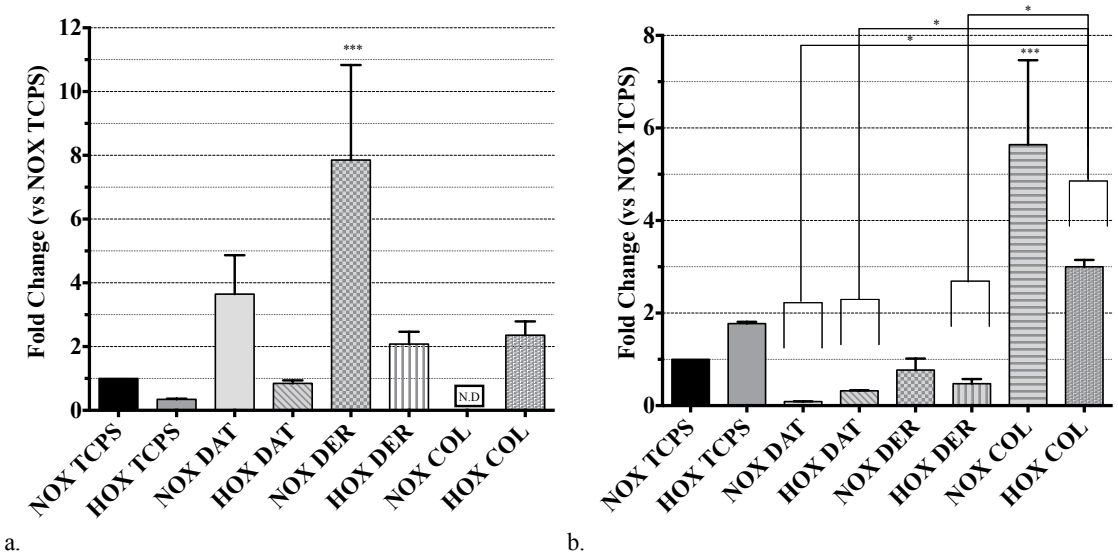

Figure 4.25: Relative (a) FGF-2 and (b) VEGF-A gene expression of ASCs cultured on varying substrates quantified using qRT-PCR. ASC were seeded onto well plates (TCPS), DAT foams (DAT), DDT foams (DER) and PureCol® gels (COL) (n = 3) and cultured in normoxic (NOX) or hypoxic (HOX) conditions for 48 hours. Relative gene expression was expressed as a fold change value (relative to NOX TCPS expression) by the delta-delta-C_T method with GAPDH as the housekeeping gene and the normoxic TCPS samples as the calibrator. A 1-way ANOVA with a Tukey's multiple comparisons post-hoc test was performed to compare means. Means were considered to be statistically different if $p < 0.05$. Means that are statistically different from all other means are marked with "***", and "*" denotes statistical differences between highlighted means. N.D. = not detected, levels of gene expression in this group were below detectable levels under the conditions in the current study.

VEGF-A expression was significantly higher for ASCs seeded in the collagen gels cultured under normoxic conditions as compared to all other groups (Figure 4.25b). Moreover, VEGF-A expression was significantly higher for ASCs seeded in the collagen gels and cultured under hypoxic conditions as compared to ASC expression in the DAT and dermal foams at the same oxygen tension.

It was expected that gene expression of both FGF-2 and VEGF-A would be significantly increased after exposure to hypoxic conditions based on previous literature reports [100]. However, no significant increase in the expression of either FGF-2 or VEGF-A was observed in the current study after exposure to hypoxic conditions. This discrepancy could be attributed to the exposure time to hypoxia. More specifically, Lee *et al.* exposed ASCs to hypoxic conditions for only 6 hours prior to RNA collection, while ASCs were exposed to hypoxic conditions for 48 hours prior to RNA extraction in this study. Additionally, Fink *et al.* reported that GAPDH expression is upregulated in ASCs cultured in hypoxic conditions [101]. Since GAPDH was used as a reference gene in this study, gene expression data might be skewed. Therefore, in future studies it would be preferable to use an alternative reference gene that is more stably expressed under the conditions described in this study. Moreover, future studies should include a time series analysis to compare the ASC gene expression patterns of different groups.

With the exceptions of ASCs seeded in dermal foams and cultured under normoxic conditions (NOX DER) for FGF-2 gene expression; and ASCs seeded in collagen gels and cultured under normoxic conditions (NOX COL) for VEGF-A gene expression, there were no significant differences in gene expression observed for either FGF-2 or VEGF-A (at a given oxygen tension) compared to ASCs seeded in 2-D and cultured under normoxic conditions (NOX TCPS). This implies that the effect of scaffold-cell interactions was not significant enough to impact gene expression of FGF-2 and VEGF-A in this experimental context. Perhaps if gene expression was quantified

after a different amount of culture time, the effect of cell-scaffold interactions might be more evident.

Protein expression is arguably a more reliable proxy of the pro-angiogenic potential of ASCs as compared to gene expression because many regulatory processes following gene transcription dictate the amount of protein translated, and secreted [102]. Therefore, it is possible that protein expression profiles of the experimental groups included in this study do not correlate directly with the gene expression profiles. Enzyme-linked immunosorbent assays (ELISA) were initially performed on ASC-conditioned media to quantify secreted VEGF-A and FGF-2, however these results were determined to be unreliable because of the protein-protein interactions between secreted growth factors and ECM-derived substrates. Western blotting is an alternative technique that could be used to quantify protein levels and verify the mRNA data.

Chapter 5

Conclusions and Future Work

5.1 Summary and Conclusions

Diabetic foot ulcers are chronic wounds that cost an average of $17,500 per ulcer episode to treat [3]. Moreover, recurrence within the first 5 years of healing is as high as 70% [3]. Current treatment strategies include antibiotic treatment to manage potential bacterial infections, offloading, surgical revascularization of ischemic limbs, surgical debridement of necrotic or infected tissue, and the application of moist wound bed preparations [103]. Unfortunately the cause of diabetic foot ulcers is unknown but several risk factors including, but not limited to, neuropathy, vasculopathy and trauma [1] have been identified. Individuals presenting with foot ulcers often have different combinations of risk factors, which necessitates individualized treatment [104]. Although these interventions can be beneficial, there is ongoing investigation of alternative treatment strategies to enhance healing, reduce overall treatment costs, and eliminate the need for lower limb amputations in patients who fail to respond to conventional approaches. In particular, stem cell-based therapies are being investigated in the hopes of improving treatment outcomes.

In particular, ASCs are being explored as a potential stem cell population for treating chronic wounds because adipose tissue is abundant and can be acquired using minimally invasive procedures. ASCs are multipotent and have the potential to contribute

to regeneration through direct cell engraftment and differentiation, as well as through the primary mechanism of beneficial paracrine factor secretion. Previous clinical studies have demonstrated that ASCs can be safely transplanted in allogenic or autologous applications [48]. ASCs have been investigated to treat wounds in animal models [8], [97] and their use generally results in accelerated wound closure times. The mechanisms of ASC-mediated wound healing are not fully understood but evidence points to growth factor and chemokine secretion as a critical factor [84], [98].

Depending on processing conditions, collagenous foam scaffolds are permissive to fibroblast infiltration [105], they can stimulate macrophages and fibroblasts to induce tissue remodeling [106], they are conformable, and they are chemotactic [10]. Similarly, decellularized tissues are largely comprised of collagen, but may contain other ECM bioinductive proteins such as fibronectin and other basement membrane components. Moreover, enzymatic degradation products of ECM-derived matrices yield fragments that influence cell-specific migration and proliferation *in vitro* [42] and these products could be beneficial at the site of the wound.

DAT is an ECM-derived biomaterial of interest since adipose tissue is abundant and easily harvested. Porous DAT foams can be fabricated by lyophilizing a homogeneous suspension of DAT [11]; moreover, porosity of these foams can be controlled by adjusting the freezing rate and the protein concentration in the homogenized DAT suspension. In the previous work, DAT foams were histologically observed to be resorbed and remodeled over a period of 12 weeks *in vivo;* furthermore,

DAT foams elicited a strong angiogenic response and functional blood vessels were discovered towards the center of implanted foams [11]. Moreover, ASCs seeded onto DAT foams were adherent and viable after 14 days in culture [11] indicating that DAT foams may be useful as an ASC delivery vehicle. However, with static seeding methods, ASCs formed a monolayer on the surface of foams and did not infiltrate into scaffolds [11], thereby limiting the effective cellular dose of the prospective wound dressings.

This project focused on the development of a cell delivery system for the treatment of chronic wounds by enhancing ASC infiltration into the DAT foams scaffolds. The first goal of this project was to characterize and compare DAT foams that were fabricated using different protein concentrations and different DAT processing techniques (mincing vs. milling). DAT foams were quantitatively characterized by measuring porosity, equilibrium water content, swelling, and protein release. Additionally, DAT foams were qualitatively assessed using scanning electron microscopy and immunohistochemistry. Overall, DAT foams were highly porous and hydrophilic. *In vitro,* the foams were generally stable and maintained their shape after rehydration, despite some protein release over time. DAT foams were positive for structural ECM protein epitopes that were detected in native adipose tissue including: collagen I, fibronectin, collagen IV, and laminin.

The second goal of this project was to enhance ASC infiltration into the DAT foams to increase the cell density and distribution in the delivery system. Dynamic orbital shaker cell-seeding was found to enhance cell infiltration when compared to static droplet

seeding methods. Moreover, milled DAT foams fabricated using a low protein concentration were found to have the greatest cell infiltration. Further refinements of the orbital shaker cell-seeding protocol were made by quantifying the effects of orbital shaker speed and cell suspension concentration on dsDNA content. Consequently, a seeding protocol was developed, which yielded DAT foam scaffolds with uniformly distributed ASCs.

The third goal of this project was to assess how ASC behavior was influenced by cell-DAT interactions. More specifically, orbital shaker cell-ed ASC-mediated scaffold contraction was quantified over a period of 28 days in culture. Generally, foams fabricated at a higher protein concentration were more resistant to contraction and had a larger surface area by day 28 than lower concentration foams. Regardless, most groups of DAT foams contracted to at least to half of their original size. Additionally, *in vitro* proliferation of orbital shaker cell-seeded scaffolds was quantified over a period of 14 days. In general, DNA content remained stable up to day 7, but significantly decreased by day 14, likely due to ASC-mediated contraction, and consequent nutrient/waste diffusion impedance.

The final goal of this project was to conduct a pilot study to assess ASC gene expression in response to two variables: oxygen tension and cell-ECM interactions. ASCs are known to secrete growth factors relevant to wound healing [107]; moreover, hypoxic preconditioning has been reported to increase mRNA expression of both VEGF and FGF-2 [85]. In this study, the synergistic effects of cell-scaffold interactions were investigated.

ASCs were seeded onto various substrates and then cultured under normoxic (21% O_2) or hypoxic (1% O_2) conditions for 48 hours. Total RNA was collected from all groups and mRNA expression of VEGF and FGF-2 was quantified using qRT-PCR. In the majority of cases, significant differences in VEGF and FGF-2 mRNA levels were not detected but these trends should be confirmed through further exploration of expression changes over time, as well as through protein analysis.

5.2 Contributions

Overall, this thesis made important progress towards optimizing ASC-seeded DAT foams with a view towards their future development as biological dressings for the treatment of chronic wounds. The most significant contributions of this thesis to the field include:

- Detailed characterization of foam scaffolds prepared from decellularized adipose tissue in terms of both structure and composition, and elucidating how protein concentration and DAT processing conditions influence the foam characteristics. Further, the methods developed in this thesis could be applied to generate tissue-specific foams from a wide variety of decellularized tissue sources, which could be explored as bioscaffolds for a range of applications.
- Identification of a sterilization strategy for homogenized DAT that does not appear to be cytotoxic for human ASCs.
- Development of a cell-seeding protocol for DAT foams that results in uniform cellular distribution and greater cell density as compared to conventional static

droplet seeding techniques. These orbital shaker cell-seeding methods could be used as a basis to develop strategies to enhance cell infiltration into other types of porous foams.

5.3 Future Work

The work completed during the course of this Master's thesis represents a good starting point in the development of a novel cell delivery system for the treatment of chronic wounds using DAT-based bioscaffolds. DAT foam characterization and cell-seeding strategies were thoroughly investigated, but *in vitro* and *in vivo* evidence for the efficacy of ASC-seeded DAT foams for wound healing should be explored in future studies.

In particular, future work should focus on:

- Determining the shear modulus or compressive strength of the DAT foams and how they relate to foam protein concentration and DAT processing methods, to ensure that the properties are well aligned with the requirements for cutaneous wound dressings and would not induce scar tissue formation through mechanical irritation.
- Further probing the *in vitro* viability of ASCs seeded onto the DAT foams over time to confirm the hypothesis that ASC viability decreases as the foams contract.
- Testing the effects of other types of dynamic cell culture methods (i.e.: spinner flask culture or flow perfusion) and culture medium (i.e.: serum-free culture

medium) on proliferation, viability, and factor secretion of ASC seeded in DAT foams.

- Further probing the effects of ASC-ECM interactions under normoxic and hypoxic conditions by assessing the changes in the gene expression profile over time, as well as investigating the expression of additional paracrine factors that may be secreted by the ASCs. The use of an alternative reference gene that is stably expressed under the experimental conditions should also be used to ensure that gene expression data is not skewed.
- Evaluating cell-DAT synergistic effects on ASC factor secretion by quantifying protein levels to confirm the trends seen in mRNA expression.
- Testing ASC-seeded scaffolds in a chronic wound model *in vivo*, such as a diabetic cutaneous wound model using db/db mice.

References

[1] T. L. Dinh and A. Veves, "A review of the mechanisms implicated in the pathogenesis of the diabetic foot.," *Int J Low Extrem Wounds*, vol. 4, no. 3, pp. 154–159, Sep. 2005.

[2] D. J. Margolis, J. Kantor, and J. A. Berlin, "Healing of diabetic neuropathic foot ulcers receiving standard treatment. A meta-analysis.," *Diabetes Care*, vol. 22, no. 5, pp. 692–695, May 1999.

[3] A. J. M. Boulton, L. Vileikyte, G. Ragnarson-Tennvall, and J. Apelqvist, "The global burden of diabetic foot disease.," *Lancet*, vol. 366, no. 9498, pp. 1719–1724, Nov. 2005.

[4] J. Apelqvist and J. Larsson, "What is the most effective way to reduce incidence of amputation in the diabetic foot?," *Diabetes Metab. Res. Rev.*, vol. 16, pp. S75–83, Sep. 2000.

[5] J. M. Gimble and F. Guilak, "Adipose-derived adult stem cells: isolation, characterization, and differentiation potential," *Cytotherapy*, vol. 5, no. 5, pp. 362–369, Jan. 2003.

[6] L. E. Flynn, "The use of decellularized adipose tissue to provide an inductive microenvironment for the adipogenic differentiation of human adipose-derived stem cells," *Biomaterials*, vol. 31, no. 17, pp. 4715–4724, Jun. 2010.

[7] W.S. Kim, B.S. Park, J.H. Sung, J.M. Yang, S.B. Park, S.J. Kwak, and J.S. Park, "Wound healing effect of adipose-derived stem cells: a critical role of secretory factors on human dermal fibroblasts.," *J. Dermatol. Sci.*, vol. 48, no. 1, pp. 15–24, Oct. 2007.

[8] G. Di Rocco, A. Gentile, A. Antonini, F. Ceradini, J. C. Wu, M. C. Capogrossi, and G. Toietta, "Enhanced healing of diabetic wounds by topical administration of adipose tissue-derived stromal cells overexpressing stromal-derived factor-1: biodistribution and engraftment analysis by bioluminescent imaging.," *Stem Cells Int*, vol. 2011, p. 304562, 2010.

[9] V. Russo, S. Young, A. Hamilton, B. G. Amsden, and L. E. Flynn, "Mesenchymal stem cell delivery strategies to promote cardiac regeneration following ischemic injury.," *Biomaterials*, vol. 35, no. 13, pp. 3956–3974, Apr. 2014.

[10] C. A. Fleck and R. Simman, "Modern collagen wound dressings: function and purpose.," *J Am Col Certif Wound Spec*, vol. 2, no. 3, pp. 50–54, Sep. 2010.

[11] C. Yu, J. Bianco, C. Brown, L. Fuetterer, J. F. Watkins, A. Samani, and L. E. Flynn, "Porous decellularized adipose tissue foams for soft tissue regeneration.," *Biomaterials*, Feb. 2013.

[12] A. E. B. Turner, C. Yu, J. Bianco, J. F. Watkins, and L. E. Flynn, "The performance of decellularized adipose tissue microcarriers as an inductive substrate for human adipose-derived stem cells," *Biomaterials*, vol. 33, no. 18, pp. 4490–4499, Jun. 2012.

[13] G. Frühbeck, “Overview of Adipose Tissue and Its Role in Obesity and Metabolic Disorders,” in *Adipose Tissue Protocols*, vol. 456, no. 1, Totowa, NJ: Humana Press, 2008, pp. 1–22.
[14] S. Cinti, “Transdifferentiation properties of adipocytes in the adipose organ.,” *Am. J. Physiol. Endocrinol. Metab.*, vol. 297, no. 5, pp. E977–86, Nov. 2009.
[15] S. Gesta, Y.H. Tseng, and C. R. Kahn, “Developmental origin of fat: tracking obesity to its source.,” *Cell*, vol. 131, no. 2, pp. 242–256, Oct. 2007.
[16] N. E. Wehrli, G. Bural, M. Houseni, K. Alkhawaldeh, A. Alavi, and D. A. Torigian, “Determination of age-related changes in structure and function of skin, adipose tissue, and skeletal muscle with computed tomography, magnetic resonance imaging, and positron emission tomography.,” *Seminars in Nuclear Medicine*, vol. 37, no. 3, pp. 195–205, May 2007.
[17] W. D. van Marken Lichtenbelt, J. W. Vanhommerig, N. M. Smulders, J. M. Drossaerts, G. J. Kemerink, N. D. Bouvy, P. Schrauwen, and G. J. Teule, “Cold-activated brown adipose tissue in healthy men,” *New England Journal of Medicine*, vol. 360, no. 15, pp. 1500–1508, 2009.
[18] R. Atit, S. K. Sgaier, O. A. Mohamed, M. M. Taketo, D. Dufort, A. L. Joyner, L. Niswander, and R. A. Conlon, “Beta-catenin activation is necessary and sufficient to specify the dorsal dermal fate in the mouse.,” *Developmental Biology*, vol. 296, no. 1, pp. 164–176, Aug. 2006.
[19] S. E. Wozniak, L. L. Gee, M. S. Wachtel, and E. E. Frezza, “Adipose tissue: the new endocrine organ? A review article,” *Digestive diseases and sciences*, vol. 54, no. 9, pp. 1847–1856, 2009.
[20] J. M. Friedman and J. L. Halaas, “Leptin and the regulation of body weight in mammals.,” *Nature*, vol. 395, no. 6704, pp. 763–770, Oct. 1998.
[21] A. Strobel, T. Issad, L. Camoin, M. Ozata, and A. D. Strosberg, “A leptin missense mutation associated with hypogonadism and morbid obesity.,” *Nat Genet*, vol. 18, no. 3, pp. 213–215, Mar. 1998.
[22] T.H. Chun, “Peri-adipocyte ECM remodeling in obesity and adipose tissue fibrosis.,” *Adipocyte*, vol. 1, no. 2, pp. 89–95, Apr. 2012.
[23] B. Leitinger and E. Hohenester, “Mammalian collagen receptors.,” *Matrix Biol.*, vol. 26, no. 3, pp. 146–155, Apr. 2007.
[24] S. Mori, S. Kiuchi, A. Ouchi, T. Hase, and T. Murase, “Characteristic expression of extracellular matrix in subcutaneous adipose tissue development and adipogenesis; comparison with visceral adipose tissue.,” *Int. J. Biol. Sci.*, vol. 10, no. 8, pp. 825–833, 2014.
[25] P. D. Yurchenco, Y. S. Cheng, and H. Colognato, “Laminin forms an independent network in basement membranes.,” *J. Cell Biol.*, vol. 117, no. 5, pp. 1119–1133, Jun. 1992.
[26] J. Nelson, N. V. McFerran, G. Pivato, E. Chambers, C. Doherty, D. Steele, and D. J. Timson, “The 67 kDa laminin receptor: structure, function and role in disease.,” *Biosci. Rep.*, vol. 28, no. 1, pp. 33–48, Feb. 2008.

[27] T. Sasaki, R. Fässler, and E. Hohenester, “Laminin: the crux of basement membrane assembly.,” *J. Cell Biol.*, vol. 164, no. 7, pp. 959–963, Mar. 2004.
[28] B. M. Spiegelman and C. A. Ginty, “Fibronectin modulation of cell shape and lipogenic gene expression in 3t3-adipocytes,” *Cell*, vol. 35, no. 3, pp. 657–666, Dec. 1983.
[29] D. F. Mosher and P. E. Schad, “Cross-linking of fibronectin to collagen by blood coagulation Factor XIIIa.,” *J. Clin. Invest.*, vol. 64, no. 3, pp. 781–787, Sep. 1979.
[30] A. Divoux and K. Clément, “Architecture and the extracellular matrix: the still unappreciated components of the adipose tissue.,” *Obes Rev*, vol. 12, no. 5, pp. e494–503, May 2011.
[31] P. Bork and R. F. Doolittle, “Proposed acquisition of an animal protein domain by bacteria.,” *Proc. Natl. Acad. Sci. U.S.A.*, vol. 89, no. 19, pp. 8990–8994, Oct. 1992.
[32] S. Chattopadhyay and R. T. Raines, “Review collagen-based biomaterials for wound healing.,” *Biopolymers*, vol. 101, no. 8, pp. 821–833, Aug. 2014.
[33] E. R. Kenawy, J. M. Layman, J. R. Watkins, G. L. Bowlin, J. A. Matthews, D. G. Simpson, and G. E. Wnek, “Electrospinning of poly(ethylene-co-vinyl alcohol) fibers.,” *Biomaterials*, vol. 24, no. 6, pp. 907–913, Mar. 2003.
[34] U. Hersel, C. Dahmen, and H. Kessler, “RGD modified polymers: biomaterials for stimulated cell adhesion and beyond.,” *Biomaterials*, vol. 24, no. 24, pp. 4385–4415, Nov. 2003.
[35] M. P. Lutolf and J. A. Hubbell, “Synthetic biomaterials as instructive extracellular microenvironments for morphogenesis in tissue engineering.,” *Nat. Biotechnol.*, vol. 23, no. 1, pp. 47–55, Jan. 2005.
[36] S. F. Badylak, “Decellularized allogeneic and xenogeneic tissue as a bioscaffold for regenerative medicine: factors that influence the host response.,” *Ann Biomed Eng*, vol. 42, no. 7, pp. 1517–1527, Jul. 2014.
[37] S. Nagata, R. Hanayama, and K. Kawane, “Autoimmunity and the clearance of dead cells.,” *Cell*, vol. 140, no. 5, pp. 619–630, Mar. 2010.
[38] J. E. Valentin, A. M. Stewart-Akers, T. W. Gilbert, and S. F. Badylak, “Macrophage participation in the degradation and remodeling of extracellular matrix scaffolds,” *Tissue Engineering Part A*, vol. 15, no. 7, pp. 1687–1694, 2009.
[39] C. D. Mills, K. Kincaid, J. M. Alt, M. J. Heilman, and A. M. Hill, “M-1/M-2 macrophages and the Th1/Th2 paradigm.,” *J. Immunol.*, vol. 164, no. 12, pp. 6166–6173, Jun. 2000.
[40] J. M. Anderson, A. Rodriguez, and D. T. Chang, “Foreign body reaction to biomaterials.,” *Semin. Immunol.*, vol. 20, no. 2, pp. 86–100, Apr. 2008.
[41] J. E. Valentin, N. J. Turner, T. W. Gilbert, and S. F. Badylak, “Functional skeletal muscle formation with a biologic scaffold.,” *Biomaterials*, vol. 31, no. 29, pp. 7475–7484, Oct. 2010.

[42] J. E. Reing, L. Zhang, J. Myers-Irvin, K. E. Cordero, D. O. Freytes, E. Heber-Katz, K. Bedelbaeva, D. McIntosh, A. Dewilde, S. J. Braunhut, and S. F. Badylak, "Degradation products of extracellular matrix affect cell migration and proliferation.," *Tissue Engineering Part A*, vol. 15, no. 3, pp. 605–614, Mar. 2009.

[43] T. J. Keane, R. Londono, N. J. Turner, and S. F. Badylak, "Consequences of ineffective decellularization of biologic scaffolds on the host response.," *Biomaterials*, vol. 33, no. 6, pp. 1771–1781, Feb. 2012.

[44] P. Thevenot, A. Nair, J. Dey, J. Yang, and L. Tang, "Method to Analyze Three-Dimensional Cell Distribution and Infiltration in Degradable Scaffolds," *Tissue Eng Pt C-Meth*, vol. 14, no. 4, pp. 319–331, 2008.

[45] J. Zeltinger, J. K. Sherwood, D. A. Graham, R. Müeller, and L. G. Griffith, "Effect of Pore Size and Void Fraction on Cellular Adhesion, Proliferation, and Matrix Deposition," *Tissue Eng.*, vol. 7, no. 5, pp. 557–572, Oct. 2001.

[46] B. S. Kim, A. J. Putnam, T. J. Kulik, and D. J. Mooney, "Optimizing seeding and culture methods to engineer smooth muscle tissue on biodegradable polymer matrices.," *Biotechnol Bioeng*, vol. 57, no. 1, pp. 46–54, Jan. 1998.

[47] J. F. Alvarez-Barreto, S. M. Linehan, R. L. Shambaugh, and V. I. Sikavitsas, "Flow perfusion improves seeding of tissue engineering scaffolds with different architectures," *Ann Biomed Eng*, vol. 35, no. 3, pp. 429–442, 2007.

[48] J. M. Gimble, A. J. Katz, and B. A. Bunnell, "Adipose-Derived Stem Cells for Regenerative Medicine," *Circ. Res.*, vol. 100, no. 9, pp. 1249–1260, Apr. 2007.

[49] J. K. Fraser, I. Wulur, Z. Alfonso, and M. H. Hedrick, "Fat tissue: an underappreciated source of stem cells for biotechnology.," *Trends Biotechnol.*, vol. 24, no. 4, pp. 150–154, Apr. 2006.

[50] J. B. Mitchell, K. McIntosh, S. Zvonic, and S. Garrett, "Immunophenotype of Human Adipose-Derived Cells: Temporal Changes in Stromal-Associated and Stem Cell–Associated Markers," *Stem Cells,* 2006.

[51] F. Guilak, K. E. Lott, H. A. Awad, Q. Cao, K. C. Hicok, B. Fermor, and J. M. Gimble, "Clonal analysis of the differentiation potential of human adipose-derived adult stem cells.," *J. Cell. Physiol.*, vol. 206, no. 1, pp. 229–237, Jan. 2006.

[52] B. Puissant, C. Barreau, P. Bourin, C. Clavel, J. Corre, C. Bousquet, C. Taureau, B. Cousin, M. Abbal, P. Laharrague, L. Penicaud, L. Casteilla, and A. Blancher, "Immunomodulatory effect of human adipose tissue-derived adult stem cells: comparison with bone marrow mesenchymal stem cells," *Br J Haematol*, vol. 129, no. 1, pp. 118–129, Apr. 2005.

[53] K. McIntosh, S. Zvonic, S. Garrett, J. B. Mitchell, Z. E. Floyd, L. Hammill, A. Kloster, Y. Di Halvorsen, J. P. Ting, R. W. Storms, B. Goh, G. Kilroy, X. Wu, and J. M. Gimble, "The immunogenicity of human adipose-derived cells: temporal changes in vitro.," *Stem Cells*, vol. 24, no. 5, pp. 1246–1253, May 2006.

[54] M. Rodbell, “Metabolism of Isolated Fat Cells. I. Effects of Hormones On Glucose Metabolism and Lipolysis.,” *J. Biol. Chem.*, vol. 239, pp. 375–380, Feb. 1964.

[55] J. H. Moore Jr., J. W. Kolaczynski, L. M. Morales, R. V. Considine, Z. Pietrzkowski, P. F. Noto, and J. F. Caro, “Viability of fat obtained by syringe suction lipectomy: effects of local anesthesia with lidocaine,” *Aesth. Plast. Surg.*, vol. 19, no. 4, pp. 335–339, 1995.

[56] A. J. Katz, M. H. Hedrick, R. Llull, and J. W. Futrell, “A novel device for the simple and efficient refinement of liposuctioned tissue.,” *Plast. Reconstr. Surg.*, vol. 107, no. 2, pp. 595–597, 2001.

[57] Y. Zhao, S. D. Waldman, and L. E. Flynn, “The Effect of Serial Passaging on the Proliferation and Differentiation of Bovine Adipose-Derived Stem Cells,” *Cells Tissues Organs*, vol. 195, no. 5, pp. {414–427}, 2012.

[58] L. L. Q. Pu, X. Cui, B. F. Fink, D. Gao, and H. C. Vasconez, “Adipose aspirates as a source for human processed lipoaspirate cells after optimal cryopreservation.,” *Plast. Reconstr. Surg.*, vol. 117, no. 6, pp. 1845–1850, May 2006.

[59] W. Wagner, F. Wein, A. Seckinger, M. Frankhauser, U. Wirkner, U. Krause, J. Blake, C. Schwager, V. Eckstein, W. Ansorge, and A. D. Ho, “Comparative characteristics of mesenchymal stem cells from human bone marrow, adipose tissue, and umbilical cord blood.,” *Exp. Hematol.*, vol. 33, no. 11, pp. 1402–1416, Nov. 2005.

[60] M. Dominici, K. Le Blanc, I. Mueller, I. Slaper-Cortenbach, F. Marini, D. Krause, R. Deans, A. Keating, D. Prockop, and E. Horwitz, “Minimal criteria for defining multipotent mesenchymal stromal cells. The International Society for Cellular Therapy position statement.,” *Cytotherapy*, vol. 8, no. 4, pp. 315–317, 2006.

[61] H. Nakagami, “Novel Autologous Cell Therapy in Ischemic Limb Disease Through Growth Factor Secretion by Cultured Adipose Tissue-Derived Stromal Cells,” *Arteriosclerosis, Thrombosis, and Vascular Biology*, vol. 25, no. 12, pp. 2542–2547, Dec. 2005.

[62] L. Cai, B. H. Johnstone, T. G. Cook, Z. Liang, D. Traktuev, K. Cornetta, D. A. Ingram, E. D. Rosen, and K. L. March, “Suppression of hepatocyte growth factor production impairs the ability of adipose-derived stem cells to promote ischemic tissue revascularization.,” *Stem Cells*, vol. 25, no. 12, pp. 3234–3243, Dec. 2007.

[63] K. Kondo, S. Shintani, R. Shibata, H. Murakami, R. Murakami, M. Imaizumi, Y. Kitagawa, and T. Murohara, “Implantation of adipose-derived regenerative cells enhances ischemia-induced angiogenesis.,” *Arteriosclerosis, Thrombosis, and Vascular Biology*, vol. 29, no. 1, pp. 61–66, Jan. 2009.

[64] J.I. Yamaguchi, K. F. Kusano, O. Masuo, A. Kawamoto, M. Silver, S. Murasawa, M. Bosch-Marce, H. Masuda, D. W. Losordo, J. M. Isner, and T.

Asahara, “Stromal cell-derived factor-1 effects on ex vivo expanded endothelial progenitor cell recruitment for ischemic neovascularization.,” *Circulation*, vol. 107, no. 9, pp. 1322–1328, Mar. 2003.

[65] A. J. Singer and R. A. Clark, “Cutaneous wound healing.,” *N. Engl. J. Med.*, vol. 341, no. 10, pp. 738–746, Sep. 1999.

[66] P. Breen, “Basics of coagulation pathways.,” *Int Anesthesiol Clin*, vol. 42, no. 3, pp. 1–9, 2004.

[67] R. A. F. Clark, “The molecular and cellular biology of wound repair,” 1996.

[68] M. P. Welch, G. F. Odland, and R. A. Clark, “Temporal relationships of F-actin bundle formation, collagen and fibronectin matrix assembly, and fibronectin receptor expression to wound contraction.,” *J. Cell Biol.*, vol. 110, no. 1, pp. 133–145, Jan. 1990.

[69] T. Leivo, U. Kiistala, M. Vesterinen, K. Owaribe, R. E. Burgeson, I. Virtanen, and A. Oikarinen, “Re-epithelialization rate and protein expression in the suction-induced wound model: comparison between intact blisters, open wounds and calcipotriol-pretreated open wounds,” *Br J Dermatol*, vol. 142, no. 5, pp. 991–1002, 2000.

[70] A. Desmoulière, M. Redard, I. Darby, and G. Gabbiani, “Apoptosis mediates the decrease in cellularity during the transition between granulation tissue and scar.,” *Am. J. Pathol.*, vol. 146, no. 1, pp. 56–66, Jan. 1995.

[71] G. E. Reiber, B. A. Lipsky, and G. W. Gibbons, “The burden of diabetic foot ulcers.,” *Am. J. Surg.*, vol. 176, no. 2, pp. 5S–10S, Aug. 1998.

[72] G. E. Reiber, L. Vileikyte, E. J. Boyko, M. del Aguila, D. G. Smith, L. A. Lavery, and A. J. Boulton, “Causal pathways for incident lower-extremity ulcers in patients with diabetes from two settings.,” *Diabetes Care*, vol. 22, no. 1, pp. 157–162, Jan. 1999.

[73] A. J. Boulton, C. A. Hardisty, R. P. Betts, C. I. Franks, R. C. Worth, J. D. Ward, and T. Duckworth, “Dynamic foot pressure and other studies as diagnostic and management aids in diabetic neuropathy,” *Diabetes Care*, vol. 6, no. 1, pp. 26–33, 1983.

[74] J. D. Ward, A. J. Boulton, J. M. Simms, D. A. Sandler, and G. Knight, “Venous distension in the diabetic neuropathic foot (physical sign of arteriovenous shunting).,” *J R Soc Med*, vol. 76, no. 12, pp. 1011–1014, Dec. 1983.

[75] A. J. Boulton, J. H. Scarpello, and J. D. Ward, “Venous oxygenation in the diabetic neuropathic foot: evidence of arteriovenous shunting?,” *Diabetologia*, vol. 22, no. 1, pp. 6–8, Jan. 1982.

[76] R. Tegnér, “The effect of skin temperature on vibratory sensitivity in polyneuropathy.,” *J. Neurol. Neurosurg. Psychiatr.*, vol. 48, no. 2, pp. 176–178, Feb. 1985.

[77] G. E. Reiber, L. Vileikyte, E. J. Boyko, M. del Aguila, D. G. Smith, L. A. Lavery, and A. J. Boulton, “Causal pathways for incident lower-extremity ulcers in patients with diabetes from two settings.,” *Diabetes Care*, vol. 22, no.

1, pp. 157–162, Jan. 1999.
[78] G. Williams and J. Pickup, “Impaired microvascular hyperaemic response to minor skin trauma in type I diabetes.,” *Br Med J (Clin Res Ed)*, vol. 293, no. 6540, p. 204, Jul. 1986.
[79] M. A. M. Loots, S. B. Kenter, F. L. Au, W. Van Galen, E. Middelkoop, J. D. Bos, and J. R. Mekkes, “Fibroblasts derived from chronic diabetic ulcers differ in their response to stimulation with EGF, IGF-I, bFGF and PDGF-AB compared to controls,” *Eur. J. Cell Biol.*, vol. 81, no. 3, pp. 153–160, 2002.
[80] D. L. Steed, C. Attinger, T. Colaizzi, M. Crossland, M. Franz, L. Harkless, A. Johnson, H. Moosa, M. Robson, T. Serena, P. Sheehan, A. Veves, and L. Wiersma-Bryant, “Guidelines for the treatment of diabetic ulcers.,” *Wound Repair and Regeneration*, vol. 14, no. 6. pp. 680–692, Nov. 2006.
[81] C. K. Sen, G. M. Gordillo, S. Roy, R. Kirsner, L. Lambert, T. K. Hunt, F. Gottrup, G. C. Gurtner, and M. T. Longaker, “Human skin wounds: a major and snowballing threat to public health and the economy.,” *Wound Repair Regen*, vol. 17, no. 6, pp. 763–771, Nov. 2009.
[82] V. Falanga, “Wound healing and its impairment in the diabetic foot.,” *Lancet*, vol. 366, no. 9498, pp. 1736–1743, Nov. 2005.
[83] J. R. Hilton, D. T. Williams, B. Beuker, D. R. Miller, and K. G. Harding, “Wound dressings in diabetic foot disease.,” *Clin. Infect. Dis.*, vol. 39, pp. S100–3, Aug. 2004.
[84] J. Rehman, “Secretion of Angiogenic and Antiapoptotic Factors by Human Adipose Stromal Cells,” *Circulation*, vol. 109, no. 10, pp. 1292–1298, Mar. 2004.
[85] E. Y. Lee, Y. Xia, W.S. Kim, M. H. Kim, T. H. Kim, K. J. Kim, B.S. Park, and J.H. Sung, “Hypoxia-enhanced wound-healing function of adipose-derived stem cells: increase in stem cell proliferation and up-regulation of VEGF and bFGF.,” *Wound Repair Regen*, vol. 17, no. 4, pp. 540–547, Jul. 2009.
[86] N. M. Toyserkani, M. L. Christensen, S. P. Sheikh, and J. A. Sørensen, “Adipose-Derived Stem Cells: New Treatment for Wound Healing?,” *Ann Plast Surg*, Mar. 2014.
[87] J. Macdiarmid and J. B. Wilson, “Separation of epidermal tissue from underlying dermis and primary keratinocyte culture,” pp. 401–410, 2001.
[88] J. E. Reing, B. N. Brown, K. A. Daly, J. M. Freund, T. W. Gilbert, S. X. Hsiong, A. Huber, K. E. Kullas, S. Tottey, and M. T. Wolf, “The effects of processing methods upon mechanical and biologic properties of porcine dermal extracellular matrix scaffolds,” *Biomaterials*, vol. 31, no. 33, pp. 8626–8633, Nov. 2010.
[89] N. Rajan, J. Habermehl, M.F. Coté, C. J. Doillon, and D. Mantovani, “Preparation of ready-to-use, storable and reconstituted type I collagen from rat tail tendon for tissue engineering applications.,” *Nat Protoc*, vol. 1, no. 6, pp. 2753–2758, 2006.

[90] L. Flynn, J. L. Semple, and K. A. Woodhouse, “Decellularized placental matrices for adipose tissue engineering,” *J. Biomed. Mater. Res.*, vol. 79, no. 2, pp. 359–369, Nov. 2006.
[91] R. Zhang and P. X. Ma, “Poly (α-hydroxyl acids)/hydroxyapatite porous composites for bone-tissue engineering. I. Preparation and morphology,” 1999.
[92] I. G. Fels, “Hydration and density of collagen and gelatin,” *J. Appl. Polym. Sci.*, vol. 8, no. 4, pp. 1813–1824, 1964.
[93] G. Sitterley, “Collagen Attachment Protocols, Solubility, and Stability,” *BioFiles*, vol. 3, no. 5, pp. 1–3, Oct. 2008.
[94] R. Komsa-Penkova, R. Spirova, and B. Bechev, “Modification of Lowry's method for collagen concentration measurement,” *Journal of Biochemical and Biophysical Methods*, vol. 32, no. 1, pp. 33–43, Apr. 1996.
[95] E. Bell, B. Ivarsson, and C. Merrill, “Production of a tissue-like structure by contraction of collagen lattices by human fibroblasts of different proliferative potential in vitro.,” *Proc. Natl. Acad. Sci. U.S.A.*, vol. 76, no. 3, pp. 1274–1278, Mar. 1979.
[96] H. A. Awad, D. L. Butler, M. T. Harris, R. E. Ibrahim, Y. Wu, R. G. Young, S. Kadiyala, and G. P. Boivin, “In vitro characterization of mesenchymal stem cell-seeded collagen scaffolds for tendon repair: effects of initial seeding density on contraction kinetics.,” *J. Biomed. Mater. Res.*, vol. 51, no. 2, pp. 233–240, Aug. 2000.
[97] M. K. Maharlooei, M. Bagheri, Z. Solhjou, B. M. Jahromi, M. Akrami, L. Rohani, A. Monabati, A. Noorafshan, and G. R. Omrani, “Adipose tissue derived mesenchymal stem cell (AD-MSC) promotes skin wound healing in diabetic rats,” *Diabetes Research and Clinical Practice*, vol. 93, no. 2, pp. 228–234, Aug. 2011.
[98] S. C. Heo, E. S. Jeon, I. H. Lee, H. S. Kim, M. B. Kim, and J. H. Kim, “Tumor Necrosis Factor-α-Activated Human Adipose Tissue–Derived Mesenchymal Stem Cells Accelerate Cutaneous Wound Healing through Paracrine Mechanisms,” *J. Invest. Dermatol.*, vol. 131, no. 7, pp. 1559–1567, Mar. 2011.
[99] S. Liu, H. Zhang, X. Zhang, W. Lu, X. Huang, H. Xie, J. Zhou, W. Wang, Y. Zhang, Y. Liu, Z. Deng, and Y. Jin, “Synergistic Angiogenesis Promoting Effects of Extracellular Matrix Scaffolds and Adipose-Derived Stem Cells During Wound Repair,” *Tissue Engineering Part A*, vol. 17, no. 5, pp. 725–739, Mar. 2011.
[100] Y.-H. Lee, J.-J. Chang, M.-C. Yang, C.-T. Chien, and W.-F. Lai, “Acceleration of wound healing in diabetic rats by layered hydrogel dressing,” *Carbohydrate Polymers*, vol. 88, no. 3, pp. 809–819, Apr. 2012.
[101] T. Fink, P. Lund, L. Pilgaard, J. G. Rasmussen, M. Duroux, and V. Zachar, “Instability of standard PCR reference genes in adipose-derived stem cells during propagation, differentiation and hypoxic exposure.,” *BMC Mol. Biol.*, vol. 9, p. 98, 2008.

[102] D. Greenbaum, C. Colangelo, and K. Williams, “Comparing protein abundance and mRNA expression levels on a genomic scale,” *Genome ...*, 2003.
[103] American Diabetes Association, “Standards of medical care in diabetes--2006.,” *Diabetes care*, vol. 29. pp. S4–42, Jan-2006.
[104] M. Lepäntalo, J. Apelqvist, C. Setacci, J. B. Ricco, G. de Donato, F. Becker, H. Robert-Ebadi, P. Cao, H. H. Eckstein, P. De Rango, N. Diehm, J. Schmidli, M. Teraa, F. L. Moll, F. Dick, and A. H. Davies, “Chapter V: Diabetic foot.,” *Eur J Vasc Endovasc Surg*, vol. 42, pp. S60–74, Dec. 2011.
[105] C. J. Doillon and F. H. Silver, “Collagen-based wound dressing: effects of hyaluronic acid and fibronectin on wound healing.,” *Biomaterials*, vol. 7, no. 1, pp. 3–8, Jan. 1986.
[106] C. A. Fleck and D. Chakravarthy, “Understanding the Mechanisms of Collagen Dressings,” *Adv Skin Wound Care*, vol. 20, no. 5, pp. 256–259, May 2007.
[107] S. K. Kapur and A. J. Katz, “Review of the adipose derived stem cell secretome.,” *Biochimie*, vol. 95, no. 12, pp. 2222–2228, Dec. 2013.

Appendix A

Immunostaining Negative Controls

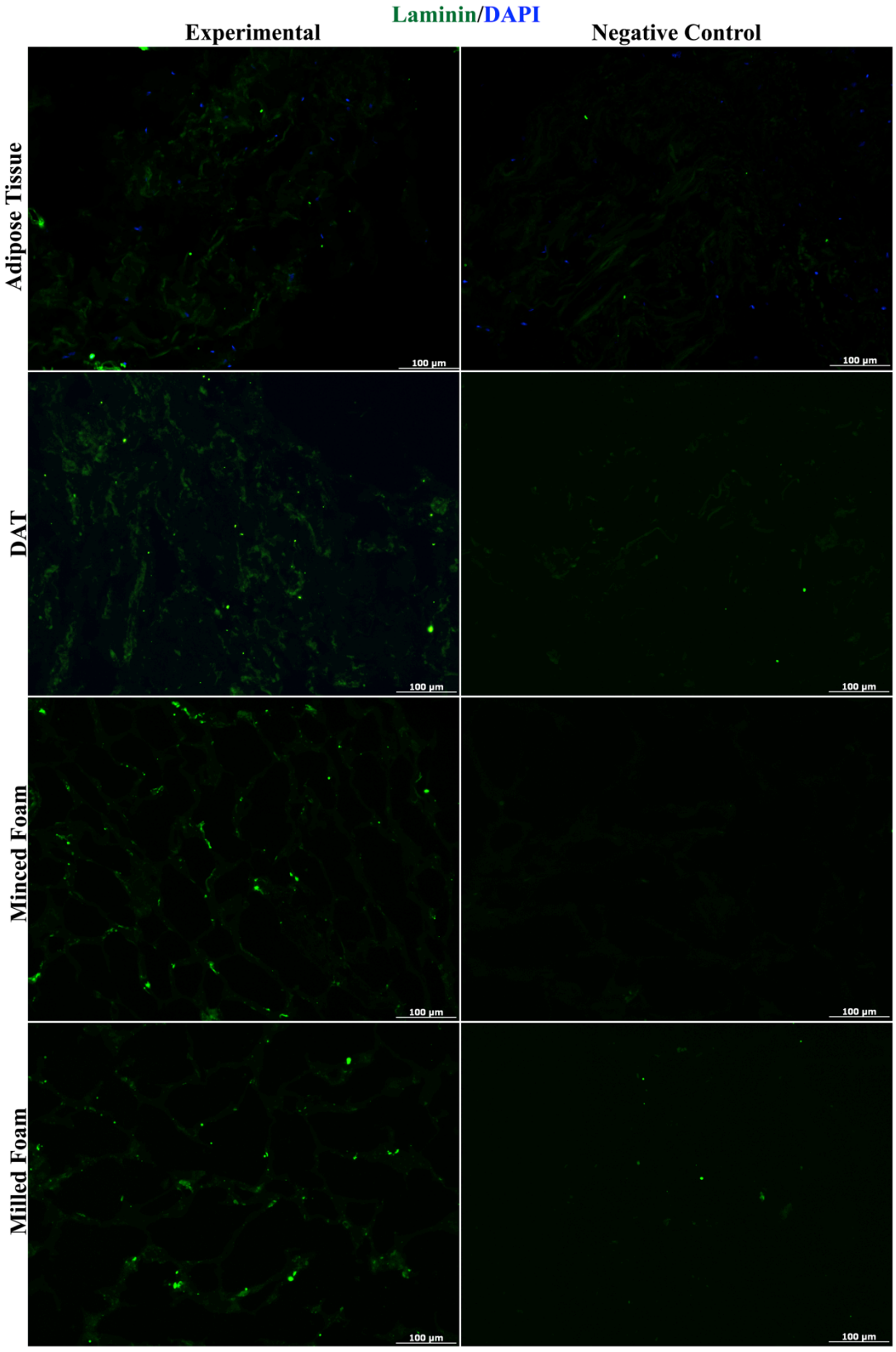
Laminin/DAPI
Experimental
Negative Control
Adipose Tissue
DAT
Minced Foam
Milled Foam
100 µm

Figure A1: Laminin immunostaining negative controls. On each microscope slide, 2 sections were subject to the immunostaining protocol. One section was stained using all antibodies (left column), while primary antibody was intentionally omitted from the other section (right column). Each pair of images was captured using identical exposure times, confirming the staining was specific with minimal non-specific background staining visualized.

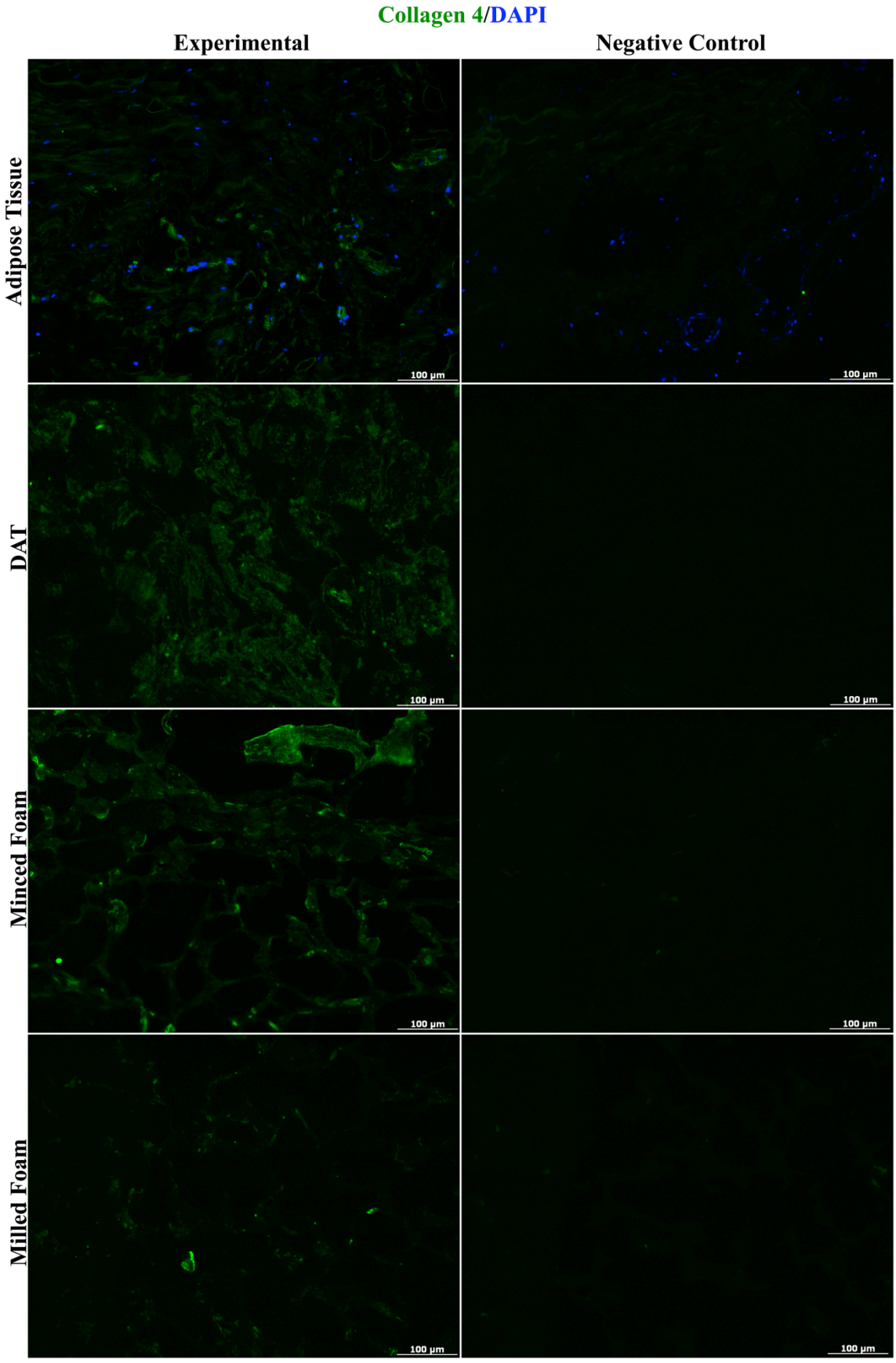
Collagen 4/DAPI
Experimental
Negative Control
Adipose Tissue
DAT
Minced Foam
Milled Foam
100 µm

Figure A1: Collagen type IV immunostaining negative controls. On each microscope slide, 2 sections were subject to the immunostaining protocol. One section was stained using all antibodies (left column), while primary antibody was intentionally omitted from the other section (right column). Each pair of images was captured using identical exposure times, confirming that the staining was specific.